Estimation of Cable Forces at the Ashton Bridge through Ambient Vibration Testing

Prepared by:

Kaboyamodimo Nare

Supervised by:

Prof. Pilate Moyo (PrEng, FSAAE, FSAICE, MASSAf)

Mr. Bukhosi Raphael Nyoni

Dissertation submitted in fulfilment of the requirements for the degree of
Master of Engineering (Structural Engineering and Materials)

Department of Civil Engineering
University of Cape Town, Private Bag Rondebosch, 7700
South Africa 7700

November 2022

Declaration

I know the meaning of plagiarism and declare that all the work in the document, save for that which is properly acknowledged, is my own. This thesis/dissertation has been submitted to the Turnitin module (or equivalent similarity and originality checking software) and I confirm that my supervisor has seen my report and any concerns revealed by such have been resolved with my supervisor.

Signed: Signed by candidate Date: 25/07/2023

Dedication

To my parents

Abstract

The Ashton Bridge is a concrete tied arch bridge which was part of a project conducted under the auspices of the Western Cape Government. AECOM SA were the consulting engineers. The construction of bridge was started by Basil Read and completed by Haw & Inglis after the former went into business rescue. The bridge was officially opened on the 15th of August 2021 after being transversely launched to its final position.

Hanger cables distribute forces and become more dynamically active as span lengths increase. It is for this reason that the accurate evaluation of forces in the hanger cables is important during construction and for bridge maintenance purposes because they are the main elements that determine the integrity of the structure.

Superstructure and cable vibration data was collected on site after the final stage of cable tensioning. Finite element models of each cable were created using the software, Sofistik. Thereafter, the force in the cable models was iterated until the theoretical natural frequencies matched the ones from site measurements. The superstructure vibration test results were used to calibrate the main model and isolate cable frequencies in cases where the peak frequencies were not easily distinguishable especially for the short cables. The estimated force was evaluated by adapting a COLTO tendon prestressing specification and considering the temperature on the day of the tests. In order to investigate the impact of the sockets on the natural frequencies and force of the cables, an analysis was conducted by removing the sockets from each cable FEM one investigation and adjusting the stiffness parameters associated with the sockets in another investigation.

Most of the cable forces matched the predicted ones with the total variation between the two being -3.18%. It is recommended that the frequency measurement of Cable 1 (Robertson end) on the North Arch be retaken because it differs markedly from the other 3 similar cables. However, the primary method for engineer's approval relied on lift-off tests that ensured that the design force was achieved in all the cables.

The total variation between the forces estimated from the measured data and the forces predicted by the bridge's FEM is acceptable. Large variations in the forces in short cables are attributed to their high sensitivity to temperature changes. The sockets play a significant role in the frequency and ultimately the force in the cables depending on their proportion in the cable system. Hence, they should be modelled accurately to simulate the geometric and material properties.

As the length of a cable decreases, the socket proportions become larger and more influential in the cable system behaviour. Consequently, the cable may start to behave more as a beam than a cable. However, the point at which the cable transitions to beam behaviour or the combination of the cable and beam behaviour is not known and requires further study.

Acknowledgements

Firstly, I would like to thank the course convener and lecturers of CIV5131Z for a well-structured course that provided much needed guidance and knowledge in the compilation of the dissertation.

Thank you to my mother, Surrender Nare for encouraging and supporting me during my studies. Many thanks to my late father, Dennis Nare whose continuous pride in my academic journey has always been a source of encouragement in difficult moments. I trust that he is looking down from the heavens beaming with pride. I would also like to thank my aunt, Boitumelo Nare, for always checking up on my progress and holding me accountable to my deliverables throughout the research.

The Western Cape Government is acknowledged for its continuous investment into local infrastructure projects such as the rehabilitation of Trunk Road 31 from Ashton to Montagu. In addition to improving the livelihoods of the communities, these projects also enhance the technical skills of the personnel tasked to bring them to life.

I would like to express my gratitude to my supervisors Professor Pilate Moyo and Bukhosi Nyoni for their insights, guidance, and great assistance during the collection of data on site as well as for the analysis. David Ward of Teufelberger Radaelli is acknowledged for assisting in acquiring the manufacturer drawings that were used to create the models.

I also wish to thank my senior colleagues and mentors Abe Newmark, Philip Ronné, Heinrich van Wijk and Rodney Kayonga for going above and beyond in my professional and academic career. My acknowledgements also extend to AECOM SA for affording me the time and resources to undertake my postgraduate studies.

Bruce Bintley and David Middleton are acknowledged for their continuous input to my professional development especially during their site visits to the Ashton Bridge. They also formed part of a cohort of engineers that inspired me to pursue a Master’s degree.

I would also like to acknowledge the contractor, Haw & Inglis (H &I), for facilitating the hiring of a cherry picker and providing an operator for data collection procedures. EC Traffic Services are also acknowledged for assisting with traffic control during the data collection period. Last but not least, I would like to acknowledge Terry February for some of the pictures that have been used in this dissertation.

Table of contents

List of Figures

List of Tables

Glossary

Accelerometer	-	a device that measures the acceleration of a structure’s motion.
Discretizing	-	the process of breaking down continuous functions into small discrete parts for analysis.
Force Matrix	-	a table detailing the redistribution of forces in hanger cables with each passing tensioning sequence.
Fully locked coil	-	a type of cable consisting of wires that are helically twisted on the inner layer and z-shaped wires that interlock on the outer later.
Harmonic	-	a wave that has a frequency which is a multiple of other frequencies of the same reference wave.
Mode shape	-	a deflection pattern associated with a particular frequency of an object.
Natural frequency	-	the oscillation frequency of a system in the absence of an external force.
Spring point	-	the point where the arch and tie beam meet.
Tie Beam	-	a horizontal beam that connects one end of the arch rib to the other.
Transverse Launching	-	the hydraulic jacking of a structure to an intended position.
Turnbuckle	-	a piece of hardware between the cylindrical socket and the fork socket used to adjust the length or tension in a cable.
Wish bone	-	a beam that transversely connects the arches of an Arch Bridge to ensure lateral stability.

Nomenclature

Latin Upper Case

A	-	Cross sectional area
E	-	Elastic Modulus
EI	-	Bending stiffness
EA	-	Axial stiffness
Hz	-	Hertz
I	-	Moment of inertia
N	-	Newton
N/m^2	-	Newton per square metre
Nm^2	-	Newton metre squared
$\boldsymbol{S_n}$	-	Sample standard deviation
T_o	-	Sample outlier parameter
°	-	Degrees
℃	-	Degrees Celsius

Latin Lower Case

GPa	-	Gigapascal
kg	-	Kilogram
kg/m	-	Kilogram per metre
kg/m^3	-	Kilogram per cubic metre
kN	-	Kilonewton
kN/m	-	Kilonewton per metre
kN/m^3	-	Kilonewton per cubic metre
m	-	Metre
m/s^2	-	Metre per second squared
m^2	-	Metre squared
m^4	-	Metre to the power of 4
mm	-	Millimetre

mm^2	-	Millimetre squared
MPa	-	Megapascal
x_0	-	Sample test result
$\bar{x}_n$	-	Sample mean

Greek Lower Case

λ^2	-	Sag extensibility
ϵ	-	Bending stiffness parameter
ζ	-	Damping ratio
ω	-	Undamped natural frequency
ω_D	-	Damped natural frequency
ε_H	-	Total error associated with tension calculated from a tensioned beam
ε_{f1}	-	Error associated with frequency
ε_l	-	Error associated with length
ε_m	-	Error associated with mass
σ	-	Stress
α	-	Inclination angle
φ	-	Coefficient of thermal expansion per ℃
γ	-	Unit weight

Acronyms and Abbreviations

AVT	-	Ambient Vibration Testing
COLTO	-	Committee of Land Transport Officials
CTE	-	Coefficient of thermal Expansion
FE	-	Finite Element
FEM	-	Finite Element Model
FRF	-	Frequency Response Function
N	-	North
PSD	-	Power Spectrum Density
S	-	South
TH2	-	2^{nd} order theory
TH3	-	3^{rd} order theory

1 Introduction

1.1 Background to Study

The Ashton Bridge was part of a project conducted under the auspices of the Western Cape Government to rehabilitate a 13km road between the towns of Ashton and Montagu about 200km northeast of Cape Town. AECOM SA were the consulting engineers. The bridge was designed for a service life of 100 years using the Code of Practice for the Design of Highway Bridges and Culverts in South Africa and in cases of elements beyond the local code specifications such as the anchor plates, the British and Euro codes were used. Construction of bridge was started by Basil Read and completed by Haw & Inglis after the former went into business rescue. The bridge was officially opened on the 15th of August 2021 after being transversely launched to its final position.

The Ashton bridge is a concrete tied arch bridge spanning 110m. The concrete elements of the bridge superstructure are the deck, 2 tie beams and 2 arches which are connected by 5 wishbones. Furthermore, the two arches consist of fully locked coil hanger cables that are connected to the tie beam via fork sockets. The inclined hanger cables are tensioned and their forces were optimised to achieve a desired structural profile taking into account the time dependant material properties (Ronné et al., 2018). Figure 1-1 shows the Ashton bridge.

Figure 1-1: The Ashton Bridge. Photographed by Terry February for AECOM SA, 2022

As span lengths of bridges increase, the lengths of the hanger cables also increase. Consequently the hanger cables become more dynamically active which increases the risk of early fatigue and deterioration (Kangas et al., 2010). Hanger cables distribute forces which in turn affects the stress concentrations on the elements of a bridge (Morgenthal et al., 2018). Hence, the accurate estimation of forces in the hanger cables is important during construction and for bridge maintenance purposes because they are the main elements that determine the integrity of the structure (Kim & Park, 2007; Kangas et al., 2010).

1.2 Problem Statement

A key parameter in the evaluation of the forces using vibration testing is the effective hanger cable length. This parameter is challenging to determine when boundary conditions consist of special anchorage systems such as in the case at the Ashton bridge (Chen et al., 2018). There also exists an uncertainty with the degree of constraint provided by the anchorage systems which then influences the accuracy of the estimated cable force (Caetano et al., 2013; Joaquim, Cismasiu & Caetano, 2017). Thus, this study will give an accurate definition of a cable's parameters and its boundary conditions to estimate the force in a cable within acceptable accuracy.

1.3 Research Aim and Objectives

The research aims to evaluate the hanger cable forces at the Ashton Bridge. The results from the research will form part of the Ashton Bridge Maintenance Manual that will be used for condition assessments of the bridge in future.

The objectives of the research are:

i) To evaluate the cable forces using the data measured on site,
ii) To investigate the effect of anchorage systems on the forces in the cable.

1.4 Scope and Limitations

The scope of this research is limited to cables that do not have dampers and intermediate supports. The software packages Sofistik and MEscope were used to create finite element models of the cables and to extract the natural frequencies from site data respectively. Autodesk Civil 3D was used to extract section properties of the fork sockets. The bending stiffness was incorporated in all the cable models based on recommendations from previous similar work discussed in the literature review. However, its effect on cable systems were not investigated.

1.5 Significance of the Research

The application of checking cable forces through Ambient Vibration Testing (AVT) will provide practising engineers with a reliable and time efficient way of evaluating cable forces. A better understanding of the effect of the anchorage systems on the behaviour of the cable will be developed. The research will also demonstrate the application of AVT with minimal traffic interruptions.

1.6 Plan of Development

The dissertation will be outlined as follows:

Chapter 1- Introduction

This chapter contains the background to the study, objectives of the research, scope and limitations of the research and the significance of the research.

Chapter 2 - Literature review

This chapter provides information on the current methods used in checking forces in the cables. The theoretical principles that underlie the formulations and key considerations are discussed.

Chapter 3 – Methodology

This chapter provides a background on the hanger cable elements and tensioning procedures at the Ashton Bridge. The AVT setup, equipment and data processing are also discussed. The development and validation of analytical model discussion follows. Lastly, the extraction of the natural frequencies from the analytical models, evaluation of force as well as the methods on investigating the effects of sockets on the cable forces and frequencies are discussed.

Chapter 4 – Results and Discussion

This chapter contains the calibration of the bridge's global finite element model (FEM), the natural frequencies and forces of the cables as well the results from an investigation on the effect of cable anchorage systems on the force in a hanger cable.

Chapter 5 - Conclusions and Recommendations

This chapter presents the conclusions based on the observations made on the evaluation of the cable forces and effect of the anchorage systems. Recommendations for similar work on future assessments are also provided.

Chapter 6 - References

The list of all the research and reference work perused during the study is provided in this chapter.

Appendices

This section contains supplementary information that has not been included in the main text but could be of interest to readers to expand on the work undertaken and presented herein.

2 Literature Review

2.1 Introduction

In cable supported structures, cables are the primary load bearing elements and the indicator of structural integrity. The deterioration of a cable during its service life results in the reduction of its force. Consequently, the forces in the other cables in the system are reduced. Therefore, the accurate and regular checking of cable forces is of paramount importance during construction and the service life of a cable supported structure (Cho et al., 2013). Forces in hanger cables are evaluated using direct or indirect methods. The direct methods are broadly categorised into methods in which force determination is conducted through performing lift-off tests, using load cells, sensors and strain gauges that are installed prior to tensioning whereas the indirect methods are vibration testing systems (Morgenthal et al., 2018)

2.2 Direct Methods of Force Measurement

2.2.1 Lift-off Test

The lift-off test is a direct measurement of the force in a cable using the hydraulic jacks that are used to stress the cable. The hydraulic jacks are setup on the already tensioned cable and a quasi-stressing cycle is initiated. As the pressure in the jack is slowly increased, the cable extension is measured. At a critical force, lift-off from the anchor point occurs and the force in the cable is carried by the hydraulic jack. The applied pressure – cable extension relationship is divided into two stages which are the pre-lift off and post lift-off stages. The two stages are plotted using linear regression techniques and their intersection is at a critical applied pressure which is converted to a force that represents the force in the cable (Cho et al., 2013; Morgenthal et al., 2018; van Wijk, 2019). The concepts of using the pre-lift off and post lift-off stage to determine the force in the cable are illustrated in Figure 2-1.

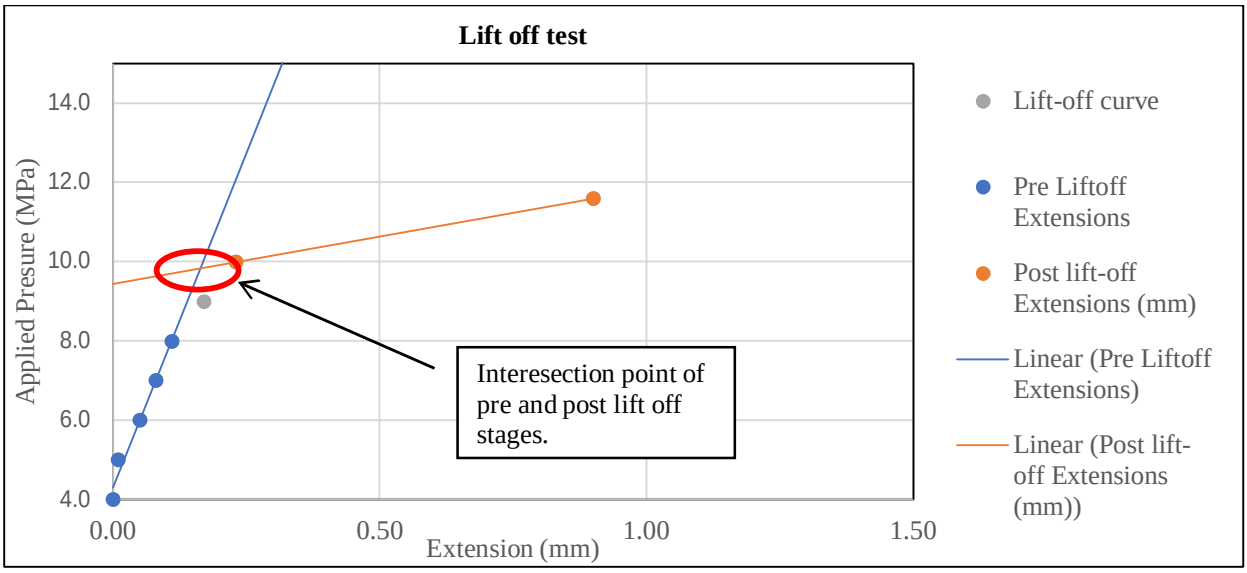

Figure 2-1: Lift-off force determination

The lift-off test method is more practical to use during construction when the equipment and personnel are already stationed on site. For a bridge that is in service, this method becomes costly and time consuming (Morgenthal et al., 2018). Additionally the error associated with the force determined through lift-off tests could be in the order of 10 to 15% if the hydraulic jacks are not calibrated properly (Caetano, 2007).

2.2.2 Load Cells

The force in a cable can be determined in situ through utilising readings from load cells. The readings obtained are used to calibrate the cells to obtain force or alternatively the dimensions and properties of the cable can be used to calculate the force. The load cells are installed on the anchorage point or across the full diameter of an element before tensioning. The drawbacks to these systems is the initial cost and that direct access to the cells is needed to obtain readings. These cells are also subject to various aging phenomena and require active maintenance and inspections (Abramson & Green, 1985; Ren, Liu & Chen, 2008). Figure 2-2 shows some of the load cells that are used when estimating cable forces.

Figure 2-2: Typical Load cells used to measure force (LCM Systems, 2017)

2.2.3 Sensors and Strain Gauges

Strain gauges or pressure sensors can be mounted onto cables prior to tensioning. When the cable is tensioned, strain readings are obtained and the cable force is subsequently determined. The method of measuring strain is simple to apply and can be used for the long-term monitoring of the forces in cables. However, the extensive wiring connections required for the systems can prove to be cumbersome particularly in the case of large cable supported structures. The large diameter hanger cables also do not provide a convenient mounting surface for strain gauges (Zhang, Qiu & Chen, 2021). Similarly to the load cells discussed in section 2.2.2, sensors and strain gauges are

also subject to various aging phenomena and require active maintenance and inspections. Figure 2-3 shows some strain gauges used to obtain strain readings.

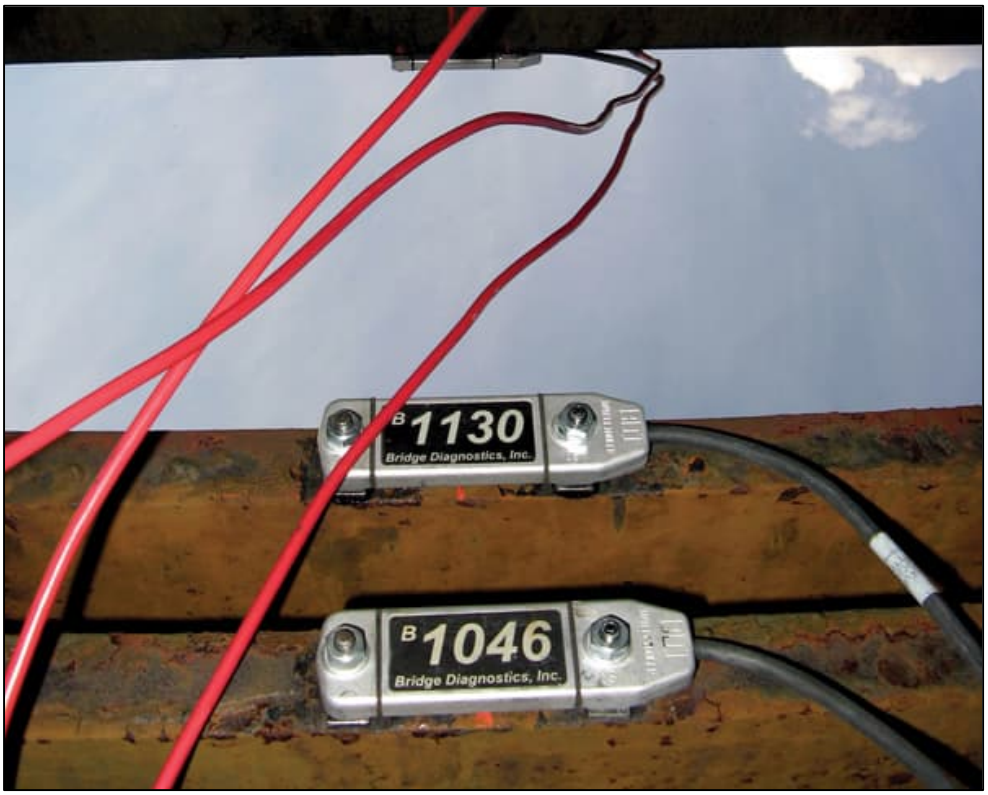

Figure 2-3: Typical strain gauges used to obtain strain readings (BDI, 2020)

2.3 Indirect Methods of Force Measurement

Indirect methods are non-destructive and can be used to estimate the force in a cable by analysing responses of a tensioned cable. The responses used to quantify the force in tensioned cables include strain, acceleration, or ferromagnetic magneto elasticity. The acceleration responses which are also known as the vibration based methods are commonly used in practice and are the subject of this research study (Cho et al., 2013). Therefore, these will be further expanded on from here onwards.

2.3.1 Vibration-based Methods

The vibration in a cable is characterised by modes that each have a natural frequency, damping value and shape. Vibration testing is then the measurement of acceleration time histories associated with these modes (Morgenthal et al., 2018). The acceleration time histories are measured using accelerometers mounted on a cable or non-contact vibrometers aimed at cables from a distance. A data acquisition system is connected to the accelerometers or vibrometers to record the acceleration time histories (Caetano, 2007; Kangas et al., 2010). Frequency Response Functions (FRF) and Average Power Spectrum Density (PSD) functions are then used to extract natural frequencies of the cables from the acceleration time histories (Schwarz & Richardson, 1999; Caetano et al., 2013). The natural frequencies are used in conjunction with the cable properties to estimate the force (Morgenthal et al., 2018). Figure 2-4 shows an accelerometer mounted on a cable.

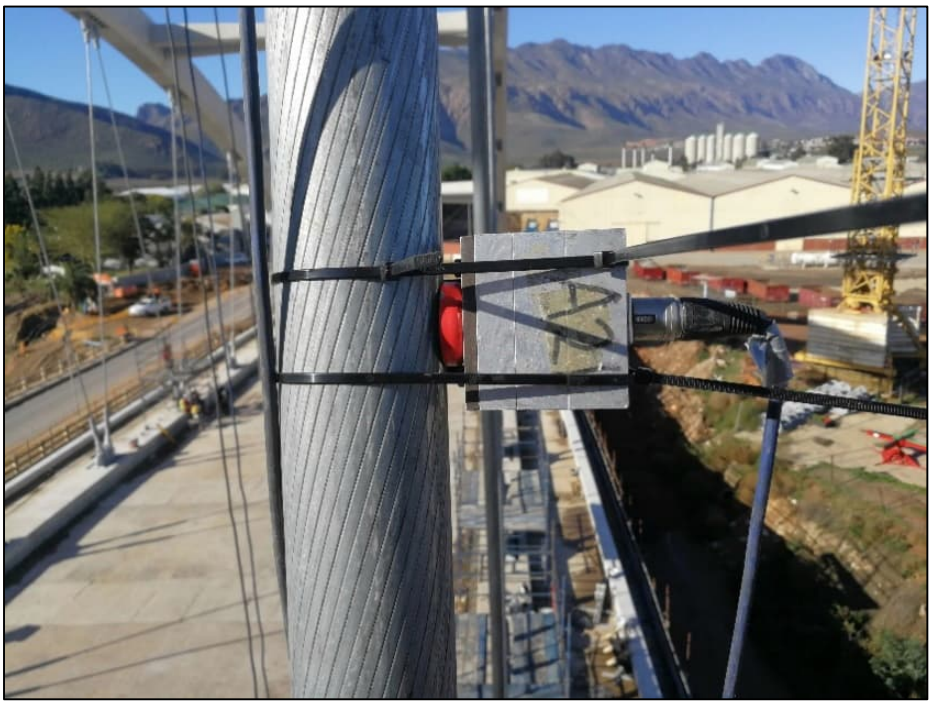

Figure 2-4: Accelerometer mounted on cable

In the case of contact measurements using accelerometers, access to the locations of the cable where the vibration testing can be conducted is required. Therefore, provision for lifting equipment should be made beforehand. Accelerometers should also be mounted at a distance which is at least a quarter of the cable length from the anchorage point to guarantee that the measured response is dominated by the cable vibrations (Caetano et al., 2013).

There are 3 types of excitation techniques used for vibrations tests which are namely forced vibration, free vibration, and ambient vibration. Forced vibration entails using equipment such as hammers to excite an element manually. For free vibration, a structure is excited through a heavy load being instantaneously released on it. In ambient vibration, the natural operating conditions such as the wind are relied upon to excite the structure. The advantage of the ambient vibration excitation technique for a bridge is that the bridge does not have to be closed down to traffic and that it is cheaper due to less equipment needed unlike for the forced and free vibration techniques (Ren & Peng, 2005; Caetano et al., 2013).

Cable properties determine the type of excitation technique used when recording vibration data. For instance, short cables essentially behave as tensioned beams whose natural frequencies' degree of dependence on the bending stiffness is a function of the level of force in the cable. Consequently, higher order frequencies are required to account for the bending stiffness effects accurately. The frequency range required to obtain the higher order frequencies is hardly achievable through ambient excitation. Hence, forced, or free vibration techniques are required in this case. Figure 2-5 shows typical hammers that are used to excite elements in cases where ambient excitation

techniques do not suffice. For longer cables, the bending stiffness effects are small and therefore a number of cable frequencies can be measured within low frequency ranges that are achievable through ambient excitation techniques (Caetano et al., 2013).

Figure 2-5: Typical impact hammer (Brüel & Kjær, n.d.)

Caetano (2007) recommends that the cable response be measured in a frequency range that corresponds to the first 10 natural frequencies of the cable. For a range of 0.2-2 *Hz* for the first mode, this translates to a frequency range of from 0 up to a range of 2 to 20 *Hz*. Key to the time resolutions are the accuracy levels required for a given test and the fundamental frequency of the cable. For example, if an error of 1% is accepted for frequency, then the fundamental frequency (f_1) that characterises the cable should have a maximum frequency resolution of $0.01f_1$. This means that measurements for one record should be $T_1 = \frac{100}{f_1}$ seconds. Equation 2.1 is an expression for the time necessary for measurement of the acceleration time histories of the cables.

$$T = \frac{50 + 50n}{f_1} \qquad 2.1$$

where:

- n is the number of time records
- f_1 is the fundamental frequency (*Hz*)

Equation 2.1 is underpinned by the following assumptions:

i) n time records give the frequency content for the recorded signals and time for reducing noise in the measurement data,

ii) When ambient excitation is used, there is a 50% overlap in time between the cable responding to the excitation and frequency signal recordings.

Given the conditions under which equation 2.1 is applicable, for a cable with a fundamental frequency of 1 *Hz* and an average frequency content based on 6 records, 350 seconds of sampling time will be required to obtain a frequency measurement with a maximum error of 1% (Caetano, 2007).

2.3.2 Inclined Hanger Cable Components

An inclined hanger cable can be schematically represented as shown in Figure 2-6 (Morgenthal et al., 2018):

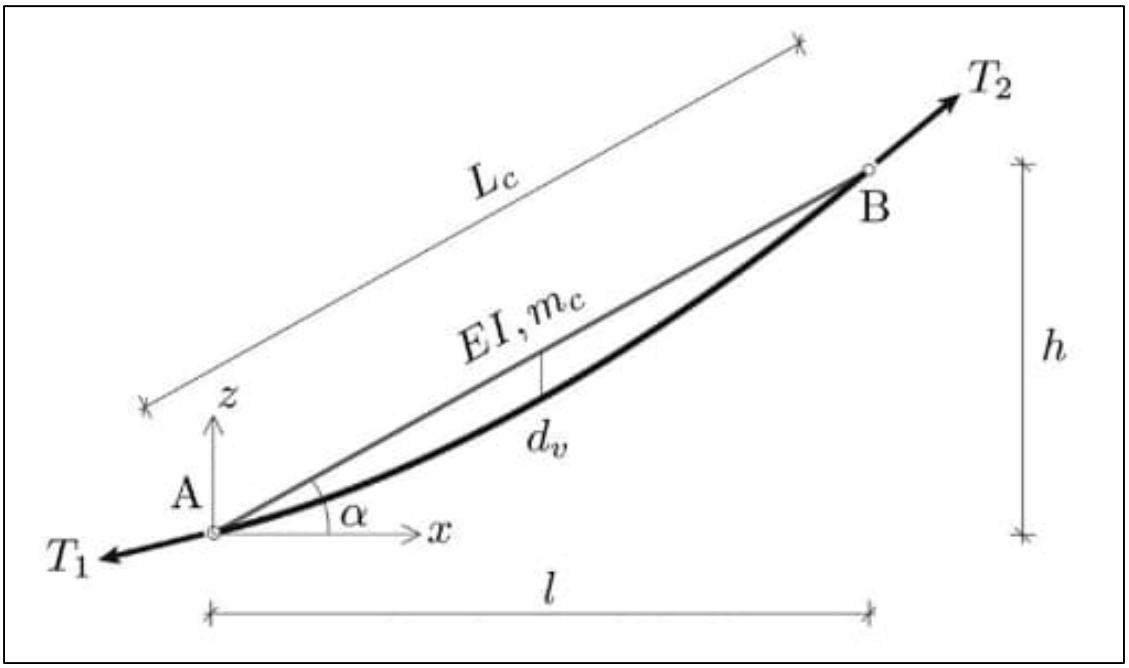

Figure 2-6: A schematic representation of an inclined cable (Morgenthal et al., 2018)

where:

- L_c is the length of the cable between the anchorage points A and B,
- h and l are the vertical and horizontal distances between the anchorages respectively,
- α is the inclination angle,
- EI and m_c are the bending stiffness and mass of the cable parameters respectively,
- d_v is the sag,
- T_1 and T_2 are the forces in the cable that are different because of gravity.

2.3.3 Hanger Cable Idealisation

The basic idealisation of a hanger cable is that of a taut string. In this method, the sag extensibility and the bending stiffness are not accounted for when estimating the force (Kangas, 2009). This is the case because of the assumption of rigid supports, a sag to span ratio less than 1/8 and that the deformation of the cable is largely elastic (Morgenthal et al., 2018). Furthermore, in the linear

theory of cables with a vertical sag, there exists longitudinal (in-plane) and transverse (out-of-plane) vibrations which are independent of each other (Mansour et al., 2018). The uncoupling of these vibrations means that a disturbance in one plane does not affect the motion in another plane. This uncoupling is valid for small levels of vibrations (Caetano, 2007). The natural frequency (f_n) is then related to the tension (T) through the following equation (Kangas, 2009; Morgenthal et al., 2018)

$$f_n = \frac{n}{2L_c}\sqrt{\frac{T}{m_c}} \quad n = 1, 2, 3 \ldots \tag{2.2}$$

Where:

- f_n is the n^{th} harmonic frequency of vibration (*Hz*)
- n is the harmonic number
- L_c is the length of the cable (m)
- T is the force (tension) in the cable (N)
- m_c is the mass per cable unit length (kg/m)

Equation 2.2 represents an accumulation of successive linear harmonics of the cable vibration. The fundamental frequency is the gap between the successive identified harmonics. When the fundamental frequency has been established the tension can be estimated by rearranging equation 2.2 to the following (Kangas et al., 2010):

$$T = m_c \left(\frac{2L_c f_n}{n}\right)^2 \tag{2.3}$$

In-plane vibrations are characterised by symmetric and anti-symmetric mode shapes. These modes are determined from the vertical component of the cable motion because the longitudinal one is small in comparison. The symmetric motion includes a non-zero additional component of cable force whereas for the antisymmetric scenario, the additional component is not included. (Caetano, 2007)

For in-plane vibrations, the cable sag must be considered when determining the fundamental frequency. Furthermore, for symmetric modes equation 2.2 is sufficient in determining the fundamental frequency. However, for antisymmetric mode shapes the stiffness of the cable influences the natural frequency to a considerable degree. The degree to which the axial stiffness influences the sag of the cable determines the mode configuration (symmetric or antisymmetric) which then defines the fundamental frequency. In a simplified approach, the weight component parallel to the cable is assumed to be small for inclined cables. Consequently, the natural frequency obtained through equation 2.2 then applies to both the in-plane and out of plane vibrations. (Morgenthal et al., 2018).

The application of the taut string model requires careful consideration depending on the degree of accuracy required. Errors arising from the cable lengths and lack of consideration of the sag and bending stiffness render the formulation inconvenient when an accurate analysis of the cable static

behaviour is needed for procedures such as cable installation (Caetano, 2007). However, it gives an upper bound criteria to check values and is a basis for more complicated models that incorporate other cable properties (Kangas et al., 2010).

2.3.4 Nonlinear Effects

The dynamic behaviour of hanger cables requires that the fundamental taut string model be refined to cater for harmonics that are largely non-linear with respect to frequency. The sag and bending stiffness of a cables are a source of non-linearity. These properties are a function of the cable system geometry and components. When the cable sag and effective bending stiffness along the cable are considered, this results in a more complete analysis of the cable's dynamic behaviour (Morgenthal et al., 2018). Sag extensibility effects are significant in lower order in-plane vibration modes whereas the bending stiffness effects play an appreciable role in the higher order modes (Kangas, 2009).

2.3.4.1 Cable sag

The geometric nonlinearity effects are accounted for by estimating an effective elastic modulus. One way of estimating the effective elastic modulus is using the Ernst's formula illustrated by equation 2.4 (Chang, Chang & Zhang, 2001; Joaquim, Cismasiu & Caetano, 2017; Zhang, Qiu & Chen, 2021):

$$E_{eff} = E_0 \frac{1}{1 + \frac{\gamma^2 L_{c_h}{}^2 E_0}{12\sigma^3}} \tag{2.4}$$

where:

E_{eff} is the effective Young's Modulus (N/m^2)

E_0 is the Young's Modulus of the cable (N/m^2)

γ is the unit weight of the cable (kg/m^3)

L_{c_h} is the horizontal component of the cable free length (m)

σ is the stress in the cable in (N/m^2)

Alternatively for in-plane vibrations, the effects of the cable geometry and sag are first accounted for by the equation 2.5 before the effective elastic modulus is estimated using equation 2.6 (Irvine & Caughey, 1974; Triantafyllou, 1984; Kangas, 2009):

$$\lambda^2 = \left(\frac{m_c g l_c \cos\alpha}{T}\right)^2 \frac{l_c}{\left(\frac{T l_{c_e}}{EA}\right)} \tag{2.5}$$

where:

m_c is the mass per cable unit length (kg/m)

g is gravity (m/s^2)
l_c is the length of the cable (m)
α is the inclination angle of the cable to the horizontal (^{o})
T is the force (tension) in the cable (N)
l_{c_e} is the effective cable length (m) considering the sag

$$l_{c_e} \cong l_c \left(1 + \frac{1}{8}\left(\frac{m_c g l_c \cos\alpha}{T}\right)^2\right)$$

$$E_{eff} = \frac{E_0}{1 + \frac{\lambda^2}{12}} \qquad 2.6$$

where:

E_{eff} is the effective Young's Modulus (N/m^2)
E_0 is the Young's Modulus of the cable (N/m^2)
λ^2 is the parameter calculated using Equation 2.5

The use of an effective Young's Modulus in the analysis of a cable's behaviour provides a more accurate estimate of the distribution of force and cable deformation. Figure 2-7 shows that for low values of λ^2, the ratio between the effective Young's Modulus and λ^2 is small. However, for the long and sagged cables when λ^2 is more than 1, the correction factor for the Young's Modulus is significant. (Caetano, 2007)

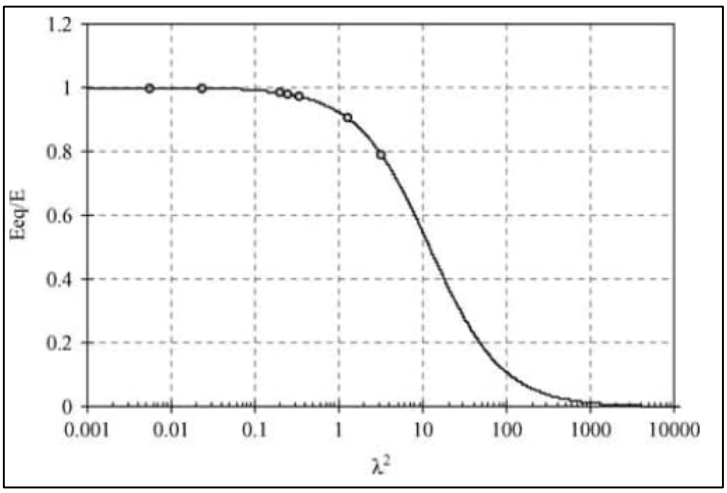

Figure 2-7: Correction factor for Young's Modulus versus λ^2 (Caetano, 2007)

Another relationship worth noting is that of the chord length and stress in a cable versus the correction factor for the Young's Modulus as illustrated in Figure 2-8. For high levels of stress in the cable, the chord or span length has a negligible influence on the correction factor for the

Young's Modulus. However at low span lengths and stress levels, the original Young's Modulus of the cable is significantly reduced. (Caetano, 2007)

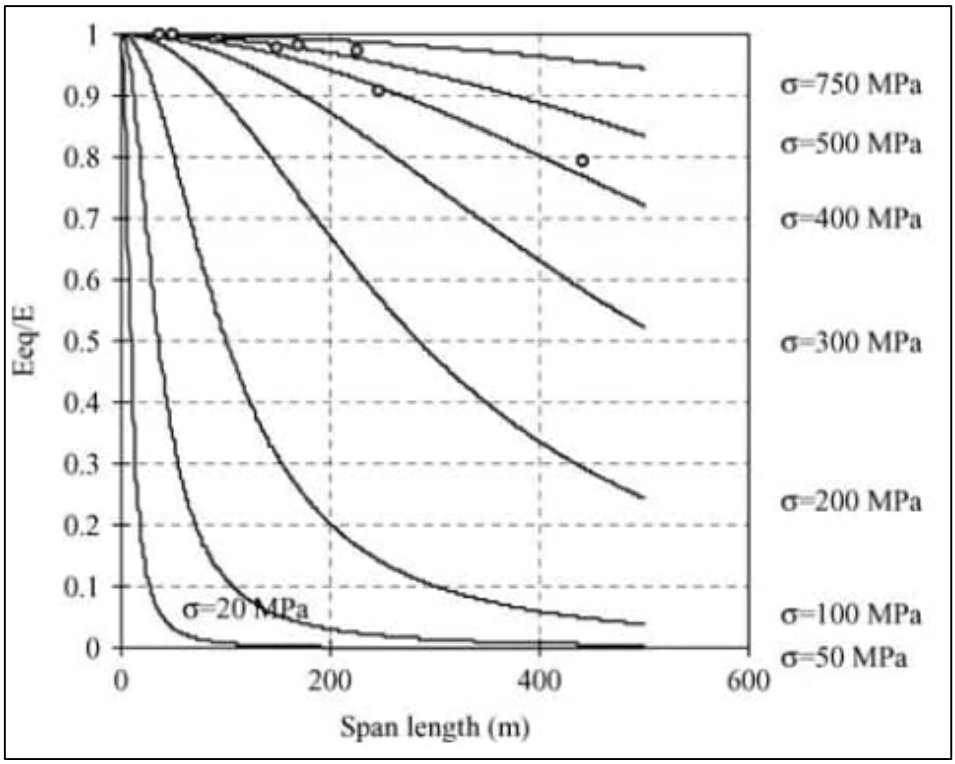

Figure 2-8: Corrrection factor for Young's Modulus versus cable length and stress (Caetano, 2007)

The typical values for λ^2 in stay cables are between 0 and 1 whereas for suspension bridges the values are greater than 100. The parameter λ^2 is an indicator of the form of deformation in stay cables. For instance, in low sagging and highly stressed cables, the small values of λ^2 indicate that the deformation is largely influenced by extensibility. The larger values of λ^2 (greater than 1), encountered when analysing very low tensioned and higher sagging cables, indicate that the cables undergo more of a geometric deformation and are inextensible (Caetano, 2007).

The parameter λ^2 determines the roots to the transcendental equations used to obtain the natural frequencies of the symmetric in-plane modes. When λ^2 is very small, the roots of the transcendental equation reduce to that of a taut string. There are no closed form solutions to these equations. However, by utilising a system of Taylor series expansions, approximate solutions can be found. The magnitude of the parameter λ^2 is largely dictated by the geometry of the cable rather than its elasticity (Irvine & Caughey, 1974; Caetano, 2007; Kangas, 2009).

2.3.4.2 Bending Stiffness

The bending stiffness effects are accounted for by the parameter, ϵ, given by the expression in equation 2.7 (Joaquim, Cismasiu & Caetano, 2017).

$$\epsilon = L_c \sqrt{\frac{T}{EI}} \tag{2.7}$$

where:

- L_c is the length of the cable (m)
- T is the force (tension) in the cable (N)
- EI is the flexural rigidity of the cable (Nm^2)

Caetano (2007) recommends that the most accurate way of estimating the force in a cable when accounting for the bending stiffness is to simultaneously identify T and ϵ using the higher order measured frequencies to enhance the bending effects.

2.3.5 Cable Dynamic Behaviour Formulation

The basis of a cable's dynamic behaviour analysis incorporating the nonlinear effects is a fourth order differential equation that works with the followings assumptions (Zui, Shinke & Namita, 1996):

i) Small sag to span ratio $\left(\frac{d_v}{L_c} \ll 1\right)$,

ii) Cable vibrations are within the x_1-z_1 plane. The x_1-z_1 axis is the rotated x-z plane in Figure 2-6 where z_1 is along the cable's undeformed line. The motion of the cable in the z_1 direction is negligible,

iii) The cable's deformed shape is defined by a parabola.

For in plane motion, the equation becomes:

$$EI\frac{\partial^4 v}{\partial x^4} - T\frac{\partial^2 v}{\partial x^2} - T'\frac{\partial^2 y}{\partial x^2} + m\frac{\partial^2 v}{\partial x^2} = 0 \tag{2.8}$$

where:

- EI is the flexural rigidity of the cable at a point x (Nm^2)
- T is the force (tension) in the cable (N)
- v $= v(x,t)$ is the deflection in the x_1 direction due to vibration at time t (m)
- y is the displacement due to the weight of the cable (m)
- T' $= T'(t)$ is the horizontal component of the additional force (tension) that is induced by vibration (N)
- m $= m(x)$ is the mass per unit length at point x (kg/m)

When the force is small and the sag is high, the parameter T', in equation 2.8, is not negligible for the first order mode of the cable vibrations. However, the effect of that horizontal component of the additional force is small from the 2nd order modes onwards. Thus equation 2.8 is then simplified by ignoring T' to become (Zui, Shinke & Namita, 1996; Caetano et al., 2013):

$$EI\frac{\partial^4 v}{\partial x^4} - T\frac{\partial^2 v}{\partial x^2} + m\frac{\partial^2 v}{\partial x^2} = 0 \qquad 2.9$$

The underlying theory of equation 2.9 is that of an axially tensioned beam that has a constant cross section with an inertia I.

The analytical models used to analyse the behaviour of the cable are categorised as follows:

i) Model 1: A beam with clamped supports where the bending stiffness is not negligible,
ii) Model 2: A simply supported beam where the bending stiffness is negligible,
iii) Model 3: A simply supported beam where the bending stiffness is not negligible.

The analytical models are derived from the circular frequencies, force, mass, length of the cable as well as the bending stiffness relations. If ϵ exceeds 50, it can be assumed that the bending stiffness effects are negligible and therefore Model 2 will be the analytical model for example (Zui, Shinke & Namita, 1996; Caetano et al., 2013).

For out of plane motion, the parameter v in equation 2.8 is adjusted as follows (Irvine, 1981; Caetano, 2007):

$$v = v(x,t) = \tilde{v}(x)e^{i\omega t} \qquad 2.10$$

where:

$i^2 = -1$

ω is the nth frequency of vibration = $\frac{n\pi}{L_c}\sqrt{\frac{T'}{m_c}}$ $n = 1,2,3,\ldots$ with L_c being the length of the cable (m), T' being the horizontal component of the additional force (tension) that is induced by vibration (N) and m_c the mass per cable unit length (kg/m)

$\tilde{v}(x)$ is the corresponding modal shape defined by an arbitrary constant A_n.

$\tilde{v}(x) = A_n.\sin\left(\frac{n\pi x}{L_c}\right)$ $n = 1,2,3,\ldots$

Alternatively, there is a less sophisticated expression that converts the non-linear frequencies of the hanger cables to equivalent taut string frequencies from which tension can be estimated using equation 2.2. The expression, which considers bending stiffness effects, is as follows (Kangas et al., 2010):

$$\frac{{f_n}^{EI}}{{f_n}^{S}} = 1 + \frac{2}{\epsilon} + \frac{4 + \frac{n^2\pi^2}{2}}{\epsilon^2} \qquad 2.11$$

where:

f_n^{EI} is the measured out of plane harmonic frequency (*Hz*)
f_n^{S} is the equivalent taut string model frequency for the n^{th} harmonic (*Hz*)
n is the mode number
ϵ is the dimensionless bending stiffness parameter

The measured non-linear harmonic frequencies are used to perform a regression analysis to estimate the fundamental frequency of the taut string model (f_n^{S}) and the dimensionless parameter (ϵ) simultaneously. The force in the hanger cable is then estimated using equation 2.2. Equation 2.11 provides a straightforward estimation of the cable force but it does not include sag extensibility effects (λ^2).

The frequencies measured from site can also be converted to taut string model frequencies using the following expression (Mehrabi & Tabatabai, 1998; Kangas, 2009):

$$\frac{f_n^{EI}}{f_n^{S}} = \varphi\beta_n - 0.24\frac{\mu}{\epsilon} \qquad 2.12$$

where:

f_n^{EI} is the measured n^{th} harmonic frequency (*Hz*)
f_n^{S} is the equivalent taut string model frequency for the n^{th} harmonic (*Hz*)
n is the mode number
$\beta_n = 1 + \frac{2}{\epsilon} + \frac{4 + \frac{n^2\pi^2}{2}}{\epsilon^2}$
$\varphi = 1 + 0.039\mu$
$\mu = \lambda^2$ for n =1 (in-plane vibrations)
$\mu = 0$ for n > 1 (in-plane vibrations) and all n (out-of-plane)

The taut sting model is then used to calculate the force in a cable using the converted frequency. Equation 2.12 presents a comprehensive practical formula that includes both the sag extensibility and bending stiffness effects. However the simplified relationship assumes fixed supports and gives results with the best accuracy when $\lambda^2 < 3.1$ and $\epsilon > 50$ (Mehrabi & Tabatabai, 1998; Kangas, 2009).

2.3.6 Finite Element (FE) Analysis

FE analysis combines all the major parameters such as the sag extensibility, boundary conditions, bending stiffness, varying cross sections and force when analysing the vibrations of a cable. This is important because the idealisation of a cable as taut string does not consider the sag and bending stiffness effects which can lead to large errors in estimating the force in a hanger cable (Mehrabi & Tabatabai, 1998). Through FE analysis, the structure is approximated by several elements that

are connected by nodes. A matrix formulation is then used to quantify the structure's response to loading (Morgenthal et al., 2018).

The basis of the FE analysis expression is derived from a horizontal cable with supports on the same level as shown in Figure 2-9. It is assumed that the cable is fixed against translation and that the in-plane, out of plane and axial vibrations are uncoupled. Furthermore, the sag to span ratio is less than 1:8 (Mehrabi & Tabatabai, 1998; Kangas, 2009).

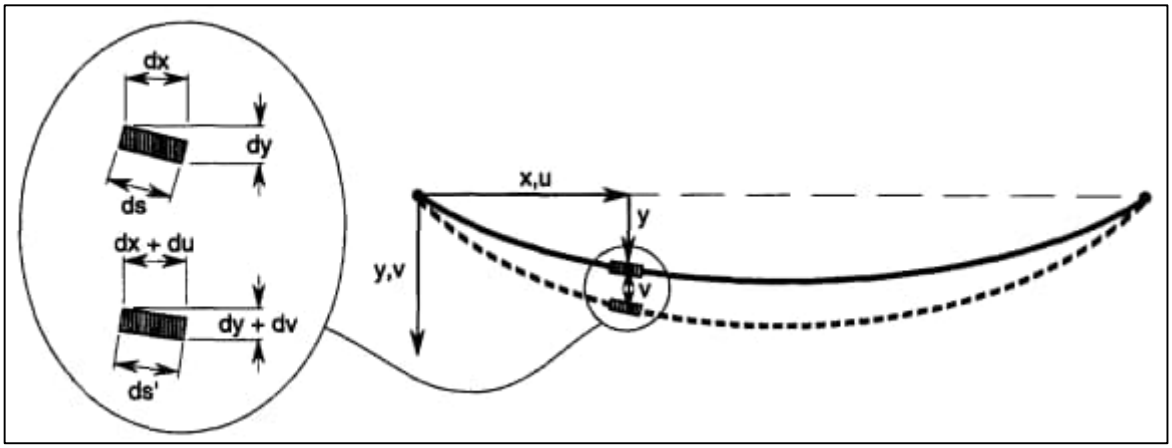

Figure 2-9 : Flat horizontal cable representation (Mehrabi & Tabatabai, 1998)

Equation 2.8 is then extended to include spring and damping effects to give the following expression (Mehrabi & Tabatabai, 1998):

$$EI\frac{\partial^4 v}{\partial x^4} - T\frac{\partial^2 v}{\partial x^2} - T'\frac{\partial^2 y}{\partial x^2} + m\frac{\partial^2 v}{\partial x^2} + k'v + c'v = 0 \qquad 2.13$$

where:

k' $= k'(x)$ is the spring constant per unit length at x

c' $= c'(x)$ is the damping factor at x

A separation of variables needs to be applied to convert equation 2.13 into an eigenvalue problem that will yield frequencies. This separation breaks the deflection into time dependent and time independent components, and separates the damped and free vibration. The separation of the variables is illustrated in equations 2.14, 2.15 and 2.16 (Mehrabi & Tabatabai, 1998; Kangas, 2009):

$$v(x,t) = w(x)q(t) \qquad 2.14$$

where:

$w(x)$ is a time independent function

$q(t)$ is a time dependent function

$q(t)$ takes the form of equation 2.15 to represent the damped, free vibration of a cable.

$$q(t) = e^{pt} \tag{2.15}$$

p is a complex number in the form of

$$p = -\zeta\omega \pm i\omega_D \tag{2.16}$$

where:

ζ is the damping ratio
ω is the undamped natural frequency (*Hz*)
ω_D $= \omega\sqrt{1-\zeta^2}$

Applying equations 2.14, 2.15 and 2.16 to equation 2.13 describes the motion of a vibrating cable and gives the more comprehensive equation of the following form (Mehrabi & Tabatabai, 1998):

$$EI\frac{\partial^4 v}{\partial x^4} - T\frac{\partial^2 v}{\partial x^2} - T'\frac{\partial^2 v}{\partial x^2} + mp^2wq + k'wq + c'wq = 0 \tag{2.17}$$

In order to solve the eigenvalue problem presented by equation 2.17, the cable is discretized into elements that are connected with internal nodes as shown in Figure 2-10.

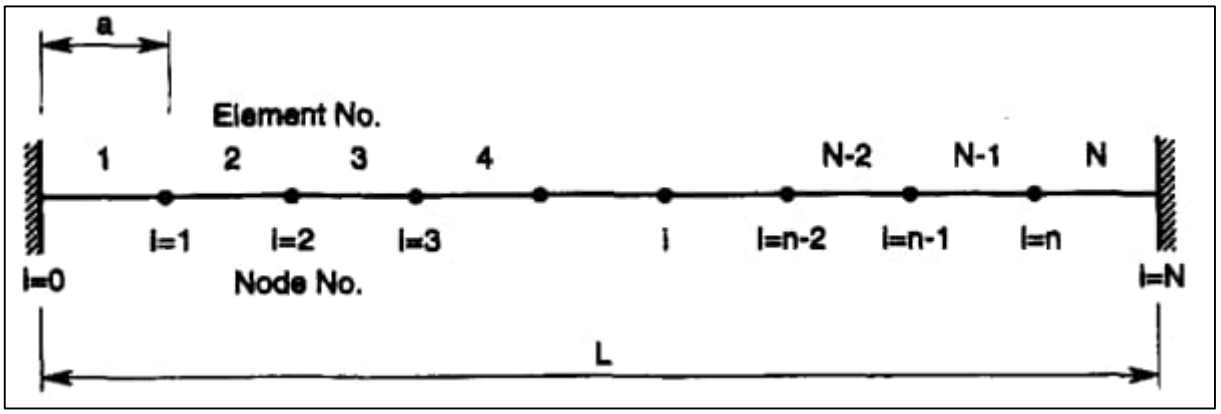

Figure 2-10: Discretization of cable (Mehrabi & Tabatabai, 1998)

The discretization process shown in Figure 2-10 results in the following matrix equation (Kangas, 2009):

$$\boldsymbol{M}\ddot{\boldsymbol{q}}(t) + \boldsymbol{C}\dot{\boldsymbol{q}}(t) + \boldsymbol{K}\boldsymbol{q}(t) = \boldsymbol{u}(t) \tag{2.18}$$

where

$\boldsymbol{M}$ is the mass matric. $\boldsymbol{M} \in \mathbb{R}^{N\times N}$
$\boldsymbol{C}$ is the damping matrix. $\boldsymbol{C} \in \mathbb{R}^{N\times N}$

$\boldsymbol{K}$ is the stiffness matrix. $\boldsymbol{K} \in \mathbb{R}^{N\times N}$
$\boldsymbol{q}(t)$ is the displacement vector at time t. $\boldsymbol{q}(t) \in \mathbb{R}^{N\times 1}$
$\dot{\boldsymbol{q}}(t)$ is the velocity vector
$\ddot{\boldsymbol{q}}(t)$ is the acceleration vector

The effects of the bending and axial stiffness as well as springs are accounted for by $\boldsymbol{K}$. If there are dampers attached along the cable, these are accounted for by the diagonal matrix $\boldsymbol{C}$. The cable's mass per unit length is entered in the diagonal matrix $\boldsymbol{M}$ (Mehrabi & Tabatabai, 1998; Kangas, 2009). Extending equation 2.17 to apply to inclined cables shown in Figure 2-6 requires that an assumption of a parabolic catenary of the cable be made (Zui, Shinke & Namita, 1996). The additional force due to vibration, T', is then transformed as follows:

$$T' = \frac{m_c g}{T}\frac{EA}{L_e}\int_0^{L_c} v dx \qquad 2.19$$

The final equation describing the motion of an inclined cable is obtained by combining equations 2.5, 2.17 and 2.19 to form the following (Kangas, 2009):

$$EI\frac{\partial^4 v}{\partial x^4} - T\frac{\partial^2 v}{\partial x^2} - m{\omega_n}^2 w + \frac{\lambda^2 T}{{L_c}^3}\int_0^{L_c} w dx = 0 \qquad 2.20$$

Equation 2.20 is applicable within the following limits (Starossek, 1991):

- $\lambda^2 \leq 24$; $\alpha \leq 60°$; $\frac{d_v}{l_c} \leq \frac{1}{80}$

  or
- $\lambda^2 \leq 24$; $\alpha \leq 30°$; $\frac{d_v}{l_c} \leq \frac{1}{33}$

Discretizing equation 2.20 gives the following matrix form (Kangas, 2009):

$$\boldsymbol{K'w} + \frac{\lambda^2 Ta}{L^3}\boldsymbol{Bw} - m{\omega_n}^2\boldsymbol{Iw} = \boldsymbol{0} \qquad 2.21$$

where:

a $= \frac{L}{n}$ is the length of each element
$\boldsymbol{B}$ is a full unit matrix
$\boldsymbol{I}$ is an identity matrix
$\boldsymbol{K'}$ is the matrix accounting for the bending stiffness and force
$\boldsymbol{w}$ is an eigenvector

Equation 2.21 can be further simplified by adding a dimensionless parameter $\boldsymbol{\Omega_n}$ for the frequency ratio which is defined as:

$$\boldsymbol{\Omega_n} = \pi\frac{\omega_n}{\omega_{1s}} \qquad 2.22$$

where:

$\omega_{1s} = \frac{\pi}{L_c}\sqrt{\frac{T}{m_c}}$ is the first harmonic frequency (*Hz*)

The final eigenvalue problem is obtained by substituting equation 2.22 into equation 2.21 to yield the following:

$$\left[N^2\frac{a^2}{T}\mathbf{K}' + \frac{\lambda^2}{N}\mathbf{B}\right]\mathbf{w} = \mathbf{\Omega_n}^2\mathbf{I}\mathbf{w} \qquad 2.23$$

Using Equation 2.23, the cable mode shapes (**w**) and the frequency ratio ($\mathbf{\Omega_n}$) can be obtained. Subsequentially, from the frequency ratio, the frequencies of the cable, $\mathbf{\omega_n}$, can be calculated for values of n = 1 to N (divisions of the mesh size).

2.3.7 Approximate Formulae for Cables with a Small Sag

In small sag to span cables $\left(\frac{d_v}{L_c} \ll 1\right)$, iteration methods such as the Newton-Raphson Method can be used to transform measured frequencies into equivalent taut string and beam frequencies. The cable is assumed to be clamped at both ends and the solutions are for the 1st and 2nd order modes. When $\epsilon > 50$, a non-dimensional parameter η_n representing the ratio between the measured frequency and the equivalent taut string frequency is introduced as shown by equation 2.24 (Zui, Shinke & Namita, 1996)

$$\eta_n = \frac{f}{{f_n}^s} \qquad 2.24$$

where:

f is the measured frequency (*Hz*)

${f_n}^s$ is the equivalent taut string model frequency for the n^{th} harmonic (*Hz*)

When $\epsilon < 50$, η_n rises rapidly and obtaining an exact solution becomes a nontrivial exercise. In this case, the behaviour of the cable becomes akin to that of a beam and the new non dimensional parameter becomes (Zui, Shinke & Namita, 1996):

$$\varphi_n = \frac{f}{{f_n}^B} \qquad 2.25$$

where:

${f_n}^B$ is the theoretical natural frequency (*Hz*) of a beam clamped at both ends

${f_n}^B = \frac{{\alpha_n}^2}{2\pi {L_c}^2}\sqrt{\frac{EI}{m_c}}$; $\alpha_1 = 4.730$; $\alpha_2 = 7.853$

Table 2-1 shows the application of the approximate formula for cables with a small sag for different ranges of $\boldsymbol{\epsilon}$.

Table 2-1: Approximate formulae for small sag-to span cables (Caetano, 2007)

$\boldsymbol{\epsilon}$	$\boldsymbol{\eta_n}$	$\boldsymbol{\varphi_n}$
$0 \leq \epsilon \leq 6$		$\varphi_1 = \sqrt{1 + \frac{\epsilon^2}{42}};\ \varphi_2 = \sqrt{1 + \frac{\epsilon^2}{85}}$
$6 \leq \epsilon \leq 8$	$\eta_1 = 1.075\sqrt{1 + \left(\frac{6.8}{\epsilon}\right)^2}$	$\varphi_1 = \sqrt{1 + \frac{\epsilon^2}{42}};\ \varphi_2 = \sqrt{1 + \frac{\epsilon^2}{85}}$
$8 \leq \epsilon \leq 17$	$\eta_1 = 1.075\sqrt{1 + \left(\frac{6.8}{\epsilon}\right)^2}$	$\varphi_2 = \sqrt{1 + \frac{\epsilon^2}{85}}$
$17 \leq \epsilon \leq 18$	$\eta_1 = \frac{\epsilon}{\epsilon - 2.2};\ \eta_2 = 0.985\frac{\epsilon}{\epsilon - 3.1}$	$\varphi_2 = \sqrt{1 + \frac{\epsilon^2}{85}}$
$18 \leq \epsilon \leq 60$	$\eta_1 = \frac{\epsilon}{\epsilon - 2.2};\ \eta_2 = 0.985\frac{\epsilon}{\epsilon - 3.1}$	
$60 \leq \epsilon \leq 200$	$\eta_1 = \frac{\epsilon}{\epsilon - 2.2};\ \eta_2 = \frac{\epsilon}{\epsilon - 2.2}$	
$\epsilon \geq 200$	$\eta_n = \frac{\epsilon}{\epsilon - 2.2}$	

2.3.8 Developing Analytical Models

The definition of cable parameters such as the free length, bending stiffness and mass determines the accuracy of the force estimate. The mass of the cable is available from the manufacturers and is fairly accurate. The bending stiffness parameter $\boldsymbol{\epsilon}$ depends on type of cable properties such as the length, curvature and cross section and is approximated through non-linear regression algorithms (Kangas, 2009). The cable free length remains a challenge to determine. The analytical models based on the tensioned beams repeated here in Table 2-2 have been extended to apply to situations covering a wide range of cable behaviour. However, these tensioned beams based analytical methods have associated errors due to the frequency, cable length and mass. The cumulative effect of the errors is expressed by equation 2.26 (Caetano, 2007; Caetano et al., 2013).

$$\varepsilon_H = 2\varepsilon_{f1} + 2\varepsilon_l + \varepsilon_m \qquad 2.26$$

where:

ε_{f1} is the error associated with frequency

ε_l is the error associated with length

ε_m is the error associated with mass

Table 2-2: Analytical models (Caetano et al., 2013)

Formulation	Boundary condition
Model 1	Clamped beam where bending stiffness is not negligible
Model 2	Simply supported beam with negligible bending stiffness
Model 3	Simply supported beam where bending stiffness is not negligible

In cases where special anchorage systems are used, there are still uncertainties about the degree of constraint that the anchorages provide, the bending stiffness and ultimately the effective length of the cable. The anchorage systems boundary condition does not explicitly fit into the clamped or simply supported categories. This necessitates numerical modelling of the cables with varying parameters until the data measured on site is matched. The numerical modelling approach of each cable element was used in the assessment of cable forces at the London Stadium in England (Caetano et al., 2013).

The numerical modelling of cable elements is done through testing various idealisations of cables for the same installation force. The cable element is modelled using its known properties of Diameter, Length, Mass, and Elastic Modulus. The anchorages are modelled with an increased cross-sectional area as well as Area Moment of Inertia to simulate their mass and stiffness properties. The idealisation of the cable and its varying boundary conditions is shown in Figure 2-11. The ratios between the measured natural frequencies and the calculated ones for each model are the correction factors applied to reduce cables to equivalent vibration chord theory cables represented by a taut string (Caetano et al., 2013).

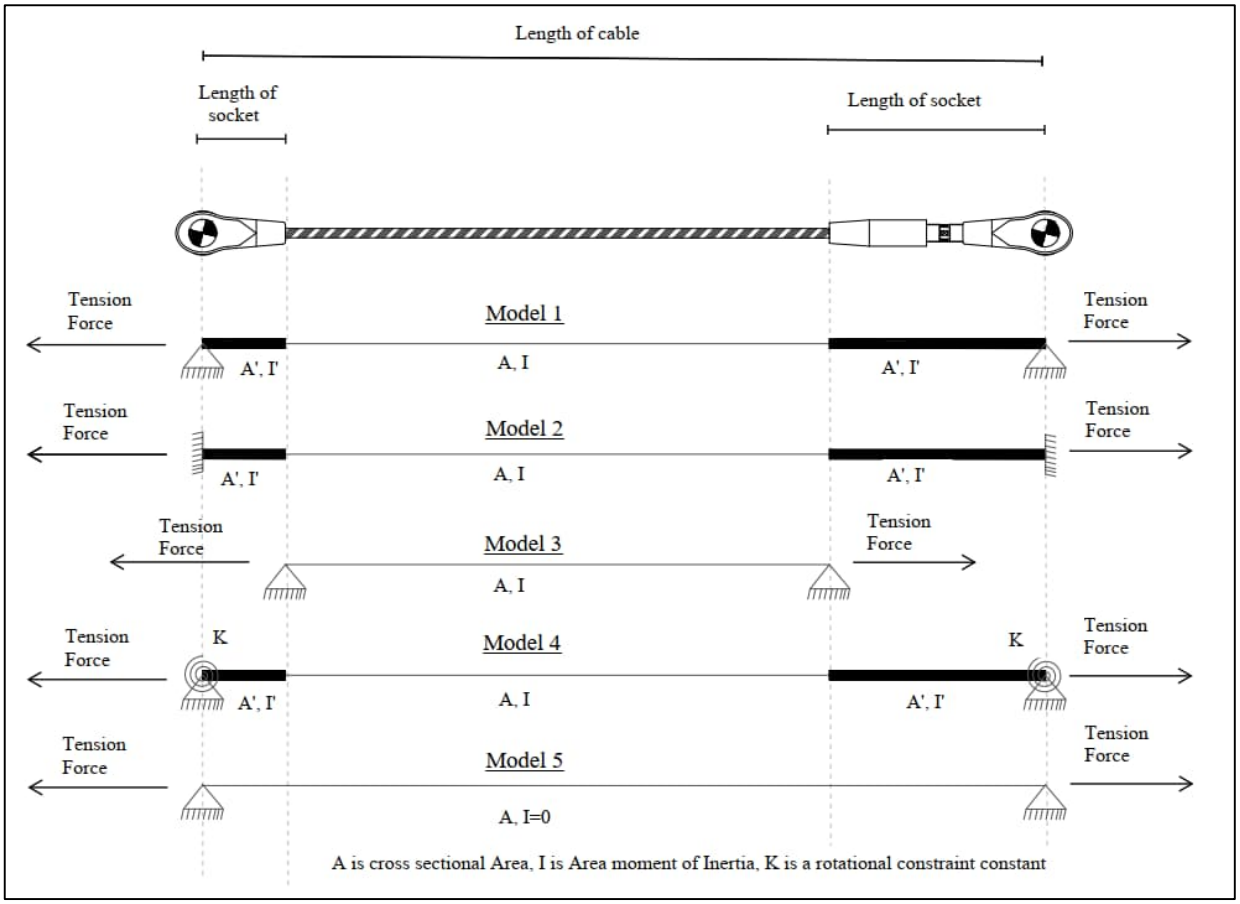

Figure 2-11: Cable idealisations (Caetano et al., 2013)

2.3.9 Form finding

Structures that transfer loads purely through axial or in-plane action adopt unique shapes under tension. These shapes are not known beforehand, and it is not trivial to formulate them using simple mathematical functions unlike in structures made of concrete, steel or masonry. The stress conditions are also not known initially. Consequently, a process known as form finding needs to be initiated to approximate the static state of equilibrium (Lewis, 2003; Veenendaal & Block, 2012). Form finding is the optimisation of the shape of a deformed element to approximate a state of equilibrium in a given stress state (Bletzinger & Ramm, 1999; Veenendaal & Block, 2012).

The types of form finding methods can be separated between the use of physical and computational models. Physical models involve the construction of prototypes of structures and can be used to verify the computational models. The main disadvantages of physical models are the cost and they require meticulous attention when refinements need to be made. Computational models involve the numerical and graphical representation of the deflections, stresses, and deformations of structures under given loads. An initial shape of the structure is assumed then through iteration, geometric adjustments are made until static equilibrium is achieved (Lewis, 2003).

2.3.10 Optimisation Exercise

The FE analysis summarised by equation 2.13 presents a formulation that considers the sag and bending stiffness. However, there remains a degree of uncertainty in the definition of the cable free length and the bending stiffness. This uncertainty results in accuracy levels that may not be acceptable (Joaquim, Cismasiu & Caetano, 2017).

The error in the cable free length can be minimised by taking measurements on several points along a cable and then performing a modal identification of the higher modes followed by measuring the length between the higher order modes close to the anchorage point (Geier, De Roeck & Petz, 2005). This method is often not used in practice because it is cumbersome. An effective Young's Modulus (E_{eff}) can be calculated to account for geometric nonlinear effects of the cable. However, the other component of the bending stiffness (EI), the cable moment of inertia (I), requires a careful consideration of the interaction of the cable strands (I_{min}) and the behaviour of the cable as a monolithic section (I_{max}). Equations 2.27 and 2.28 give the ranges of the cable moment of inertia.

$$I_{min} = \sum_{n=1}^{i} I_i \qquad 2.27$$

$$I_{max} = \sum_{n=1}^{i} \left(I_i + A_i {d_i}^2\right) \qquad 2.28$$

Where:

- I_i is the moment of inertia (m^4)
- A_i is the cross-sectional area (m^2)
- d_i is the relative position of an individual strand of the cable

Estimating a reasonable value for the cable moment of inertia in this way is challenging due to the number of possible values which in turn makes obtaining the overall bending stiffness value not trivial (Joaquim, Cismasiu & Caetano, 2017).

A multi-variable optimisation exercise is used to reduce the errors associated with the definition of the cable free length and the bending stiffness. The optimisation ultimately seeks to reduce the difference between the theoretical natural frequency and the measured natural frequency by evaluating the force, cable length and bending stiffness simultaneously. A sensitivity analysis is conducted to evaluate the degree to which the force, cable length and the bending stiffness affects the natural frequency. The goal of the sensitivity analysis is to establish objective functions and then define the optimisation problems. Joaquim et al., (2017) performed a sensitivity study on cables at the Salgueiro Maia Bridge in Portugal and established an unscaled objective function defined by equation 2.29 that was more sensitive to the bending stiffness of the cable and a scaled function that produced more balanced results through equation 2.30

$$\Delta_1^2 = \sum_{i=1}^{n} \left(f_{i,exp} - f_i\right)^2 \quad 2.29$$

$$\Delta_2^2 = \sum_{i=1}^{n} \left(\frac{f_{i,exp} - f_i}{f_{i,exp}}\right)^2 \quad 2.30$$

Where:

$f_{i,exp}$ represents the measured natural frequencies (*Hz*)
f_i represents the taut string model frequency in (*Hz*)
i is the mode number

Subsequentially, the optimisation problem was to minimise Δ_1^2 or Δ_2^2 such that the following conditions were met:

i) $T_{min} \leq T \leq T_{max}$
ii) $L_{min} \leq L \leq L_{max}$
iii) $I_{min} \leq I \leq I_{max}$

The cables length (L) ranges from the length between the end of anchorage points and to the cable free length. The cable moment of inertia (I) ranges from values calculated considering the individual strands to the values calculated considering the cable as a monolithic section. The design force is taken as the starting force (T) value. The optimisation problem is then iterated to minimise the difference between the measured natural frequency and the theoretical one by adjusting the force, cable moment of inertia and cable length values (Joaquim, Cismasiu & Caetano, 2017).

2.4 Key considerations

The natural frequencies in a cable are affected by other elements in a structure as well as the prevailing environmental conditions. The main secondary effects are discussed in detail in the following sections.

2.4.1 Isolation of Cable Frequencies

The theoretical natural frequencies and modes shapes of a bridge are obtained through the FEM constructed using idealised geometric and structural properties. The FEM has inherent inaccuracies of varying degrees due to modelling and parametric uncertainties. Thus, it is continuously updated with focus on the mass and stiffness components of the structure when the goal is to analyse the dynamic response (Chang, Chang & Zhang, 2001; Sipple & Sanayei, 2014).

The calibration of the FEM is done through reducing the difference between experimentally determined dynamic properties with the theoretical ones by adjusting parameters such as the stiffness of boundary conditions and the self-weight of elements. The modal properties obtained from the bridge's complete dynamic behaviour analysis are then used to isolate the cable's natural

frequency especially in situations where the fundamental frequency is not easily distinguishable from the measured data (Brownjohn, Dumanoglu & Severn, 1992).

2.4.2 Effect of Temperature on the Cable Forces

The variations in the ambient temperature also result in the variations in the cables forces with time. This is so because when the temperature changes, the cable either elongates or contracts and this change in length is either restricted or not restricted depending on the boundary conditions. In the case where the elongation is restricted, the cables experience stresses that in turn alter the force in the cable. Figure 2-12 shows a situation whereby the cable elongation due to the increase in temperature is not restricted. In contrast, Figure 2-13 illustrates the scenario whereby the cable elongation is restricted on both ends which leads to the development of a stress in the cable. The cable in Figure 2-13 experiences a compressive stress when temperatures rise and when temperatures decrease, tensile stress is experienced.

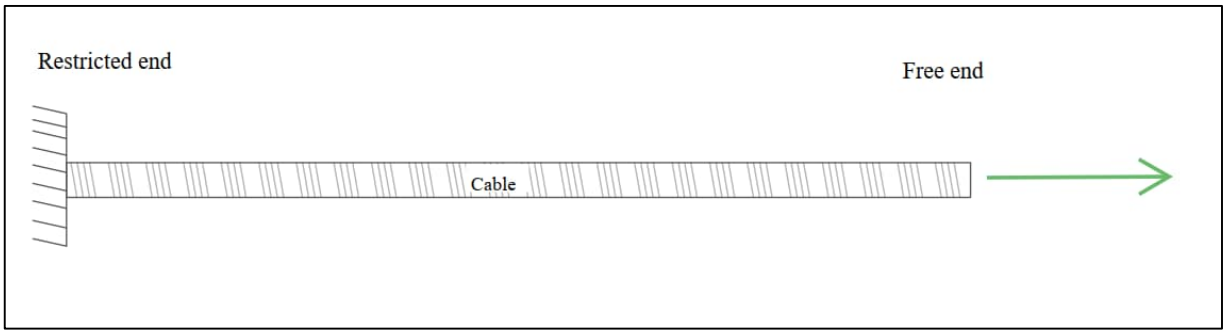

Figure 2-12: Elongation of a cable with a free end

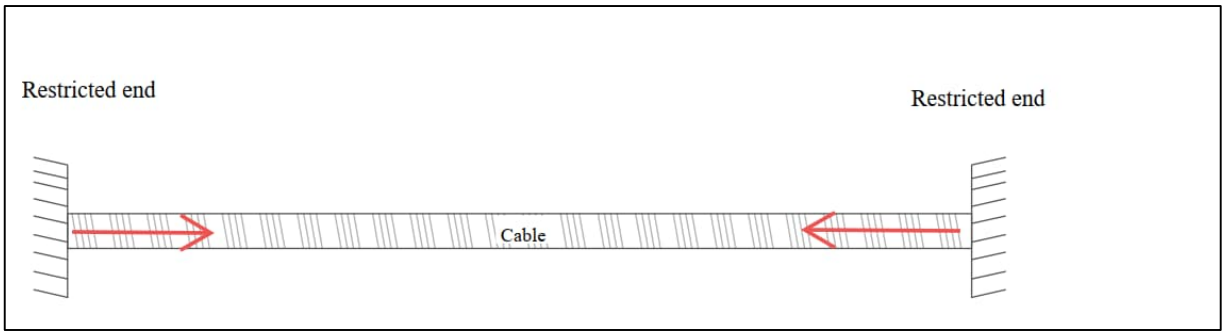

Figure 2-13: Cable with restricted ends

The change in cable force due to the temperature effects is given by (Suangga et al., 2019)

$$\Delta \boldsymbol{F_{cable}} = \boldsymbol{EA\varphi\Delta T} \qquad 2.31$$

Where:

- E is the elastic modulus of the cable material (N/m^2)
- A is the cross-sectional area of the cable (m^2)
- φ is the coefficient of thermal expansion (CTE) per ℃

ΔT is the change in temperature (℃)

The expansion and contraction of other elements in a structure due to temperature changes is also transferred to the cables. For instance, in cable stayed bridges where the cables are connected to the girder on one side and the pylon on the other, deflections of the pylon and girder due to temperature changes will translate to an elongation or contraction of the cable and ultimately affect its force. The variation in force due to elongation or contraction of the cable induced by other structural elements is given by (Suangga et al., 2019)

$$\Delta F_{due\ to\ structural\ deformation} = EA\ \frac{\Delta L}{L_i} \tag{2.32}$$

Where:

E is the elastic modulus of the cable material (N/m^2)
A is the cross-sectional area of the cable (m^2)
ΔL is the change in the length of the cable (m) due to deformation of other elements
L_i is the initial length of the cable (m)

The total change in the cable effects is thus quantified as follows:

$$\Delta F_{total} = \Delta F_{cable} + \Delta F_{due\ to\ structural\ deformation} \tag{2.33}$$

Equation 2.32 represents a simplification of the actual temperature effects on the structure. When structural elements undergo temperature variations, both the mechanical and geometric properties are altered. The alteration of the geometric properties leads to the change in the boundary conditions. The quantification of the temperature effects is thus of a complex nature and is simplified by assuming that for temperature variations, the mechanical and geometric properties change but the mass and the boundary conditions remain constant (Xia et al., 2006; Zhou, Sun & Sun, 2013).

2.5 Summary of literature review

The direct methods of cable force estimation are mostly suited for application during construction. The setting up of equipment takes time and a greater labour force than in the case of indirect methods. Moreover, during construction there is enough working area due to the site being totally closed off to the public. The application of these methods becomes more expensive and time consuming when they are applied to in service bridge because alternative means of passage must be provided to the public and contractors must establish teams and equipment on site. The turnaround time between results availability for post processing is also another reason these methods cannot be relied on when assessing an in-service bridge.

AVT is the preferred indirect method of determining the cable forces due to its ease of application and non-destructive nature. The underlying theory of vibration testing is the taut string theory. The simplifications of the taut string theory result in large errors if applied to hanger cables because the method does not account for the bending stiffness and sag. FEM and Approximate formulae are some of the methods that include the effects of the bending stiffness and sag when calculating the force.

The accuracy of the force estimated through AVT depends on the careful definition of the cable properties such as the free length, mass and bending stiffness. Moreover, in cases where special anchorage systems are used, there is a degree of uncertainty regarding the constraints imposed on the cable system. This necessitates the development of analytical models in which mass and stiffness effects of the anchorage systems are accurately simulated. Alternatively, approximate formulae and FEM differential equations can be used to develop objective functions that minimise the errors between the theoretical natural frequencies and the measured natural frequencies by simultaneously varying the force, bending stiffness and cable free length.

A cable's natural frequency is affected by the bridge's global dynamic behaviour. Hence, it is important to conduct a full-scale dynamic analysis to calibrate the bridge's FEM in order to use it to isolate the cable natural frequencies in situations where the fundamental frequencies are not clear from the measured data. Additionally, the effects of temperature on the cables as well as the entire structure need to be accounted for when determining the forces in the cable.

The natural frequency in the local cable model is determined after form finding. In this process, the forces and boundary conditions of the cable system are first considered through the FE analysis process when making geometric adjustments to achieve static equilibrium. The frequency is then obtained computationally and iterated until it matches the field data before the force in the cable can be extracted.

3 Methodology

3.1 Introduction

This chapter focuses on the Ashton bridge hanger cables as the case study of the dissertation. It begins with an overview of the Ashton Bridge then the AVT, the development and validation of the Analytical Models are discussed. The extraction of natural frequencies from analytical models, evaluation of forces and the methodology followed when investigating the effects of sockets are then discussed. A summary of all the methods followed in this study is then provided.

3.2 Case Study: Ashton Bridge

The subject of this research is the Ashton Bridge along route 62 in South Africa's Western Cape Province town, Ashton. The bridge was first constructed next to its final position on temporary support work. When it was complete, it was used as a bypass while the old bridge was being demolished. When the demolition of the old bridge was completed, permanent abutments were constructed. The final stage of construction was the transverse launching of the new bridge to its final position. The author worked as a resident engineer and as part of the design team in the latter stages of the project. The following sub chapters describe the geometry and characteristics of the cables, the tensioning operations as well as the force redistribution in the cables that provided the predicted forces that were compared to the ones estimated using AVT.

3.2.1 Cable Elements

The Ashton Bridge contains 48 fully locked coil hanger cables that are connected to the arch ribs and tie beams by steel fork sockets via a pin connection. They were manufactured and tested for compliance by Teufelberger Radaelli in Italy. The hanger cable system is made up of 3 components which are the fork socket, cable section and the adjustable fork socket. These components are shown in Figure 3-1. The inclined hanger cables have a gross diameter of 76mm, lengths ranging from 4.638 m to 19.670m (pin to pin) and the angles of inclination range from 68° to 80°. Figure 3-2 shows the cross section and z-layers layout around the strands of the cables used at the Ashton Bridge.

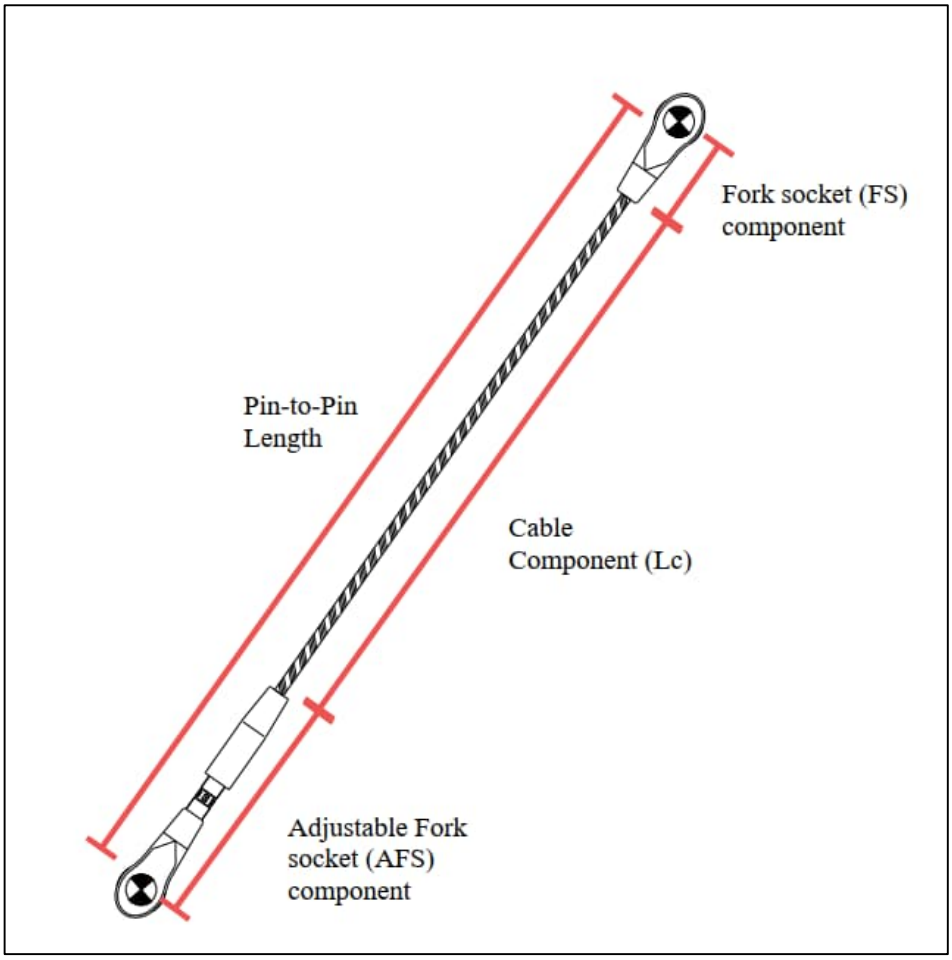

Figure 3-1: Hanger cable components

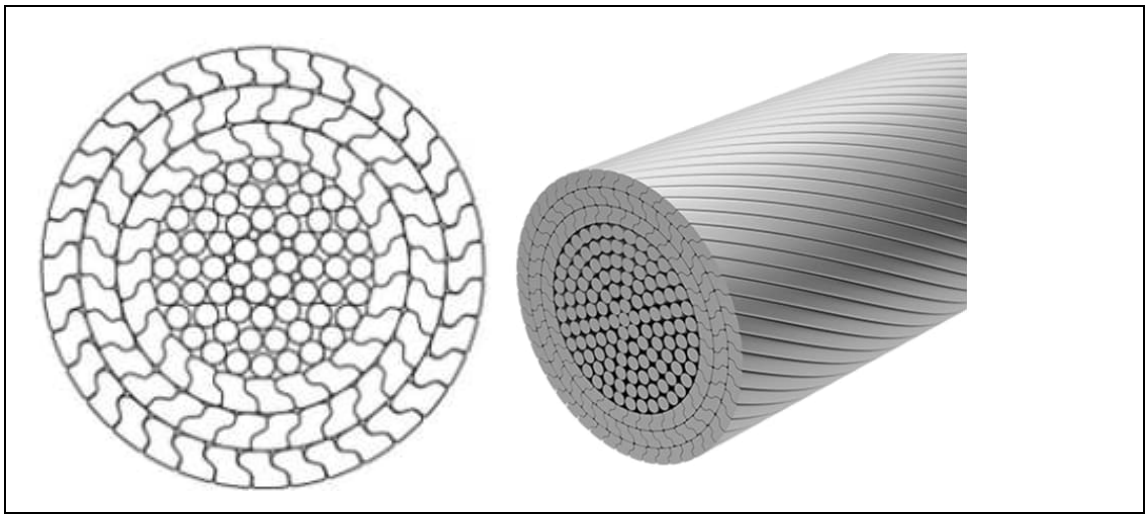

Figure 3-2: Cross section of fully locked coil cable (Teufelberger Radaelli, 2022a)

Figure 3-3 shows the adjustable fork sockets that connect the hanger cables to the tie beam. Figure 3-4 shows the layout of the adjustable fork sockets and cables at the Ashton Bridge.

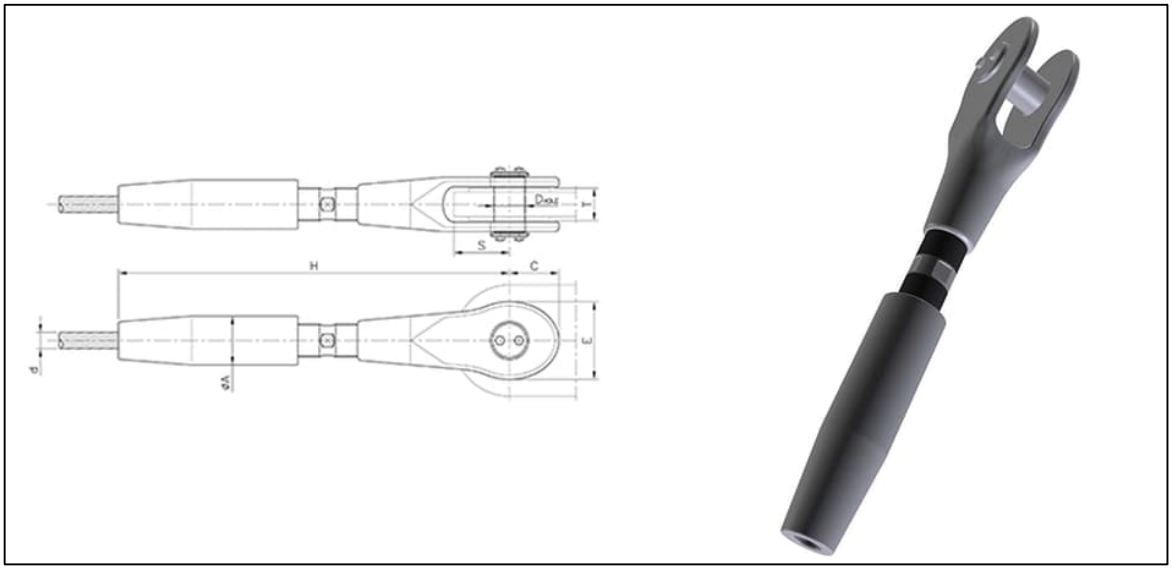

Figure 3-3: Adjustable fork socket connecting cables to the tie beam (Teufelberger Radaelli, 2022b)

Figure 3-4: Connection between the adjustable fork socket and the cable. Photographed by Terry February for AECOM SA, 2020.

Figure 3-5 shows the fork socket at the interface of the hanger cables with the arch rib. Figure 3-6 shows the layout of the fork sockets and the hanger cables at the Ashton Bridge.

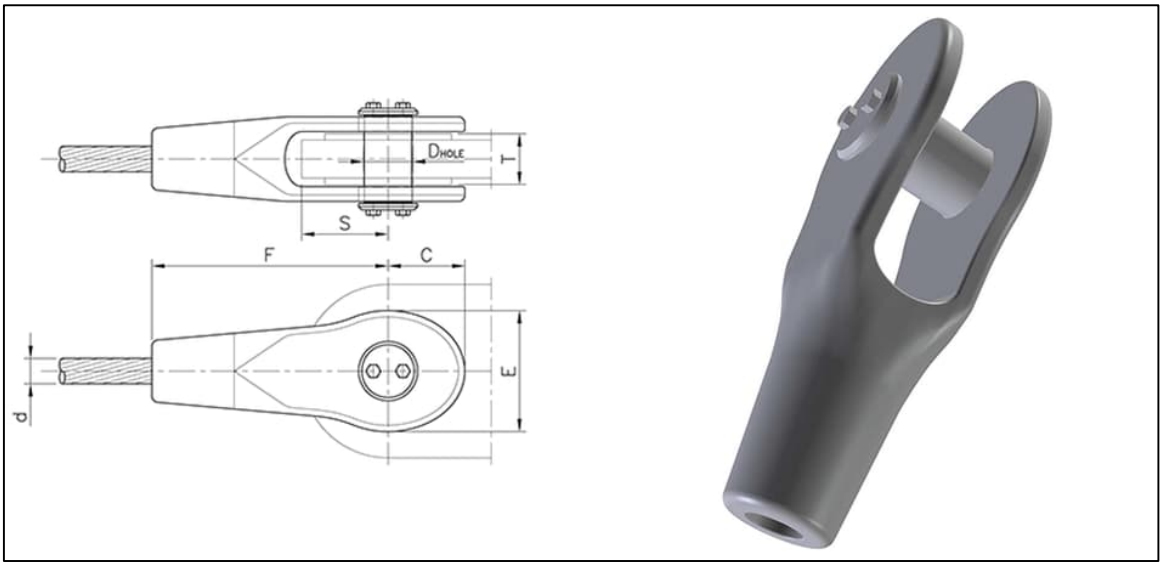

Figure 3-5: Fork socket connecting the cable to the arch rib (Teufelberger Radaelli, 2022c)

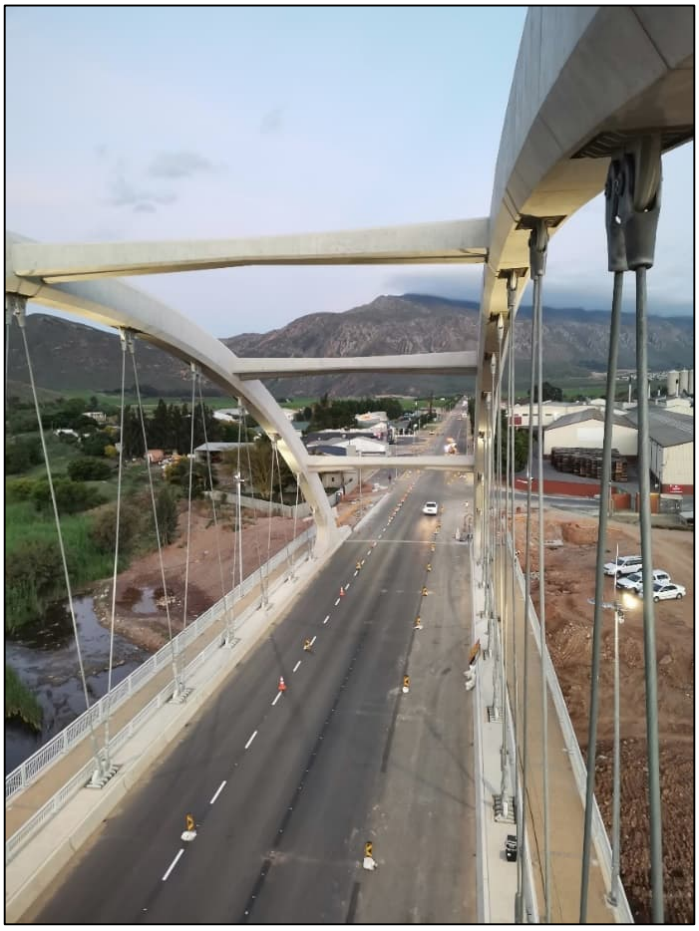

Figure 3-6: Layout of the fork socket and cables at the arch rib interface.

3.2.2 Cable Layout and Numbering

The cables are symmetrical on both arches and were numbered from 1 to 24 starting on the Western End. On each arch, the cables are divided into 2 sections, one section constituting of cables 1 to 12 and the other with cables 13 to 24. The cables in one section were paired with cables in the other section that had the same geometric properties such as the pin-to-pin length and the angle of inclination to the tie beam. For instance, Cable 1 was paired with Cable 24, Cable 2 was paired with Cable 23, Cable 3 was paired with Cable 22 and so on. The prefixes N and S were used to differentiate between the cables on the North Arch and the ones on the South Arch respectively. Figure 3-7 shows the cable numbering and Figure 3-8 shows the general layout of the cables on both arches.

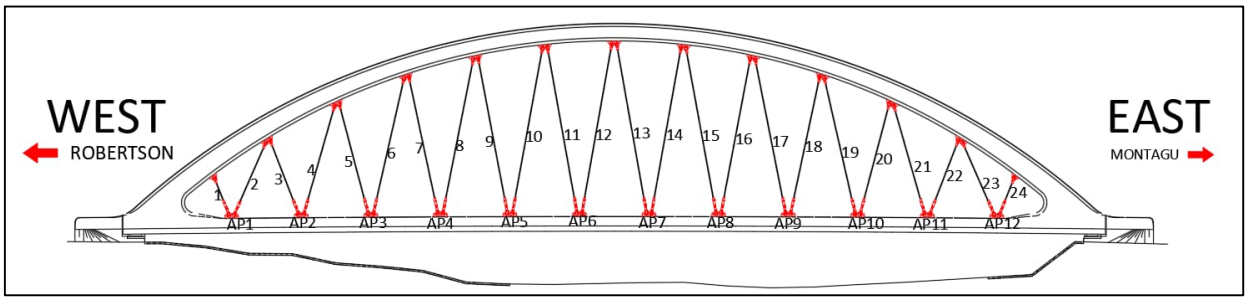

Figure 3-7: Cable numbering

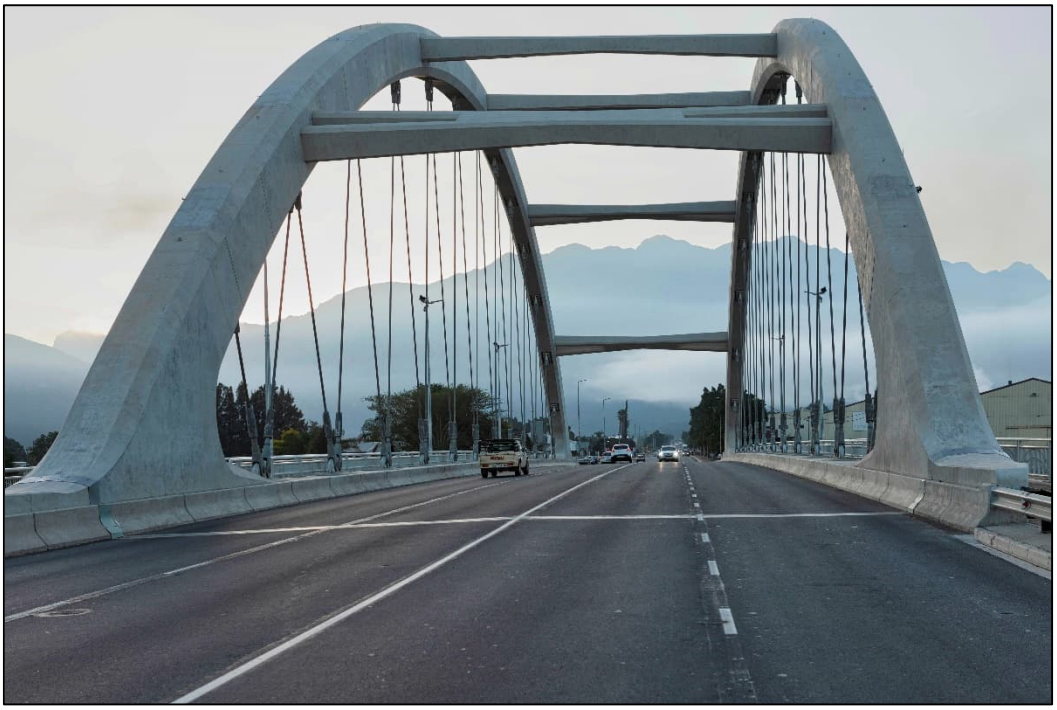

Figure 3-8: Western Side view of cables on the arch ribs. Photographed by Terry February for AECOM SA, 2022

3.2.3 Tensioning and Force Check

The hanger cables were tensioned in 4 stages with the first 3 stages taking place when the bridge was in its temporary position and the final stage of tensioning was when the bridge was in its final position. The purpose for each tensioning stage was as follows:

i) Stage 1 - to remove slack from the cables.
ii) Stage 2 - to lift the deck from the temporary supports.
iii) Stage 3 - to achieve the desired deck profile before the bridge was opened to traffic.
iv) Stage 4 - the final stage of tensioning after the calibration of the FEM using actual displacements to allow for long-term creep and shrinkage of the structure

Before tensioning commenced, the hydraulic jacks' calibration certificates were checked and the tensioning designed forces were aligned according the jacks' output. The cables were tensioned in pairs. One pair of cables was tensioned on one arch before the identical pair was tensioned on the other. The tensioning was also performed in 12 sequences to ensure uniform distribution of forces. Figure 3-9 shows a pair of cables (S12 and S13) being tensioned simultaneously.

Figure 3-9: Tensioning of cable S12 and S13 pair

When tensioning the cables, the gap between the area above the pin and the fork socket reduces as the cable extends. After some increments in the force the gap finally closes, and the turnbuckle needs to be adjusted to reopen it so that more force can be transferred into the cable. When the desired force has been transferred into the cable the turnbuckle is tightened to lock in the force. This procedure is illustrated in Figure 3-10

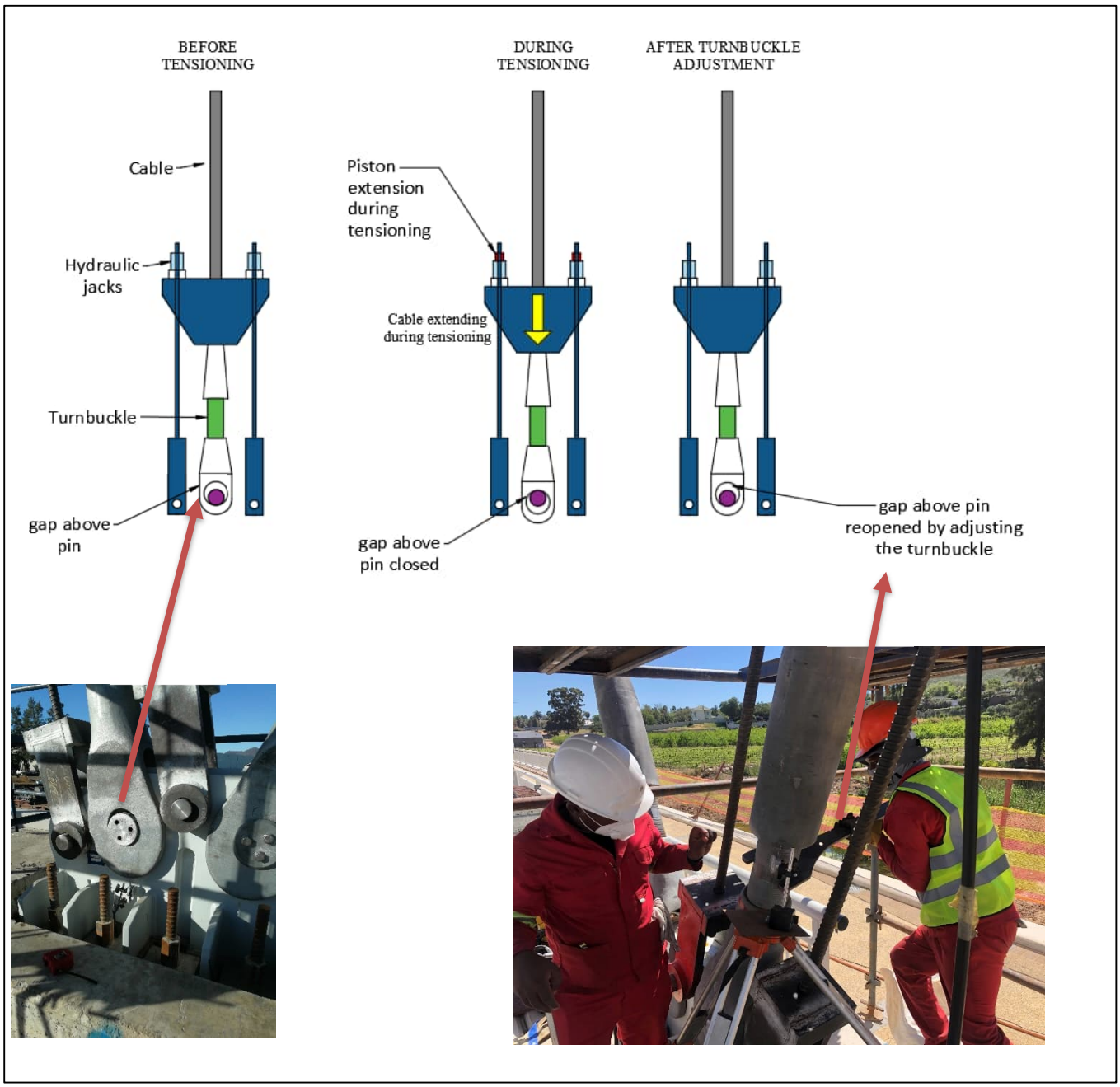

Figure 3-10: Tensioning procedure

The forces in the cables were verified using lift-off tests as well live monitoring of the structural deformation. Figure 3-11 shows the set up for the lift-off test during tensioning. The red hydraulic jacks labelled C and D exerted a force on the adjustable fork socket and the cable extended towards the tie beam as illustrated in Figure 3-10. The extension of the cable during tensioning and lift-off tests was measured using a dial gauge. A spike in the dial gauge readings indicated lift-off and the pressure was gradually increased to get more points for the pressure versus extension graph and determine the lift-off force as described in Section 2.2.1. Prior to tensioning each cable, a lift-off test was conducted to check the residual force in the cable. If the residual force was higher than the tensioning force, then the cable would not be tensioned, and tensioning would proceed onto the following sequence.

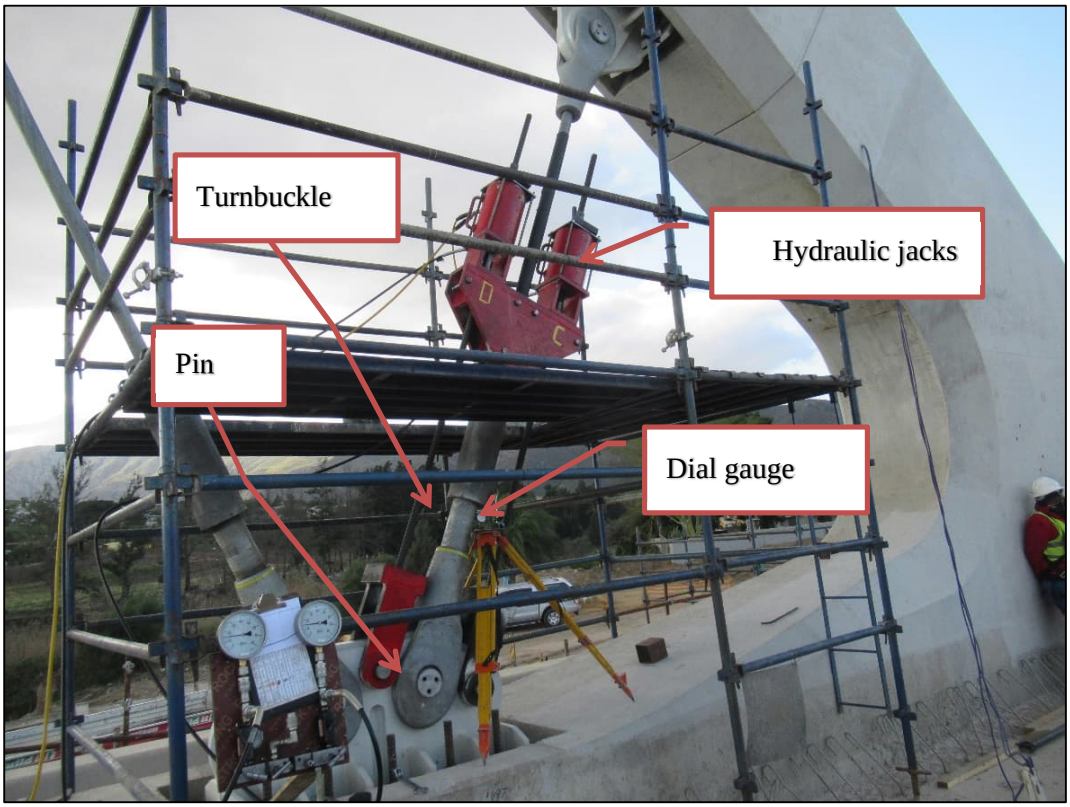

Figure 3-11: Lift-off test set up at the Ashton Bridge

Figure 3-12 shows a close-up view of the dial gauge setup on a surveying tripod stand during tensioning and lift-off tests procedures.

Figure 3-12: A close up view of the dial gauge setup

When the hanger cables were tensioned, the relationship between the turnbuckle adjustment and the force transferred into the cable was investigated. This relationship formed a basis to overcome the system losses when the cable force determined through a lift-off test differed from the design force by more than 6%. Figure 3-13 shows the turnbuckle with the threaded region of the socket that was adjusted during tensioning operations as illustrated in Figure 3-10.

Figure 3-13: Threaded turnbuckle region adjusted during tensioning

The following variables were defined and determined through measurements and calculations:

i) The circumference (C) of the turnbuckle in the threaded region was 480mm,
ii) The thread pitch was 6mm,
iii) The number of sides of 2 because a rotation resulted in adjustments at the top and bottom interfaces of the turnbuckle with other elements in the socket. This meant that a full rotation would produce a 12mm cable extension.

The relationship was quantified and formulated as follows:

- After tensioning a cable, a lift off test was performed. Before the turnbuckle was tightened, a mark starting on the bottom of the turnbuckle and ending on the fork socket was made,
- After the turnbuckle was tightened the gap between the mark on the fork socket and the one on the turnbuckle was measured. Figure 3-14 shows the gap between the two marks on the turnbuckle and the fork socket,

Figure 3-14: The gap measured between the two white marks after the turnbuckle was tightened

- The angle of the turnbuckle rotation was calculated through the circle geometry relationship in equation 3.1

$$S = R\theta \qquad 3.1$$

where:

S is the rotation length (mm)

R is radius of the turnbuckle (mm) which can expressed as a function of the circumference as $R = \frac{C}{2\pi}$

θ is the central angle in radians

- For example, if the turnbuckle rotation was 50mm, the central angle of rotation was calculated as follows:

$$\theta = \frac{2S\pi}{C} = \frac{2 \times 50 \times \pi}{480} = 0.65\, radians$$

- One full rotation gave a 12mm cable elongation. Therefore 0.65 radians rotation would result in the following elongation

$$\frac{0.65}{2\pi} \times 12 = 1.24mm\ cable\ elongation$$

- An elongation per pressure increment rate was obtained using the applied pressure readings and the resulting elongation readings captured using the dial gauge. For instance, if the elongation rate of the cable was 2mm per pressure increment in MPa then a turnbuckle rotation of 50mm would result in the following pressure gain

$$\frac{1.24mm}{2mm/Mpa} = 0.62\ MPa$$

- The pressure gained from the turnbuckle rotation was added to the pressure found at lift-off prior to tightening the turnbuckle. The total value for pressure was converted into a force using the hydraulic jacks' calibration certificate.
- A final lift-off test was conducted to verify the force. The turnbuckle would not be tightened after this final lift-off test.
- The turnbuckle thread length reduction was recorded for all stages of tensioning.
- The total cable elongation also accounted for the structural deformation of the arch ribs and tie beam which were being monitored live by the surveyor.

3.2.4 Redistribution of Cable Forces

The cable forces redistributed after every tensioning sequence. The redistribution effects were experienced in the cables tensioned from the first sequence to the eleventh sequence. The cables tensioned in the 12th and final sequence retained their installation force. This is illustrated in Table 3-1 where the number highlighted in blue represents the tension values and the figures in column L are the final forces in the cables after tensioning. In this case, the cables tensioned in sequence 3 (cables N5, N20, S5 and S20) were tensioned to a force of 1570 kN but at the end of the tensioning procedure they had a force of 1237 kN due to the redistribution effects. Cables N9, N16, S9 and S16 of sequence 5 were tensioned to a force of 1683 kN and that reduced to 1307 kN after the final sequence of tensioning. It can also be seen that the cables tensioned in the last sequence (N10, N15, S10 and S15) retained their initial force as their final force after the tensioning was completed.

Table 3-1: Force matrix table

Sequence Number	Cable No		Forces (kN)												
			A	B	C	D	E	F	G	H	I	J	K	L	M
1	1	24	821	712	658	651	657	663	624	630	636	582	574	579	614
2	3	22	1059	1466	1312	1259	1252	1263	1197	1198	1215	1179	1140	1149	1203
3	5	20	1162	1073	1570	1429	1372	1377	1327	1300	1325	1312	1233	1237	1293
4	7	18	1310	1285	1170	1679	1522	1483	1467	1404	1404	1405	1341	1322	1373
5	9	16	1158	1155	1123	1014	1683	1532	1534	1478	1380	1383	1362	1307	1352
6	11	14	1160	1164	1166	1141	998	1617	1622	1598	1328	1330	1333	1262	1301
7	4	21	591	527	442	409	414	431	757	730	741	697	615	613	634
8	8	17	736	737	706	618	506	454	436	780	731	728	655	598	627
9	12	13	684	689	701	702	611	347	350	328	878	878	881	801	836
10	2	23	659	618	592	594	605	613	562	556	559	1006	979	979	986
11	6	19	708	683	595	506	466	473	419	347	353	337	729	710	737
12	10	15	928	934	939	910	789	621	619	556	364	364	343	633	664

The final stage of tensioning (Stage 4) took place before the asphalt paving works were completed and all handrails were installed on the pedestrian sidewalk. Consequently, there was an additional dead load component to the cable forces. This was accounted for in the column M highlighted in green. This column represents the final forces in the cables as predicted by the bridge's FEM. However, according to the site tensioning records for sequence 1, the pre lift-off test results indicated that the residual forces in the cables were greater than the tensioning force (821 kN). The tensioning records from the pre lift-off tests can be found in Appendix A. Therefore, the cables in sequence 1 were not tensioned because the design force was already in the cables. The lift-off test results for these cables were the put in the force matrix table to get the final cable force prediction as shown in Table 3-2.

Table 3-2: Force matrix correction for sequence 1

Sequence Number	Cable No	Forces (kN)												
		A	B	C	D	E	F	G	H	I	J	K	L	M
1	N1	995	885	832	825	831	837	798	804	810	756	748	753	788
1	N24	1016	906	853	846	852	858	819	825	831	777	769	774	809
1	S1	846	736	683	676	682	688	649	655	661	607	599	604	639
1	S24	856	746	693	686	692	698	659	665	671	617	609	614	649

The final forces from Sequence 2 to 12 in Table 3-1 and Sequence 1 from Table 3-2 were then used for verification through AVT.

3.3 Ambient Vibration Testing

After the transverse launching of the Ashton bridge to its final position, the hanger cables were tensioned for the final stage (Stage 4). The final forces in the cables predicted by the bridge's FEM were required to be validated and recorded in the maintenance manual. AVT was used to estimate the cable forces. The source of excitation used was the wind. A full scale AVT was also conducted on the bridge superstructure to determine the modal properties.

3.3.1 Test Setup on site

3.3.1.1 Cables

The AVT of the 48 cables was conducted by dividing the cables into 8 sets (6 cables each) and then testing each set of cables for 15 minutes. Accelerometers were positioned at a third of the cables' length from the anchorage point, orientated in the central longitudinal plane of the bridge. Additionally, they were placed on the side of the cable in which the accelerometers were facing downwards towards the tie beam. Figure 3-15 shows the accelerometers mounted on the cables and Figure 3-16 shows a close-up view of an accelerometer secured onto a cable.

Figure 3-15: Position of accelerometers along the cables

Figure 3-16: Accelerometer secured onto a cable

3.3.1.2 Bridge Superstructure Measurements

Accelerometers were set up on the deck and the arch then vibration data was recorded data for 15 minutes. Reference positions on the arch and deck were selected. Accelerometers placed at the reference positions were not moved for the duration of the tests. Vibration data was recorded in the vertical and transverse directions. The following sections describe and illustrate the tests on the arch and deck.

3.3.1.2.1 Deck set up

Accelerometers were positioned along 3 longitudinal alignments. These alignments were the 2 tie beams at the anchor plate positions as well as along the central longitudinal beam in the deck. The total number of testing points on the deck was 36. Figure 3-17 shows the AVT set up for the deck.

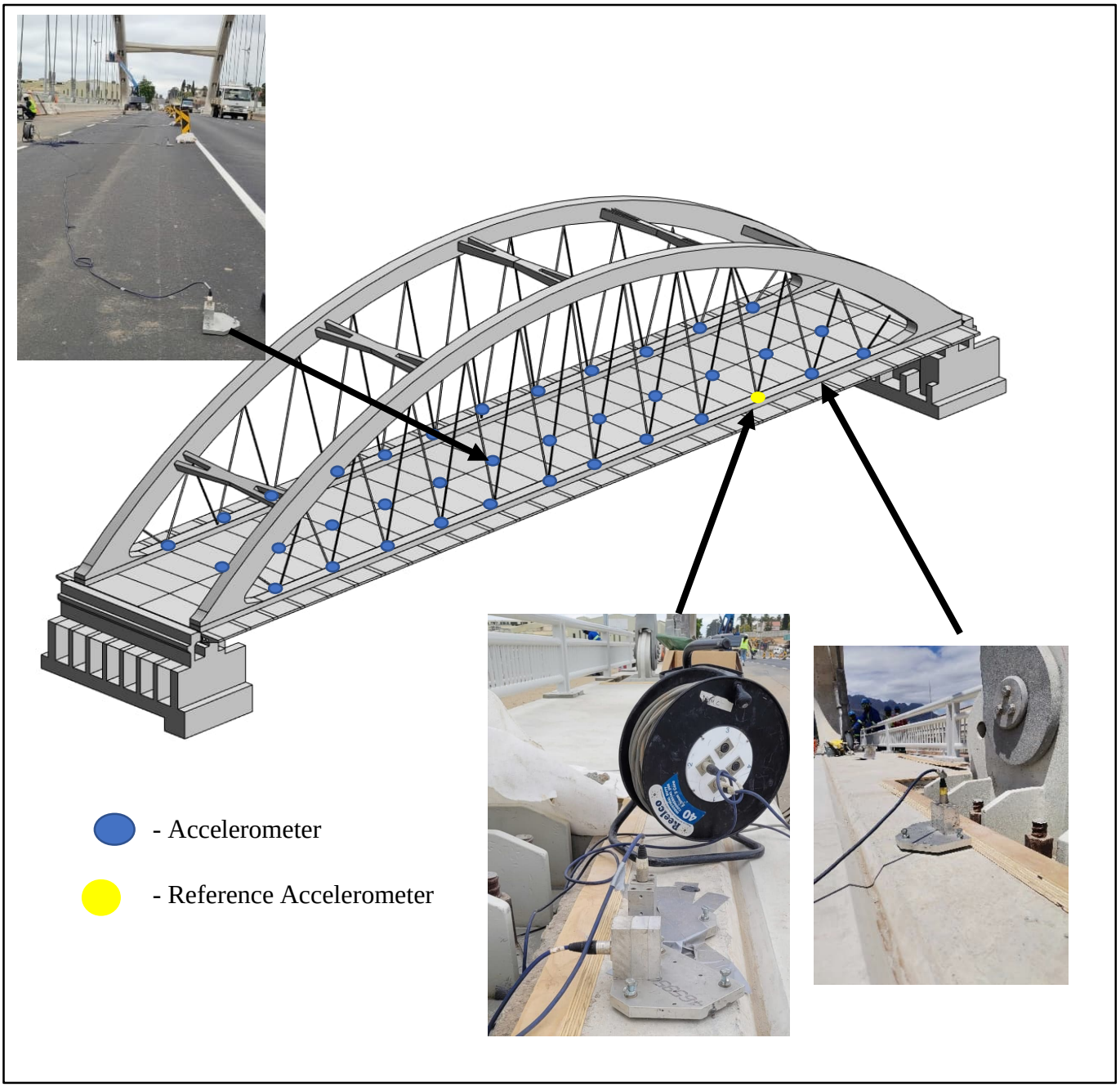

Figure 3-17: Deck AVT set up

3.3.1.2.2 Arch set up

Accelerometers were placed in line with the wishbones on both arches. In total 10 positions were used to record the arch vibrations. Figure 3-18 shows the Arch AVT set up.

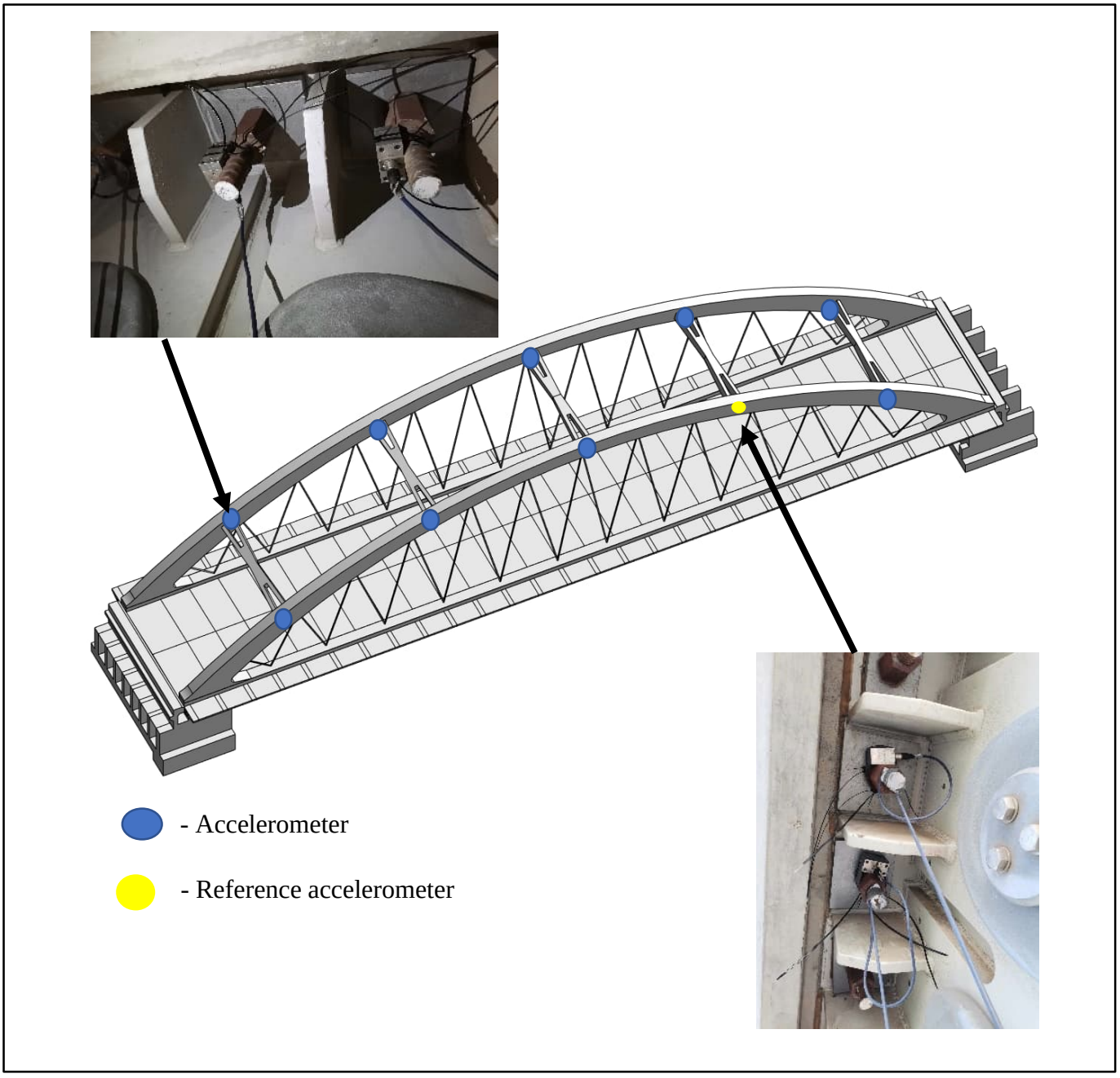

Figure 3-18: Arch AVT setup

3.3.2 Equipment and site organisation

AVT was conducted on the cables on the 6th of December 2021 while the bridge was open to traffic to ensure minimum disruption to the traffic. To create sufficient working space, two of the bridge's four lanes were closed and delineators were used to divert the traffic. A cherry picker was used to access the cable positions to mount the accelerometers. Flag persons and traffic accommodation personnel assisted in stopping traffic momentarily and to realign the delineators when the cherry picker had to move to the other arch. Figure 3-19 shows the working space demarcation.

Figure 3-19: Working space demarcation

The bridge superstructure vibration tests were conducted on the 8th and 9th of December 2021. The deck tests were conducted using the same working area shown in Figure 3-19. The traffic was shifted to the centre of the bridge for the arch tests as shown in Figure 3-20.

Figure 3-20: Working space during arch vibration tests

The vibration testing equipment comprised of the following:

- 8-channel digital signal analyser,
- 8 force balance accelerometers and cables,
- Portable generator,
- Computer containing the data acquisition software,
- 96 cable ties to tie the accelerometers onto the cable,
- 4 cable drums to connect to the signal analyser.

Figure 3-21 shows the force balance accelerometers and the setup of the data acquisition system on the tie beam. The cable drum was connected to the signal analyser where each accelerometer's measuring data had a unique channel.

Figure 3-21: Force balance accelerometers (left) and set up of the data acquisition system (right)

3.3.3 Identifying Natural Frequencies

The FRF of the measured data for the cables was calculated using a range from 0 to 250 Hz with an associated frequency resolution of 0.1 to 2 Hz. The FRF for the superstructure measurements was calculated using a range from 0 to 256 Hz with an associated resolution of 0.06 to 5 Hz. The modal properties of the cables and the bridge were extracted from the measured vibration data through a software called MEscope. In the case of cables, the first peak was identified for the natural frequency whereas in the case of the bridge measurements, the several peaks identified were used to qualify the mode shape and extract the associated frequency. Figure 3-22 shows how the peak frequencies were extracted using MEscope.

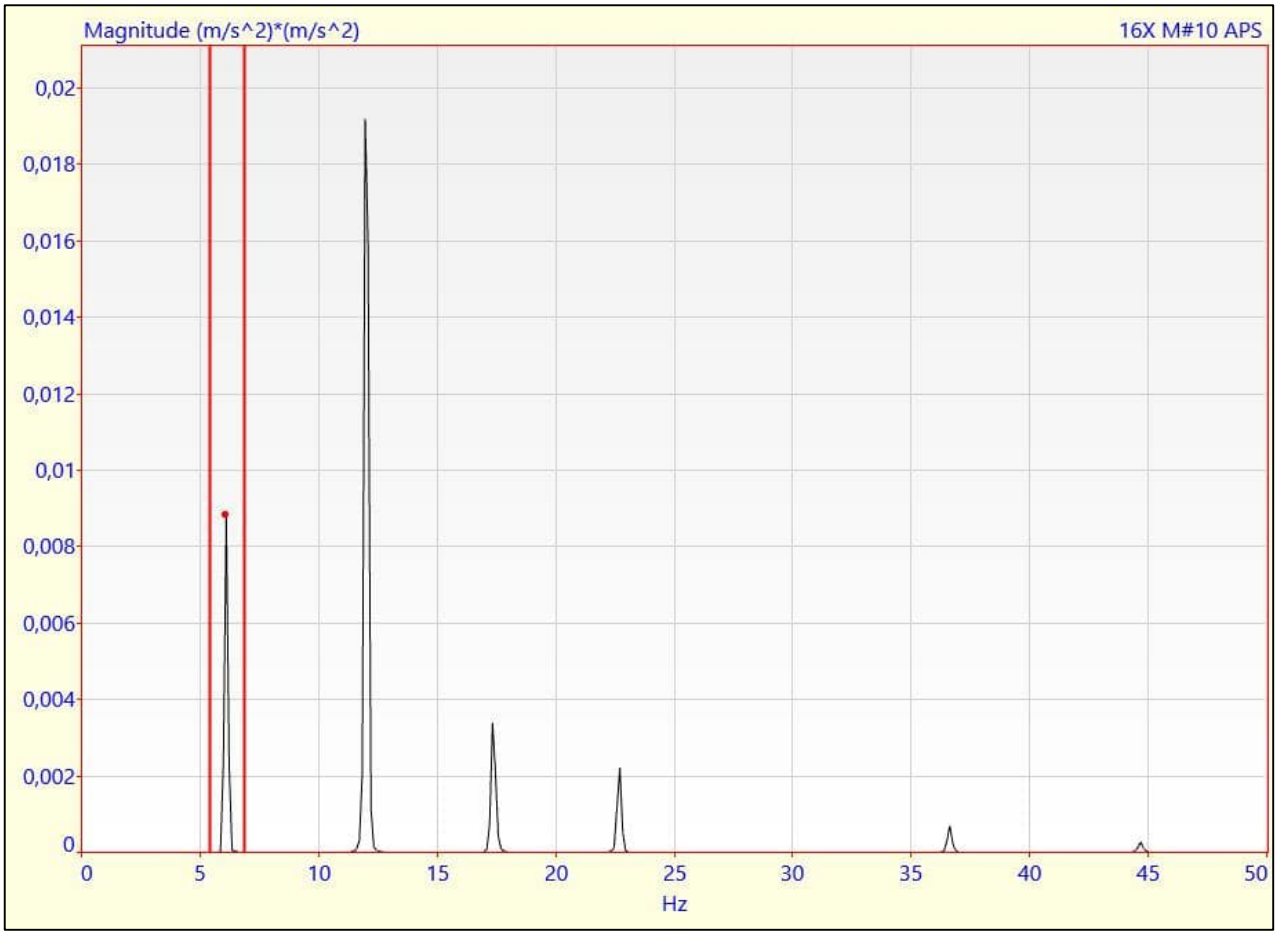

Figure 3-22: Identification of peak frequencies in MEscope

The measured frequencies of cables with similar geometries and symmetrical about the arches were grouped together to analyse the standard deviations. For instance, the one group of measured frequencies consisted of cables N2, N23, S2 and S23, another one would contain cables N11, N14, S11 and S14 and so on. The results were tested for outliers using Method 1 specified in the Committee of Land Transport Officials (COLTO) specifications for quality control. Method 1 of testing results for outliers is illustrated in the equation 3.2 and Table 3-3 (Committee of Land Transport Officials, 1998).

$$T_o = \frac{(x_0 - \bar{x}_n)}{S_n} \qquad 3.2$$

where:

- T_o is the result used to check if the test result is an outlier
- x_0 is the test result that differs from the mean the most
- $\bar{x}_n$ is the mean of the test results
- $\boldsymbol{S_n}$ is the standard deviation

The absolute value of T_o from equation 3.2 must be greater than the critical value listed in Table 3-3 (for the given sample size) for a test result to be considered as an outlier. In this case, the sample size was four because each group consisted of four similar cables. Therefore the absolute value of T_o was checked to be greater than 1.46 for the particular test result to be considered as an outlier (Committee of Land Transport Officials, 1998).

Table 3-3: Outlier assessment values (Committee of Land Transport Officials, 1998)

Sample size	Critical value
4	1.46
5	1.67
6	1.82
7	1.94
8	2.03
9	2.11
10	2.18
11	2.23
12	2.29
13	2.33
14	2.37
15	2.41
16	2.44
17	2.47
18	2.50
19	2.53
20	2.56

3.3.4 Bridge Model Calibration

The natural frequencies determined from the bridge's superstructure AVT were compared to the one's predicted by the bridge's FEM at the end of construction. The criteria used in classifying the bridge's FEM as being sufficiently calibrated was when the theoretical frequencies were within 10% of the one measured on site. Additionally, the FEM was used to classify the type of mode that was associated each frequency.

During construction, the bridge's FEM was calibrated by adjusting the self-weight of the concrete elements and the elastic modulus of the concrete. These adjustments were made to account for the creep and shrinkage effects as well as to obtain the accurate self-weight of the structure for hydraulic jacking procedures when changing bearings. Additionally, the post tensioning forces of the superstructure were modelled. This phase of calibration was done before AVT. In the case of calibration influenced by the AVT results, the stiffness values of the springs used to simulate the bearings were adjusted in the FEM. Figure 3-23 shows the bearing layout and articulation at the Ashton Bridge. Figure 3-24 shows the location of the bearings in relation to the superstructure. Figure 3-25 shows the close-up view of the spring elements simulating the bearings in the FEM.

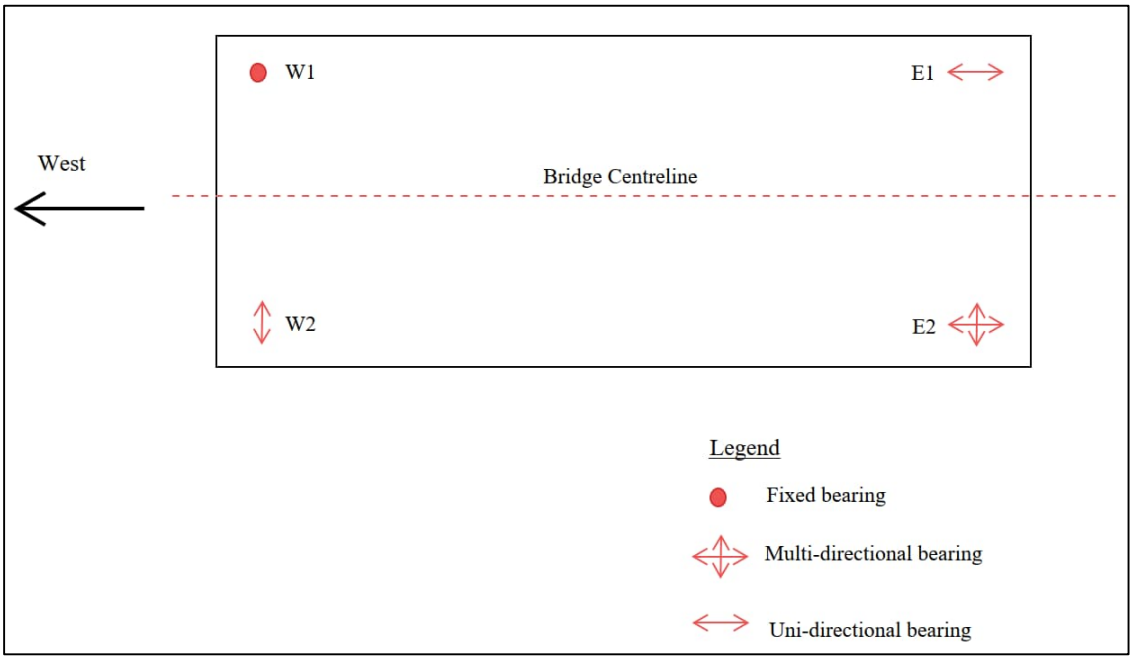

Figure 3-23: Plan view of the Ashton Bridge illustrating the bearing layout and articulation

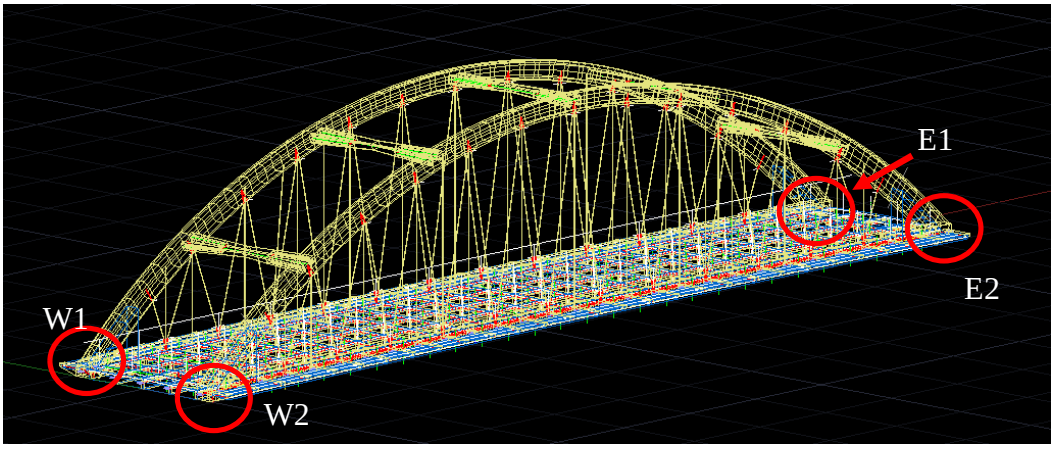

Figure 3-24: Location of bearings in relation to the superstructure

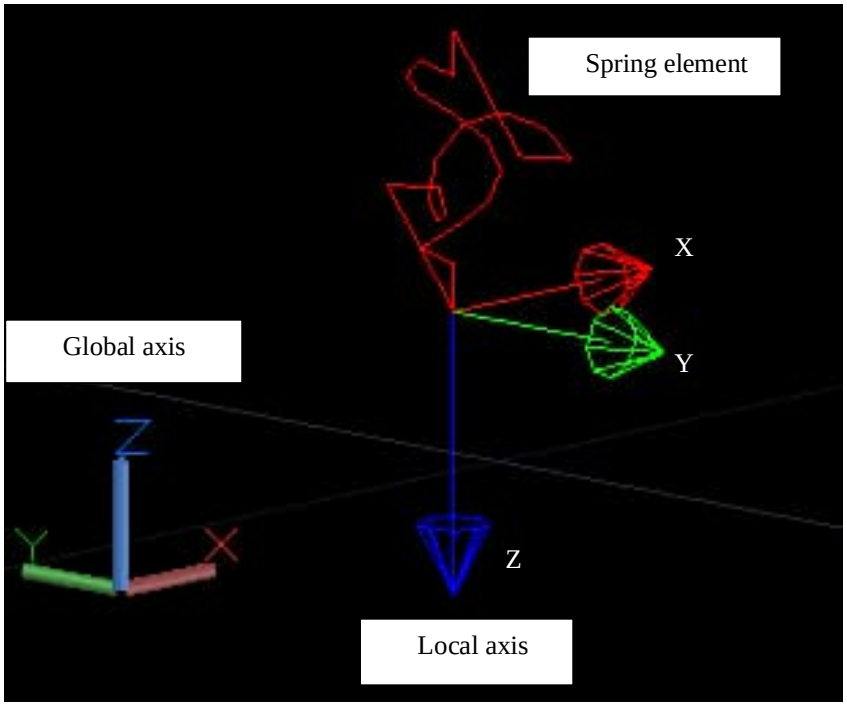

Figure 3-25: Close up view of the spring element in the model

The initial axial spring stiffness values in the FEM are listed in Table 3-4.

Table 3-4: Initial axial spring stiffness values

Bearing	Stiffness values in the Global axis (kN/m)			Stiffness values in the Local axis (kN/m)		
	x	y	z	x	y	z
W1 (fixed)	-	-	10 000 000	100 000	100 000	-
W2 (Unidirectional)	-	-	10 000 000	100 000	-	-
E1 (Unidirectional)	-	-	10 000 000	-	100 000	-
E2 (Multidirectional)	-	-	10 000 000	-	-	-

3.4 Development of the Cable Analytical Models

The cables' FEM were created in Sofistik. The cable element was used to model the cable section of the system whereas a combination of beam and plate elements were used to model the sockets. Additionally, the cable section of the system of the short cables was also modelled using the beam element property. The details of the modelling of each component are discussed in the following sections.

3.4.1 Socket Modelling

The geometry of the fork sockets varied along their length and breadth. Consequently, the stiffness properties also varied. An Autodesk Civil 3D drawing of the sockets provided by the manufacturer was used to extract dimensions to model the sockets. The drawing supplied by the manufacturer as well as the labels of the components are shown in Figure 3-26.

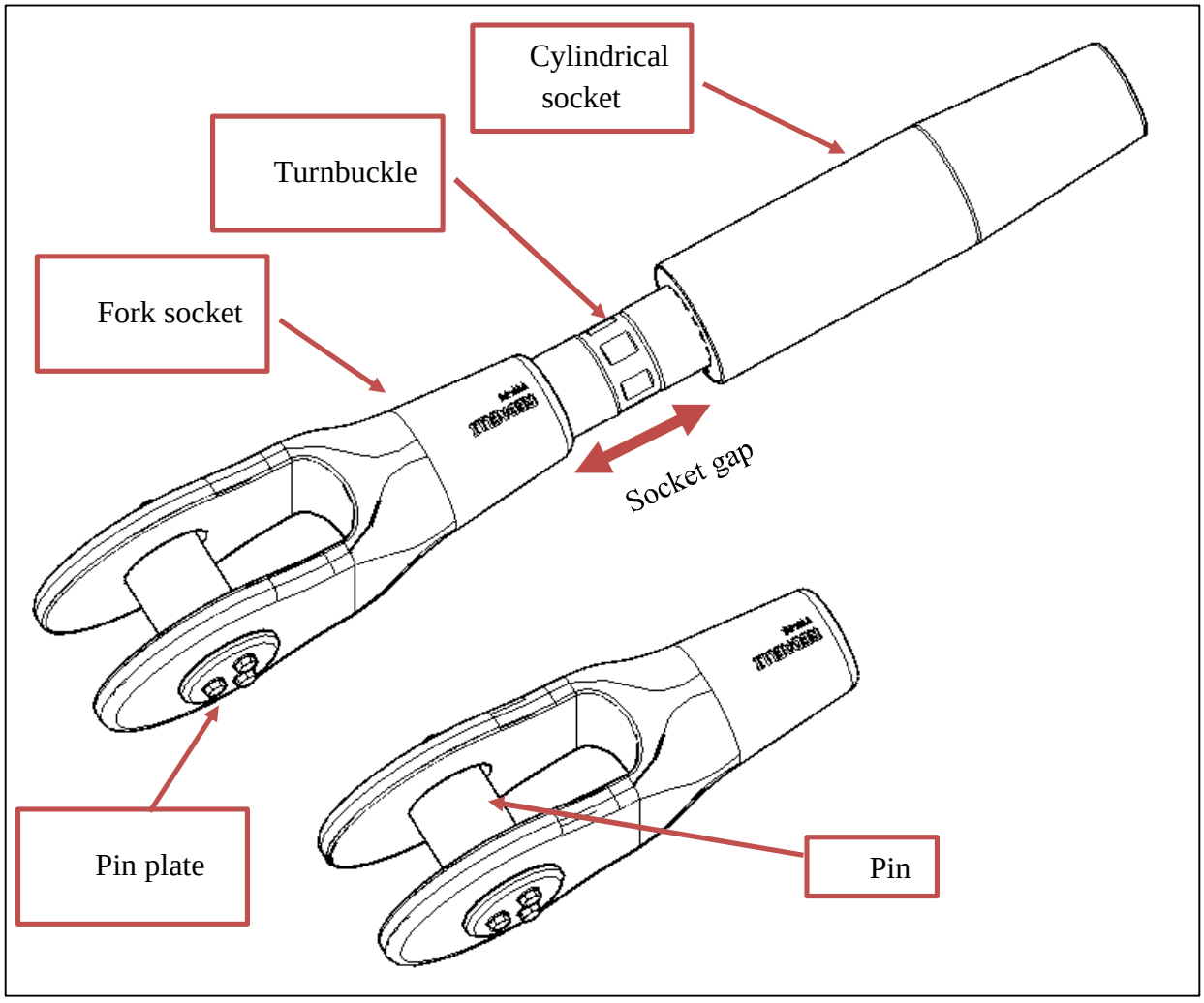

Figure 3-26: Ashton bridge top and bottom sockets. Drawings supplied by manufacturer Teufelberger Radaelli

The sockets were modelled using a combination of plate and beam elements as illustrated in Figure 3-27

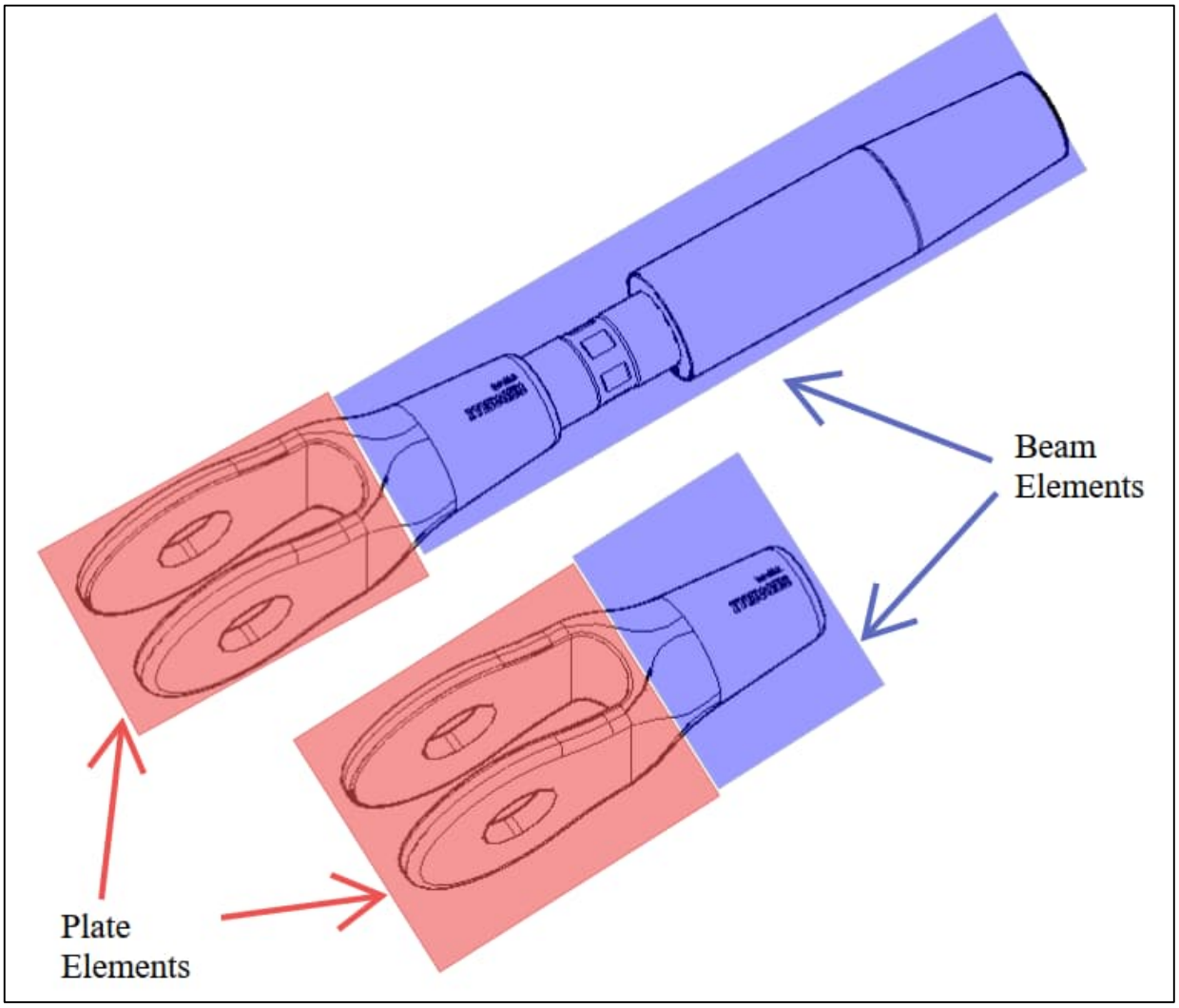

Figure 3-27: Element assignment of socket components

The length of the fork socket was the same in each cable model. However, the length of the adjustable fork socket was different in each cable model due to the different cable forces and turnbuckle adjustments during tensioning. The length from the bottom of the pin plate to the top of the cylindrical socket and the thread length reduction (socket gap in Figure 3-26) of the turnbuckle were measured after each tensioning phase. The parameters measured are shown in Figure 3-28

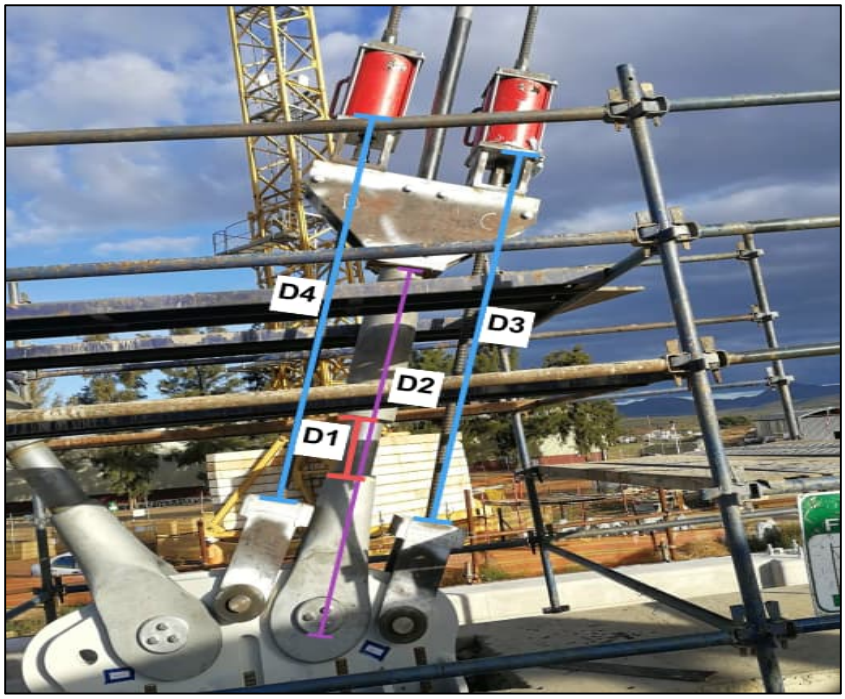

Figure 3-28: Parameters measured before and after tensioning

The D3 and D4 measurements were taken from the bottom of the hydraulic jacks to the top of the stressing brackets to ensure that the hydraulic jacks were transferring equal forces into the cable. The D2 was the measurement taken from the bottom of the pin plate to the bottom of the cross head that served as a platform for the hydraulic jacks. D1 was measured from the bottom of the cylindrical socket to the bottom of the mark made by tape on the fork socket. Figure 3-29 shows close up view of the tape mark on the fork socket. The D1 measurement was used to determine the turnbuckle thread reduction.

Figure 3-29: Tape mark made on fork socket for D1 measurements

In order to standardise the socket gaps in all the analytical models, the average of D1 measurements for all the cables was calculated and used as the standard value. The final value used for the socket gap was 290 mm and the value for the socket length was 1820 mm . The detailed calculation of the lengths of the sockets can be found in Appendix B.

The fork socket plate and beam elements were modelled using the following properties:

- Material: Steel Casting with a Yield strength of 495 MPa and a Tensile Strength of 690 MPa (BS 3100, 1991; Radaelli, 2017),
- Self-weight of 62.82 kN/m^3 accounting for the mass of the socket (Teufelberger Radaelli, 2022c).

The adjustable fork socket plate and beam elements were modelled using the following properties:

- Material: Steel Casting with a Yield strength of 495 MPa and a Tensile Strength of 690 MPa (BS 3100, 1991; Radaelli, 2017),
- Self-weight of 54.17 kN/m^3 accounting for the mass of the socket (Teufelberger Radaelli, 2022b).

The detailed calculations of the self-weight of the sockets can be found in Appendix C

3.4.2 Final Cable Model

The cable elements from the Bridge's FEM that was being used by the consulting engineer, AECOM SA, were extracted to create local models for each cable with some alterations to the material and geometric properties. Firstly, the mass recorded in the materials report (32.4 kg) was converted to a unit weight value of 81.45 kN/m^3. Secondly, the cables in the local models incorporated the sockets modelled using the drawing supplied by the manufacturer. Finally the elastic modulus of 158312 N/mm^2 was used and the diameter was changed to 70.8 mm^2 after considering the test results from the manufacturer's report which stipulated the effective metallic area of the cable (Radaelli, 2017). The standard CTE value of $12 \times 10^{-6}\ {}^{0}C^{-1}$ was used in modelling the cables. The same CTE value was also used in the bridge's global model.

The short cables (N1, N24, S1 and S24) adjacent to the spring points were modelled using two approaches. Firstly, the beam element property was used to simulate their behaviour as tensioned beams. Secondly, the cable element property was used because it only transfers axial forces and when performing non-linear analysis, the cable is always in tension (Sofistik AG, 2022a). A sanity check of the two models was conducted resulting in one of them being selected as the analysis model for the short cables. The cable element property was used to model the rest of the bridge's cables.

The cable models were discretized into a number of nodes in order to capture the inner cables vibrations when masses are applied to the nodes during a dynamic analysis (Sofistik AG, 2022a). The pinned end boundary conditions were used to simulate the restraint provided by the socket pin connection to the anchor plate. The final analytical model is shown Figure 3-30 and the main members in the bridge's global FEM are listed in Table 3-5.

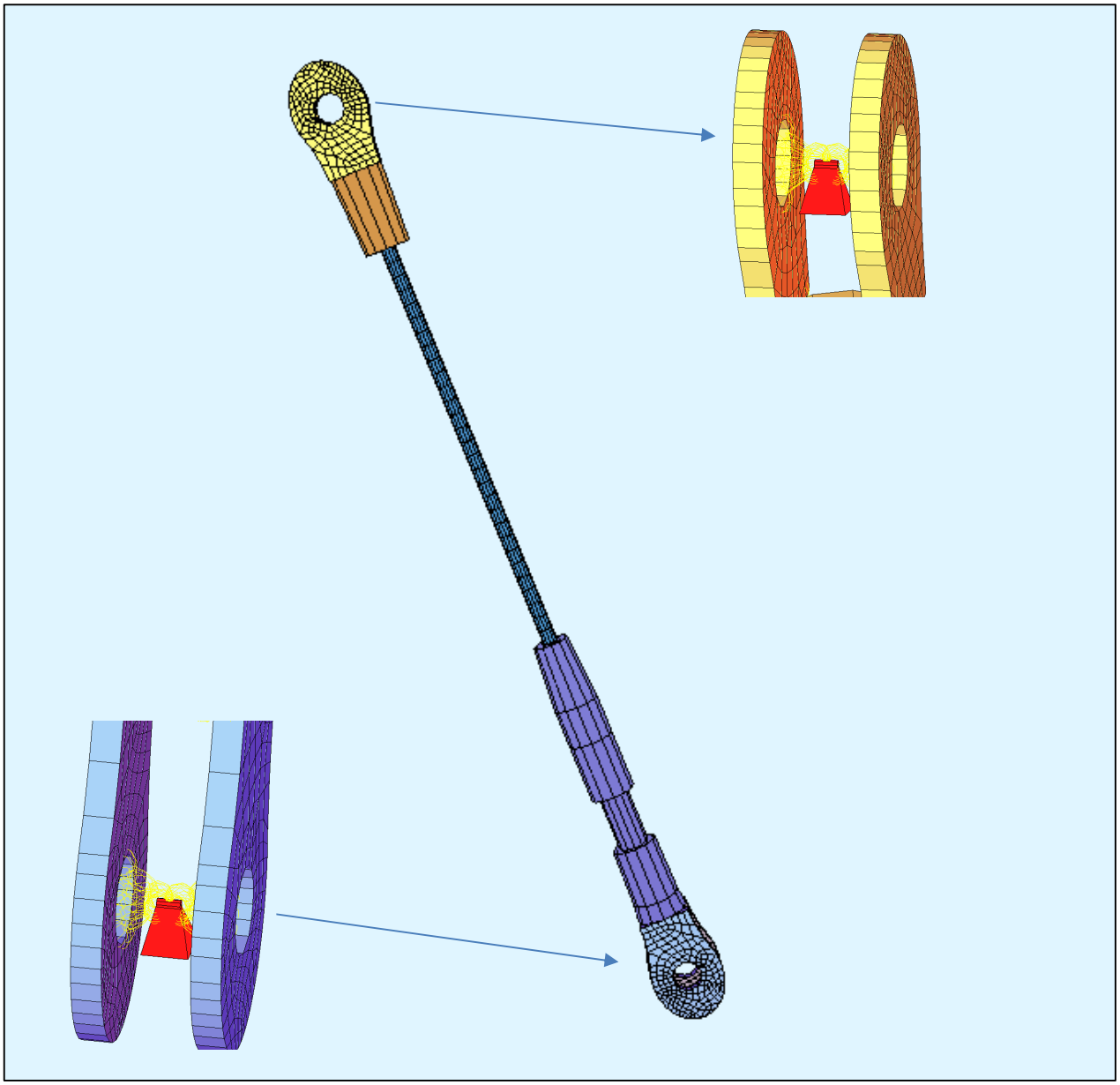

Figure 3-30: Final cable model

Table 3-5: Superstructure members

Bridge Member	Element and Concrete Properties
Arch ribs	Beam element. γ = 25.6 kN/m^3; φ = 12 × 10^{-6} ^{0} C^{-1}; E = 34 GPa
Arch and Tie Beam interface	Shell element to represent the spring point γ = 0 kN/m^3; φ = 12 × 10^{-6} ^{0} C^{-1}; E = 31.5 GPa
Deck Slab	Shell element γ = 25.5kN/m^3; φ = 12 × 10^{-6} ^{0} C^{-1}; E = 31 GPa
Deck longitudinal and transverse beams	Beam elements γ = 25.5kN/m^3; φ = 12 × 10^{-6} ^{0} C^{-1}; E = 31 GPa
Tie Beam	Beam element γ = 25.9kN/m3; φ = 12 × 10^{-6} ^{0} C^{-1}; E = 34 GPa
Wish Bones	Beam elements connecting the two arch ribs γ = 25.5kN/m^3; φ = 12 × 10^{-6} ^{0} C^{-1}; E = 31 GPa

3.5 Validation of the Analytical Model

A nonlinear analysis was conducted in the FEM followed by form finding using the total load in the system. The reactions and cable force from the FEM were checked through hand calculations. The following sections describe the FEM validation in detail.

3.5.1 Sofistik 2nd and 3rd order theory

The 2nd and 3rd order theory analysis performed by Sofistik is illustrated in Figure 3-31. In the 2nd order theory (TH2), the material stiffness is reduced due to the compression force Pz. Consequently, there is an additional deflection dux in the x direction and the beam increases in length. The additional deflection also increases the bending moment at the bottom due to Pz. This analysis is called the pi-delta analysis method. In the 3rd order theory (TH3), the same analysis as TH2 is performed except that the beam length does not increase. Equilibrium is reached through iteration on the actual deformed shape (Sofistik AG, 2022a).

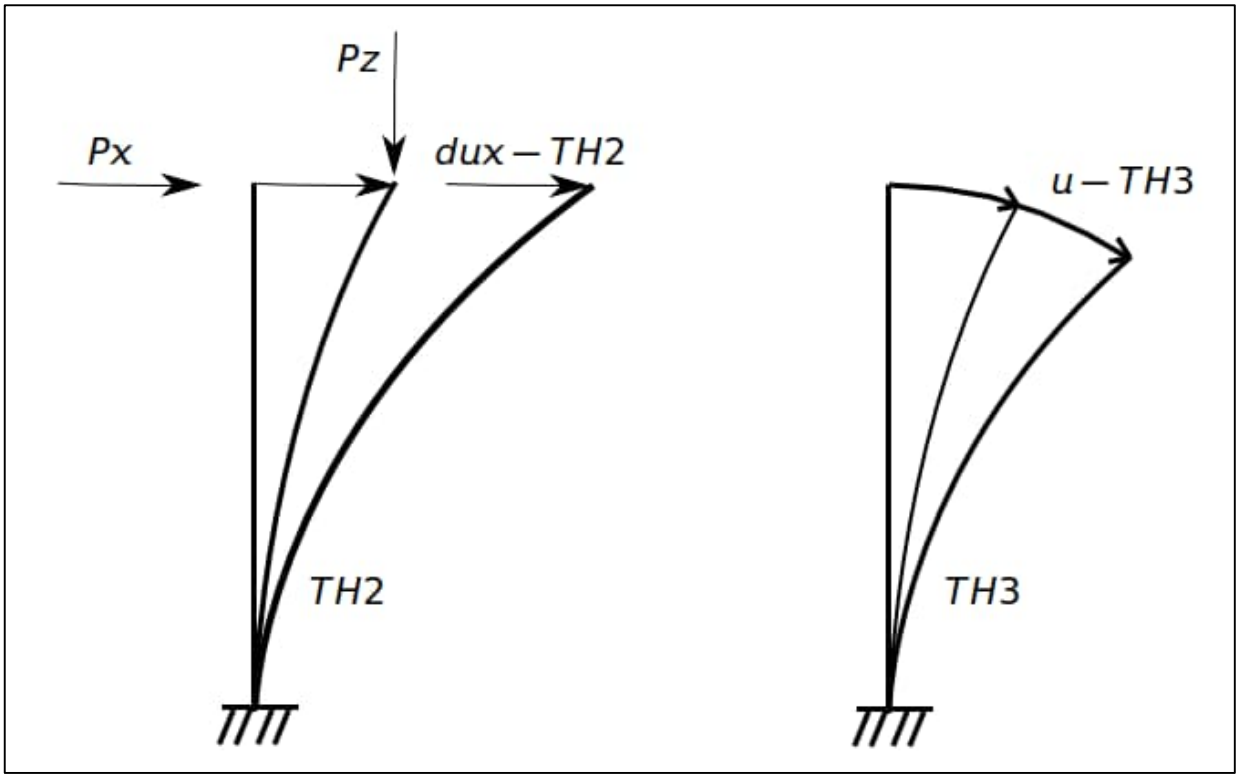

Figure 3-31: Sofistik 2nd and 3rd order theory analysis on a column (Sofistik AG, 2022a)

Figure 3-32 illustrates the differences between TH2 and TH3 analysis on a beam. In the TH2 analysis there is no normal force (N = 0) when the beam deflects. However in the TH3 analysis, there is a normal force N when the beam deflects and the length increases (Sofistik AG, 2022a).

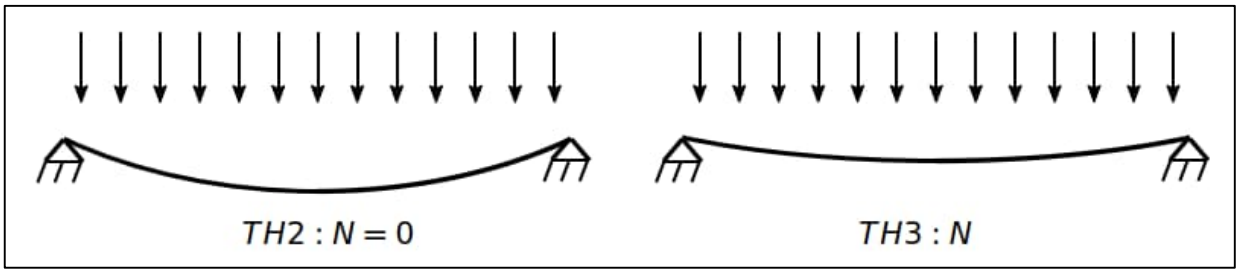

Figure 3-32: Sofistik 2nd and 3rd order theory analysis on a beam (Sofistik AG, 2022a)

The validation of the analytical models was performed using the 3rd order analysis theory.

3.5.2 Form Finding

Form finding was conducted using the deadload and the prestress force (T). The deadload comprised of the weights from the fork socket (W_{socket}), Adjustable fork socket ($W_{adjustable\ socket}$) and the Cable (W_{cable}). A 3rd order analysis was performed using Sofistik's ASE module. When the form finding was completed, the model was validated through checking the reactions (R). Figure 3-33 shows the parameters that were used for validating the models.

From Figure 3-33, the following equations were the criteria used to check the model:

$$Rv_a + Rv_b \cong W_{socket} + W_{cable} + W_{adjustable\ socket} + T_{Av} + T_{Bv} \quad 3.3$$

$$Rh_a + Rh_b = T_{Ah} + T_{Bh} \quad 3.4$$

$$T_B > T_A \quad 3.5$$

The reason for the ≅ in equations 3.3 is that T_A and T_B are not strictly equal because of gravitationally effects (Morgenthal et al., 2018). To simplify the hand calculations, T_A and T_B were assumed to be equal. However, in the FEM of the cables, T_B was checked to be more than T_A as stipulated by Equation 3.5. A typical validation calculation can be found in Appendix D.

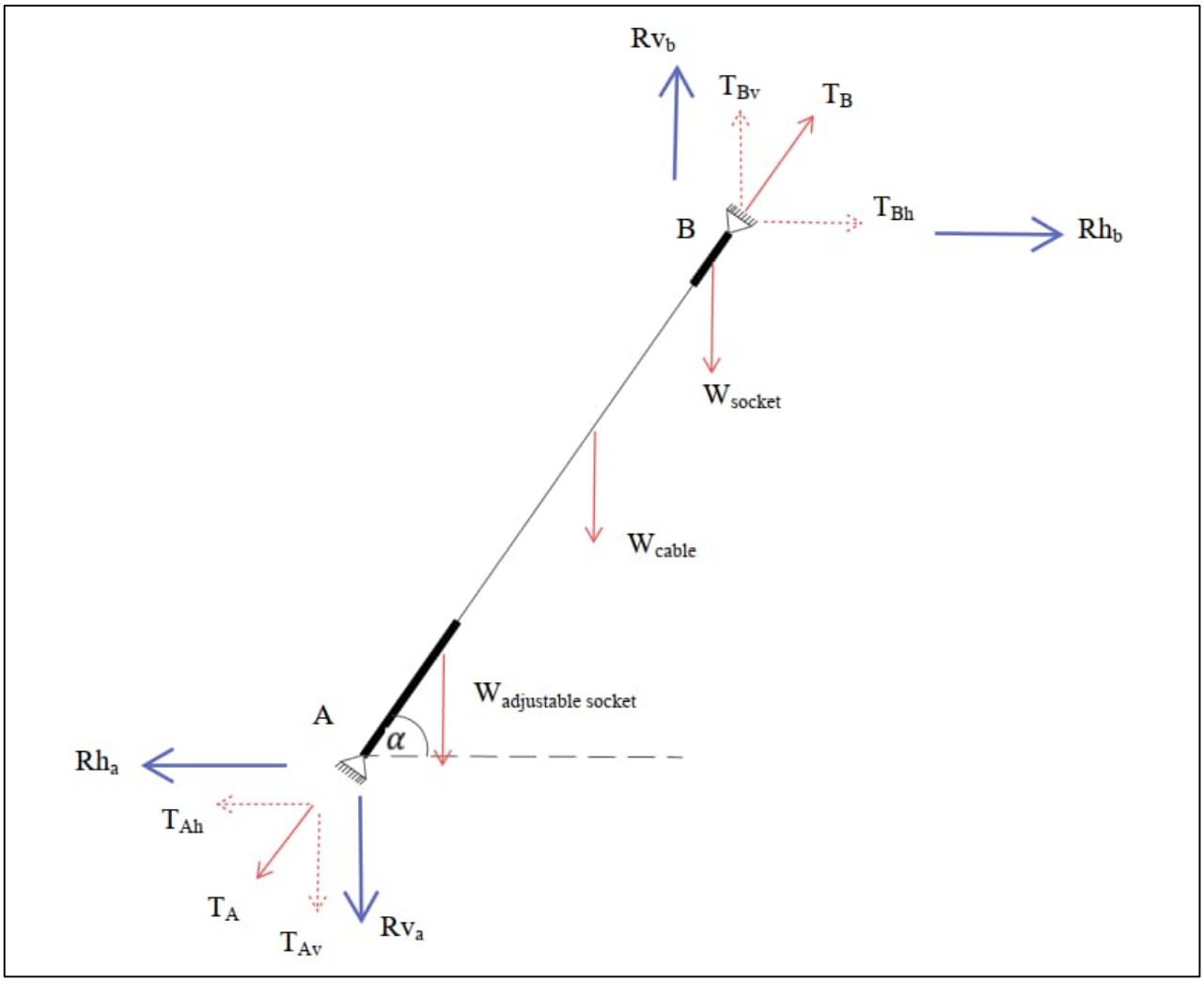

Figure 3-33: Model validation parameters

3.6 Extraction of the Natural Frequencies from Analytical Models

After the completion of form finding, Sofistik's ASE module performed the dynamic modal analysis of the cable element using the Lanczos method. The Lanczos method is an iteration method that can provide many eigenvalues relatively quicker than simultaneous vector methods which demand greater computational power if more iterations are needed for convergence to be achieved. 6 natural frequencies were computed. Load cases were created for the mode shapes and their associated frequencies (Sofistik AG, 2022a).

3.7 Evaluation of Force in the Cable

The force predicted by the bridge's FEM was used as the initial prestress force for form finding. Thereafter, the dynamic modal analysis was performed to provide the natural frequency at the predicted force. The natural frequency obtained from the cable FEM was then compared to the one that was obtained from site measurements. If the two were not matching, the prestress force would be changed, another form finding process would be initiated followed by a dynamic modal analysis until the natural frequency from the cable FEM matched the one from site measurements. When the computed natural frequency and the one from the site measurements matched, the average value of $T_A$and T_B at the cable ends was taken as the force in the cable.

The temperature effects were accounted for by creating upper and lower bound limits for the estimated force relative to the predicted force values. The maximum and minimum temperatures on the day of the tests (6th of December 2021) were 22℃ and 13℃ respectively (AccuWeather, 2021). A temperature range of ± 9℃ was then used to calculate the thermal effect on the cables and simulate the effects on the rest of the bridge elements in the FEM. The change in force in the cable due to thermal effects (ΔF_{cable}) was calculated as follows:

$$\Delta F_{cable} = EA\varphi\Delta T \tag{3.6}$$

where:

- E = 158312 N/ mm^2 was the elastic modulus of the cable material
- A was the cross-sectional area of the cable using the effective diameter 70.8 mm^2
- φ was the CTE = 12.5 × 10^{-6} ^{0} C^{-1}
- ΔT was the temperature range ± 9℃

In beam elements, Sofistik accounts for the temperature effects by applying uniaxial strain loads. Corresponding axial constraint stresses are also computed. Thereafter, the axial forces and bending moments due to the thermal strains are calculated. To maintain internal equilibrium in unconstrained systems, the forces and moments are set equal to external loads. For unconstrained systems, deformations are obtained and stresses occur. The loading is then converted to an equivalent thermal load using a reference thermal expansion factor. This enables temperature distributions to be broken down into constant, linear and nonlinear sections as shown in Figure

3-34. Sofistik's HYDRA module is used for more complex thermal analysis problems. In this study, temperature effects were approximated using uniaxial strain loads (Sofistik AG, 2022b).

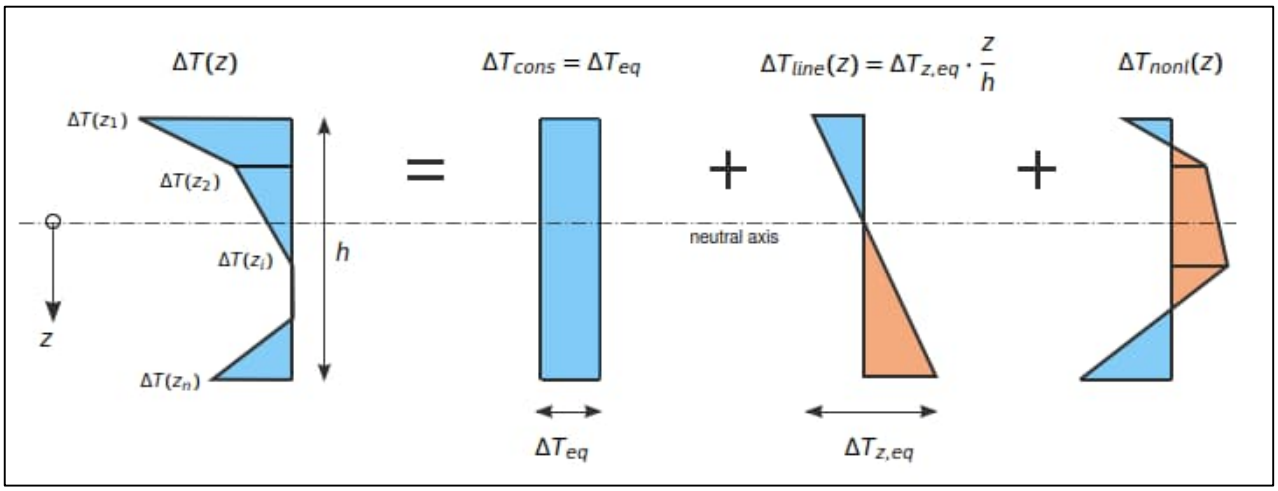

Figure 3-34: Illustration of temperature distribution decomposition into its constant, linear and nonlinear components (Sofistik AG, 2022b)

For shell elements, temperature loads are applied as absolute temperatures for fire designs, a range in-plane with the element or a temperature difference at the top and bottom (gravity direction) extreme fibres of the element. In this study, a temperature range was applied in-plane of the shell elements in the deck slab and spring points elements with the resulting axial strains used to extract deformations (Sofistik AG, 2022b).

The change in force in the cable due to structural deformation in response to the temperature changes ($\Delta F_{due\ to\ structural\ deformation}$) was calculated as follows:

$$\Delta F_{due\ to\ structural\ deformation} = EA\ \frac{\Delta L}{L_i} \qquad 3.7$$

where:

- E = 158312 N/ mm^2 was the elastic modulus of the cable material
- A was the cross-sectional area of the cable using the effective diameter 70.8 mm^2
- L_i was the cable length (mm)
- ΔL was the change in the cable length extracted from the bridge's FEM after applying a ± 9℃ temperature range across the other bridge elements

Finally, the total change in force used to calculate the upper and lower bound limits was calculated using equation 3.8.

$$\Delta F_{total} = \Delta F_{cable} + \Delta F_{due\ to\ structural\ deformation} \qquad 3.8$$

For cables N1, N24, S1 and S24, the upper and lower bound values calculated for each cable were compared. The maximum upper and minimum lower bound values were then used as the governing

bounds for the cable group because these cables already had the design force in them as discussed in Section 3.2.4. A detailed calculation of the upper of lower bound force values considering the temperature effects can be found in Appendix E.

The evaluation criteria for the estimated forces was adapted from the Committee of Land Transport Officials (COLTO) specifications for the prestressing tendons. The estimated cable forces falling within the upper and lower bound region were considered to have 0% variation from the predicted forces whereas the percentage variation of forces that were not in the upper and lower bound region was calculated. The total variation between all the estimated cable forces and the predicted ones was checked to be in the ±3% range for them to be acceptable in this study (Committee of Land Transport Officials, 1998).

3.8 Effect of sockets

The effect of the sockets on the cable force was investigated by removing the sockets from the cable FEM and then extending the cable to the pin connection point as illustrated in Figure 3-35. The force in Model B was iterated until the natural frequency matched the one from site measurements before the cable force was evaluated.

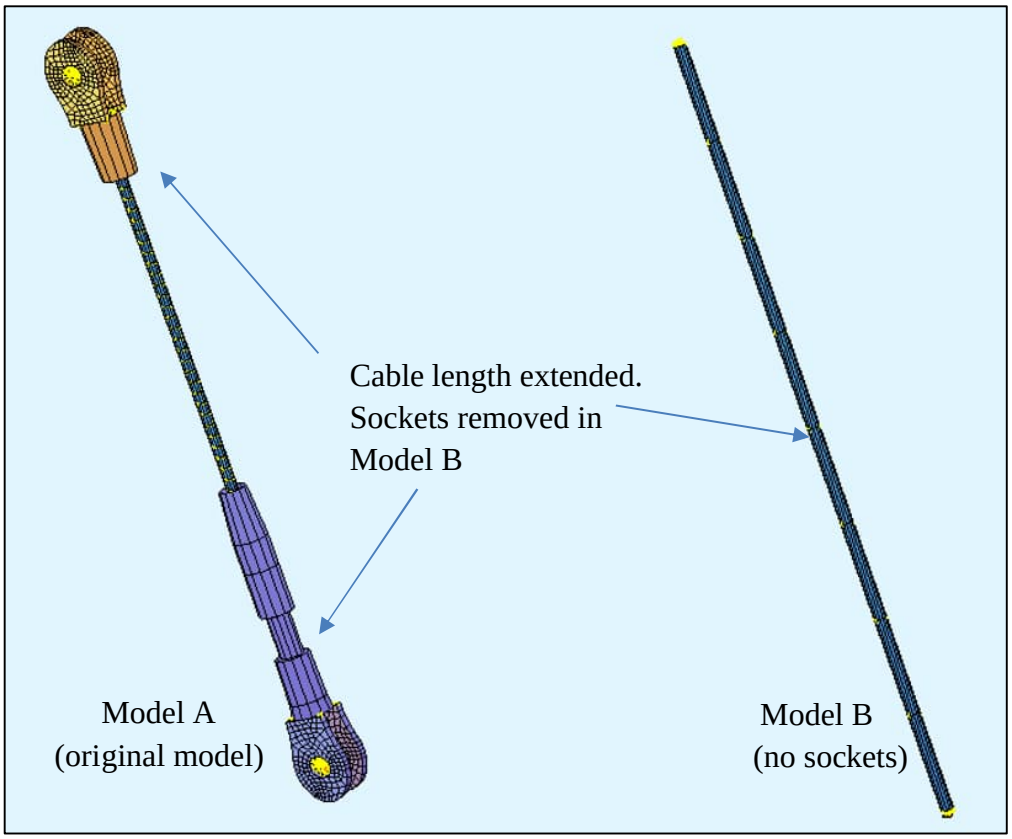

Figure 3-35 Model adjustment by removing sockets

In a second study, the stiffness values of the sockets were factored up and down and the resultant percentage change in the frequency of the cables was calculated.

3.9 Summary of Methodology

The site measurements took place on site on the 6th, 8th and 9th of December 2021 after the final stage of cable tensioning. The standard deviation and outlier checks were performed on the cable frequency measurements. Thereafter a FEM of each cable was created and validated. For short cables, the cable and beam element properties were used to model the cables followed by conducting a sanity check to select the analysis model. An iteration process involving the prestress force, form finding and frequency extraction was carried out until the frequencies in each cable FEM matched the one from the site measurements before the cable force was estimated. Temperature effects were used to create upper and lower bound limits of the estimated force relative to the predicted one. The estimated force was then evaluated by adapting a COLTO tendon prestressing specification to check the total variation of the estimated forces to be within ±3% from the predicted ones. The effects of the sockets on the cable natural frequencies and force were investigated by removing the sockets from each cable FEM and by also adjusting the socket stiffness parameters. Table 3-6 shows the final design forces evaluated.

Table 3-6: Final design forces evaluated

Cable Number (North and South)	Final Design Forces Predicted by the Bridge FEM (kN)
N1	788
N24	809
S1	639
S24	649
3 & 22	1203
5 & 20	1293
7 & 18	1373
9 & 16	1352
11 & 14	1301
4 & 21	634
8 & 17	627
12 & 13	836
2 & 23	986
6 & 19	737
10 & 15	664

4 Results and Discussion

4.1 Introduction

This chapter focuses on the calibration of the bridge's FEM as well as the extraction natural frequencies of the cables. The cable forces are also shown and evaluated. Lastly, the effect of the sockets on the force and natural frequencies of the cables is discussed. A summary of the findings is then provided.

4.2 Natural Frequencies

The bridge superstructure has an infinite number of degrees of freedom which can be simulated in its FEM. However, a limited number of the degrees of freedom can be measured experimentally. The measured frequencies from the full scale AVT were first compared to the ones predicted by the FEM at the end of construction and they matched qualitatively. The stiffness values of the springs in the FEM model were then adjusted as shown in Table 4-1 to get the measured and predicted frequency values to within 10% of each other. The numbers crossed out are the initial spring values and the numbers in green represent the new values for the calibrated model.

Table 4-1: Adjustment of spring stiffnness values

Bearing	Stiffness values in the Global axis (kN/m)			Stiffness values in the Local axis (kN/m)		
	x	y	z	x	y	z
W1 (fixed)	-	-	~~10 000 000~~ (25 000 000)	~~100 000~~ (110 000)	~~100 000~~ (150 000)	-
W2 (Unidirectional)	-	-	~~10 000 000~~ (25 000 000)	~~100 000~~ (110 000)	-	-
E1 (Unidirectional)	-	-	~~10 000 000~~ (25 000 000)	-	~~100 000~~ (150 000)	-
E2 (Multidirectional)	-	-	~~10 000 000~~ (25 000 000)	-	-	-

The calibrated FEM creates a benchmark tool which can be used in the data verification during future assessments. Cable natural frequencies can be measured, verified and isolated by checking the calibrated bridge FEM without the need for a full scale AVT. A selection of the experimentally determined natural frequencies as well as those from the bridge FEM are shown in Table 4-2. The mode shapes are also shown and classified. The frequencies predicted by the FEM were lower than the ones measured on site. This means that the structure is more rigid than initially modelled. Additionally, the close corelation between measured frequencies and the ones predicted by the

FEM is attributed to the modelling of the arch, tie beam and deck concrete elements with self-weight and stiffness parameters that considered the actual reinforcement quantity and material test results. The post tensioning forces in the beams were also modelled as part of the superstructure. The measured cable frequencies and the ones from the analytical models are presented in Table 4-3

Table 4-2: Comparison between measured frequencies and FEM predicted ones

Type of Mode and Shape	Measured Frequency (Hz)	Predicted Frequency (Hz)	% Difference
Deck 1st Bending Mode 	0.81	0.81	0
Arch Antisymmetric Mode Deck 1st Bending Mode 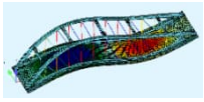	1.13	1.18	4
Arch Symmetric Mode Deck 2nd Bending Mode 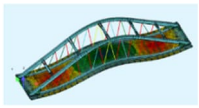	1.81	1.74	4
Arch Lateral Bending Mode Deck 1st Torsional Mode 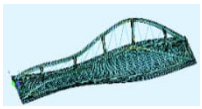	2.06	1.92	7
Deck 2nd Torsional Mode 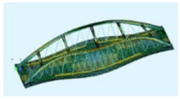	2.38	2.19	8
Arch Symmetric Mode Deck 2nd Mode 	3.06	2.80	9
Deck 3rd Bending Mode 	5.19	4.82	7

Table 4-3: Cable frequencies

Cable	North Arch First Natural Frequencies (Hz)		South Arch First Natural Frequencies (Hz)	
	Measured	Analytical Model	Measured	Analytical Model
1	17.50	17.44 (cable element) 17.46 (beam element)	27.10	27.33 (cable element) 27.28 (beam element)
2	12.07	12.07	11.60	11.60
3	13.43	13.40	12.70	12.70
4	6.35	6.34	6.34	6.34
5	9.77	9.74	9.52	9.51
6	5.61	5.58	5.37	5.36
7	7.32	7.32	7.32	7.32
8	4.27	4.26	4.52	4.51
9	6.34	6.34	6.34	6.34
10	4.40	4.41	4.15	4.15
11	5.61	5.62	5.61	5.62
12	4.52	4.53	4.51	4.52
13	4.64	4.62	4.64	4.62
14	5.73	5.72	5.73	5.72
15	4.39	4.39	4.39	4.39
16	6.34	6.34	6.10	6.10
17	4.39	4.38	4.51	4.50
18	7.44	7.42	7.44	7.42
19	5.73	5.72	5.49	5.50
20	9.52	9.51	9.50	9.51
21	6.47	6.45	6.71	6.73
22	14.77	14.79	14.28	14.27
23	11.60	11.60	11.60	11.60
24	29.90	29.91 (cable element) 29.95 (beam element)	24.20	24.00 (cable element) 24.04 (beam element)

Table 4-4 shows the statistical analysis of the measured cable frequencies.

Table 4-4: Statistical analysis of measured cable frequencies

Group No.	Cables	Measured Frequencies in Group (both North and South Arch) (Hz)				Mean (Hz)	Standard Deviation
1	1 & 24	17.5	27.1	29.9	24.2	24.68	5.32
2	2 & 23	12.07	11.6	11.6	11.6	11.72	0.24
3	3 & 22	13.43	12.7	14.77	14.28	13.80	0.92
4	4 & 21	6.35	6.34	6.47	6.71	6.47	0.17
5	5 & 20	9.77	9.52	9.52	9.5	9.58	0.13
6	6 & 19	5.61	5.37	5.73	5.49	5.55	0.15
7	7 & 18	7.32	7.32	7.44	7.44	7.38	0.07
8	8 & 17	4.27	4.52	4.39	4.51	4.42	0.12
9	9 & 16	6.34	6.34	6.34	6.1	6.28	0.12
10	10 & 15	4.4	4.15	4.39	4.39	4.33	0.12
11	11 & 14	5.61	5.61	5.73	5.73	5.67	0.07
12	12 & 13	4.52	4.51	4.64	4.64	4.58	0.07

There was a great variation in the measured frequencies in the bridge's shortest cables (Group 1) as seen by the standard deviation. The measurement 17.45 *Hz* from group 1 appears to be an outlier because it has the largest deviation from the mean of the data set. However, it was not considered as an outlier because of the following:

i) When the tests were being conducted, 6 cables were tested at a time. If there was indeed an error in the measurements it would have shown in the results of the other 5 cables. This was not the case,
ii) As can be seen in Figure 4-1, the test result does not pass the criteria check for it to be considered as an outlier.

Outlier Check for Group 1 cables:

x_0 (test result) = 17.5 *Hz*; $\bar{x}_n$ (mean) = 24.68 *Hz*; S_n (standard deviation) = 5.32; Sample size = 4; Critical value for outlier check = 1.46;

$$T_o = \frac{(x_0 - \bar{x}_n)}{S_n} = \frac{(17.5 - 24.68)}{5.32} = -1.35$$

Absolute value of T_o = 1.35 is less than the Critical value (1.46). Therefore, the test result 17.5 *Hz* is not an outlier.

Figure 4-1: Outlier test for measured frequency

However, the variation in the measured frequency of N1 differs markedly from the other cables with similar geometric properties. An AVT should be redone on that cable before the principal bridge inspections.

The mode shapes of all the cables are qualitatively similar but their frequencies are different because of the different geometry and layout of the cables. Additionally, the proportions of the sockets to the entire cable system are different for each cable. The effect of the sockets is discussed in detail in section 4.4. Figure 4-2 and Figure 4-3 show the typical mode shapes in the central longitudinal plane of the bridge in which the site measurements were taken for all the cables modelled using the cable element and beam element property respectively.

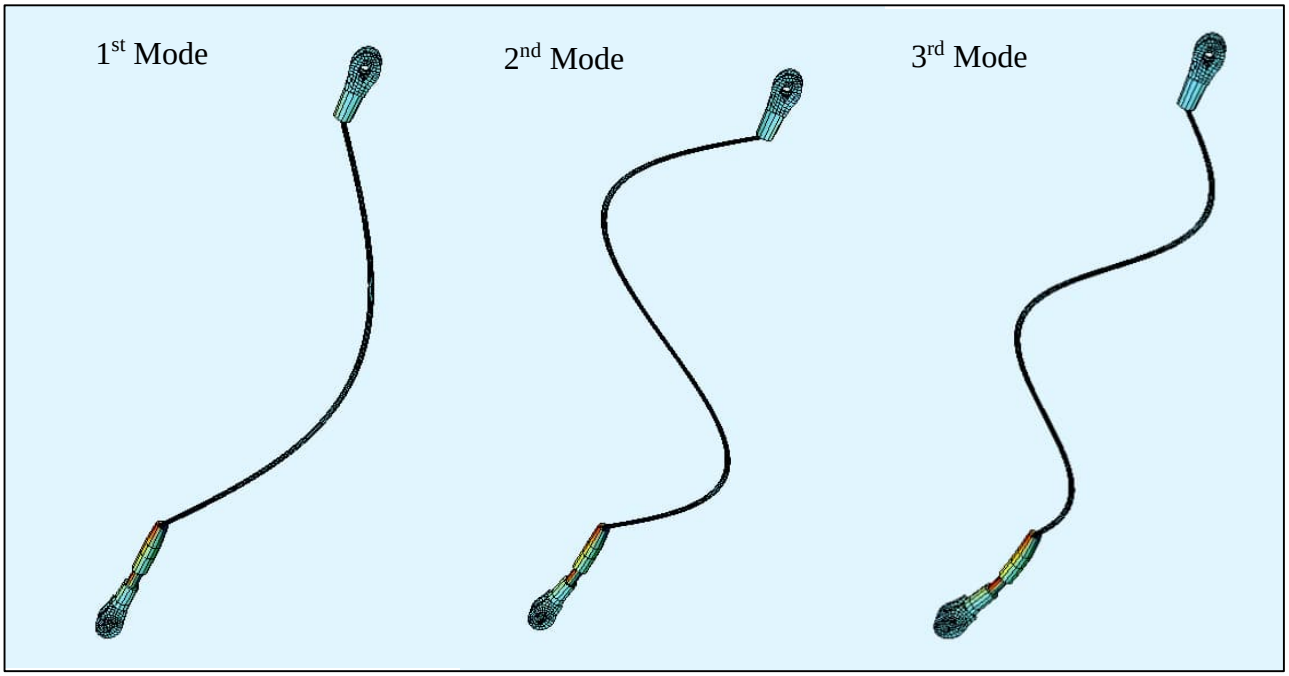

Figure 4-2: Typical mode shapes of the cables in the central longitudinal plane of the bridge (cable element analytical mode)

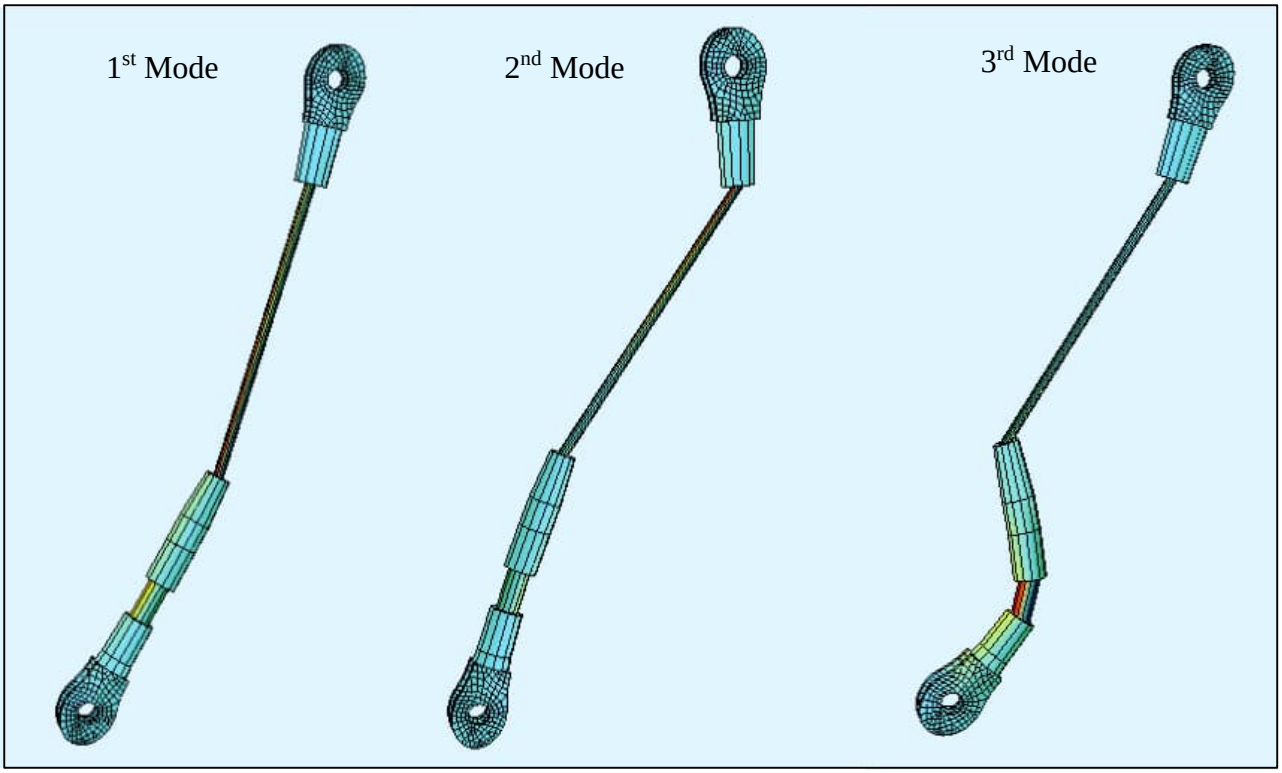

Figure 4-3: Typical mode shapes of the cables in the central longitudinal plane of the bridge (beam element analytical mode)

4.3 Cable Forces

The estimated forces from the analytical models used for the short cables are shown in Table 4-5.

Table 4-5: Estimated forces in the short cable analytical models

Cable	Estimated Force in Cable Element Model (kN)	Estimated force in Beam Element Model (kN)
N1	183	1235
N24	656	4074
S1	501	3321
S24	364	2516

The forces estimated in the model that used the beam element property were substantially higher than the ones in the model that used the cable element property. This shows that the short cables did not behave as tensioned beams entirely but rather their behaviour was a hybrid of the cable and beam action. According to the hydraulic jack calibration certificates, the pairs of hydraulic jacks

that were used to tension the cables (1 of the 2 shown in Figure 4-4) had a combined force output capacity of just over 2000 kN. The tensioning force of the cables was also higher than the final forces shown in Table 4-5 due to the redistribution of forces discussed in section 3.2.4. This made 3 of the results (N24, S1 and S24) from the beam analytical model invalid. Thus, the cable element analytical model was selected as the analysis model for the short cables.

Figure 4-4: Pair of hydraulic jacks (in red) used to tension a cable

The estimated forces for the North and South Arch cables are presented in Table 4-6 and Table 4-7 respectively. Firstly, the estimated force from the analytical model is shown then the predicted force and bounds calculated considering the temperature effects are presented in the following columns. Lastly, the estimated force is checked if it falls within the upper and lower region of tension values. For the estimated forces that did not fall within the upper and lower bound regions, a percentage deviation was calculated and is presented. Figure 4-5 is a combined graphical presentation of the results from the Table 4-6 and Table 4-7.

Table 4-6: North arch cable forces

Cable Number	Estimated Force (kN)	Force predicted by Bridge FEM (kN)	Bounds due to Temperature Range (kN)		% Deviation from Predicted Force Bound
			Upper Bound	Lower Bound	
1	182	788	1022	426	-57.32%
2	845	986	1064	908	-6.86%
3	1076	1203	1260	1146	-6.09%
4	578	634	706	562	Within bound
5	1424	1293	1362	1224	4.53%
6	741	737	812	662	Within bound
7	1304	1373	1444	1302	Within bound
8	570	627	702	552	Within bound
9	1293	1352	1426	1278	Within bound
10	714	664	743	585	Within bound
11	1172	1301	1379	1223	-4.25%
12	793	836	914	758	Within bound
13	823	836	914	758	Within bound
14	1215	1301	1379	1223	-0.73%
15	709	664	743	585	Within bound

Table 4-6: North arch cable forces (cont.)

Cable Number	Estimated Force (kN)	Force predicted by Bridge FEM (kN)	Bounds due to Temperature Range (kN)		% Deviation from Predicted Force Bound
			Upper Bound	Lower Bound	
16	1293	1352	1426	1278	Within bound
17	605	627	702	552	Within bound
18	1343	1373	1444	1302	Within bound
19	779	737	812	662	Within bound
20	1356	1293	1362	1224	Within bound
21	599	634	706	562	Within bound
22	1326	1203	1260	1146	5.22%
23	778	986	1064	908	-14.26%
24	656	809	1022	426	Within bound

Table 4-7: South arch cable forces

Cable Number	Estimated Force (kN)	Force predicted by Bridge FEM (kN)	Bounds due to Temperature Range (kN)		% Deviation from Predicted Force Bound
			Upper Bound	Lower Bound	
1	501	639	1022	426	Within bound
2	778	986	1064	908	-14.26%
3	961	1203	1260	1146	-16.16%
4	578	634	706	562	Within bound
5	1356	1293	1362	1224	Within bound
6	682	737	812	662	Within bound
7	1304	1373	1444	1302	Within bound
8	642	627	702	552	Within bound
9	1293	1352	1426	1278	Within bound
10	630	664	743	585	Within bound
11	1172	1301	1379	1223	-4.25%
12	788	836	914	758	Within bound
13	823	836	914	758	Within bound
14	1215	1301	1379	1223	-0.73%
15	709	664	743	585	Within bound
16	1195	1352	1426	1278	-6.53%
17	637	627	702	552	Within bound
18	1343	1373	1444	1302	Within bound
19	718	737	812	662	Within bound
20	1356	1293	1362	1224	Within bound

Table 4-7: South arch cable forces (cont.)

Cable Number	Estimated Force (kN)	Force predicted by Bridge FEM (kN)	Bounds due to Temperature Range (kN)		% Deviation from Predicted Force Bound
			Upper Bound	Lower Bound	
21	653	634	706	562	Within bound
22	1230	1203	1260	1146	Within bound
23	778	986	1064	908	-14.26%
24	364	649	1022	426	-16.66%

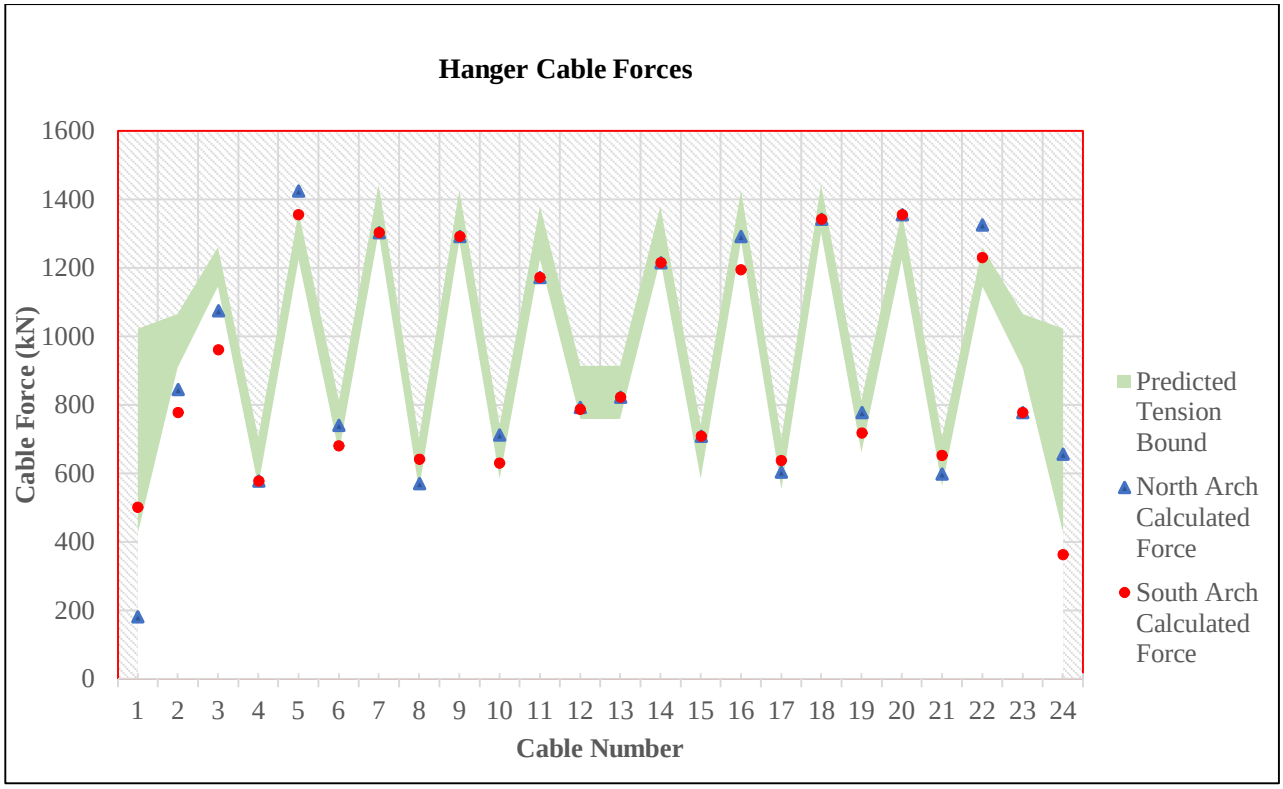

Figure 4-5: Calculated force in relation to the predicted force area

As can be seen from Table 4-6, Table 4-7 and Figure 4-5, most of the calculated forces are within the predicted force bound. However, Cables N1, N24, S1 and S24 show varying deviations from the predicted force region. Cable N1 shows the largest variation of just over 57%. Cable N24 and S1's forces are within the predicted area whereas cable S24 deviates by 16.66% from the predicted force area. The reason for the varying deviations from the predicted force in these cables is that the forces in the short cables are very sensitive to temperature changes. The formulations of the change in force are repeated here in equations 4.1, 4.2 and 4.3.

$$\Delta F_{cable} = EA\varphi\Delta T \quad (4.1)$$

$$\Delta F_{due\ to\ structural\ deformation} = EA\frac{\Delta L}{L_i} \quad (4.2)$$

$$\Delta F_{total} = \Delta F_{cable} + \Delta F_{due\ to\ structural\ deformation} \quad (4.3)$$

The ΔF_{cable} component of the change in force is the same for all cables. However, the magnitude of the $\Delta F_{due\ to\ structural\ deformation}$ component is dependent on the strain experienced by the cable $\left(\frac{\Delta L}{L_i}\right)$. The larger the change in length (ΔL) for a given length of cable (L_i), the higher the magnitude of $\Delta F_{due\ to\ structural\ deformation}$. Figure 4-6 shows that the strain in the shortest cables (1 & 24) is very sensitive to changes in length.

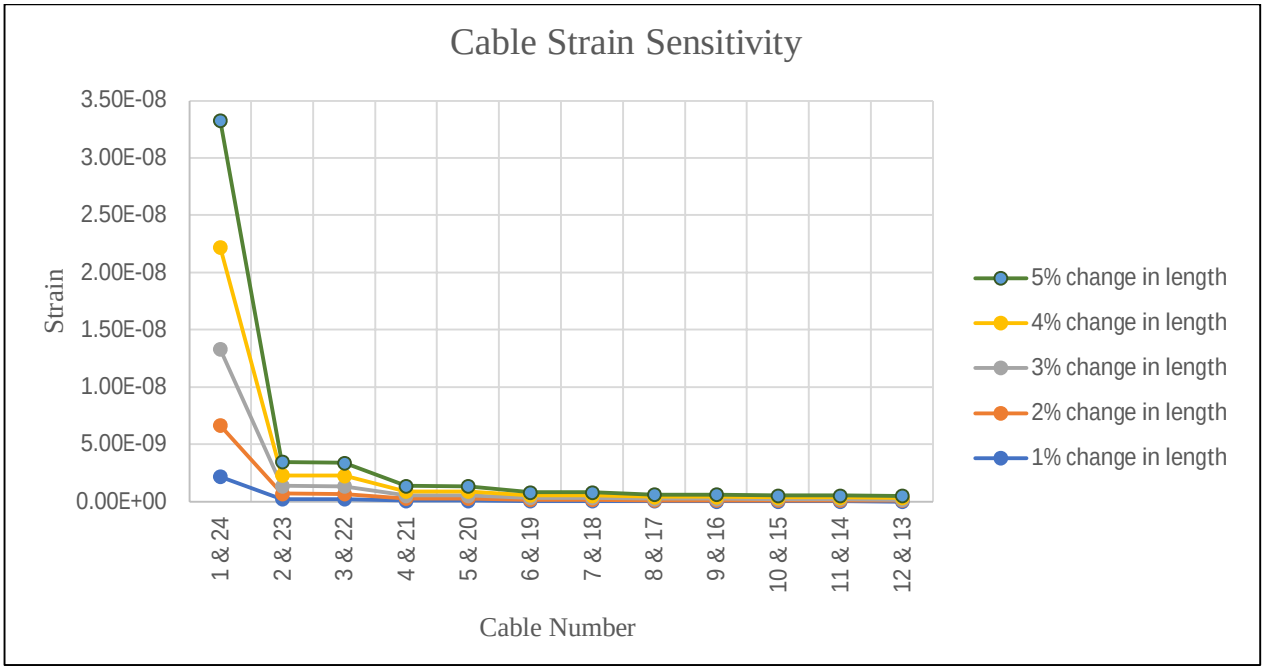

Figure 4-6: Strain parameter sensitivity to changes in length

The shortest cables in the bridge are also located adjacent to the spring points. An application of the temperature range across all the elements in the bridge's FEM shows that the spring points experience greater deformations than the rest of the elements in the bridge as can be seen in Figure 4-7. This deformation then translates to a larger change in length for the cables 1 and 24. A larger change in length means that $\Delta F_{due\ to\ structural\ deformation}$ will be larger for the shortest cables and hence ΔF_{total} for the shortest cables will also be the largest as shown in Table 4-8. For cables 1 and 24 the predicted force bound will have the largest region (Predicted Force ±213). Consequently, cables 1 and 24 experience very high variations in their forces than the other cables in the bridge. Hence these cables should be inspected in detail for fatigue during the bridge maintenance work.

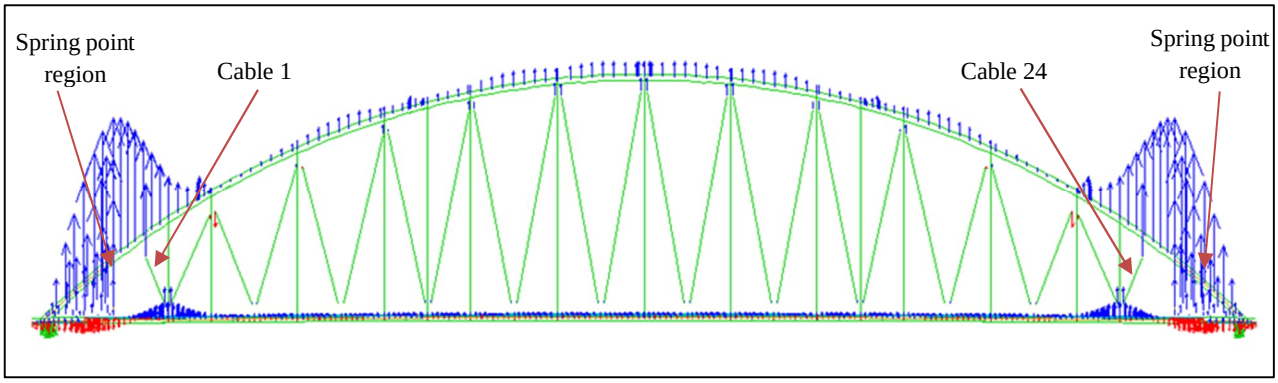

Figure 4-7: Temperature induced deformation along the structural elements

Table 4-8: Force changes due to temperature effects

Cable Number	ΔF_{cable} (kN)	$\Delta F_{due\ to\ structural\ deformation}$ (kN)	ΔF_{total} (kN)
1 & 24	70	142	213
2 & 23	70	8	78
3 & 22	70	-13	57
4 & 21	70	2	72
5 & 20	70	-1	69
6 & 19	70	5	75
7 & 18	70	1	71
8 & 17	70	5	75
9 & 16	70	4	74
10 & 15	70	8	79
11 & 14	70	7	78
12 & 13	70	8	78

Cables N2, N23, S2 & S23 as well N3, N22, S3 and S22 also show varying deviations with some results being in the predicted force bound whereas some being more than 10% out of the predicted force area. This shows that as the cables become shorter, they start to incorporate beam behaviour because the proportions of the sockets become larger and more influential in the cable system. This is expanded on when the stiffness effects of the sockets are discussed in section 4.4.

Due to the large variations in the forces of cables 1 and 24 on both arches compared to other cable groups in the bridge, the primary method for engineer's approval which were the lift-off tests were relied upon to ensure that the design force was achieved in the cables. The total average variation of the estimated forces from the predicted forces was -3.18%. This is deemed acceptable although it is slightly over the ±3% specification in the COLTO specification because of the N1 result which was not considered as an outlier and will need to be verified. Table 4-9 shows the detailed percentage variations from the predicted force for each cable.

Table 4-9: Estimated force verdict

Cable Number	North Arch		South Arch	
	Estimated Force (kN)	% Variation	Estimated Force (kN)	% Variation
1	182	-57.32%	501	0.00%
2	845	-6.86%	778	-14.26%
3	1076	-6.09%	961	-16.16%
4	578	0.00%	578	0.00%
5	1424	4.53%	1356	0.00%
6	741	0.00%	682	0.00%
7	1304	0.00%	1304	0.00%
8	570	0.00%	642	0.00%
9	1293	0.00%	1293	0.00%
10	714	0.00%	630	0.00%
11	1172	-4.25%	1172	-4.25%
12	793	0.00%	788	0.00%
13	823	0.00%	823	0.00%
14	1215	-0.73%	1215	-0.73%
15	709	0.00%	709	0.00%
16	1293	0.00%	1195	-6.53%
17	605	0.00%	637	0.00%

Table 4-9: Estimated force verdict (cont.)

Cable Number	North Arch		South Arch	
	Estimated Force (kN)	% Variation	Estimated Force (kN)	% Variation
18	1343	0.00%	1343	0.00%
19	779	0.00%	718	0.00%
20	1356	0.00%	1356	0.00%
21	599	0.00%	653	0.00%
22	1326	5.22%	1230	0.00%
23	778	-14.26%	778	-14.26%
24	656	0.00%	364	-16.66%
Total Average Variation		-3.18%		
Verdict		Accepted		

4.4 Effects of Sockets

Figure 4-8 and Figure 4-9 shows the comparison of calculated forces from models with sockets and models without sockets.

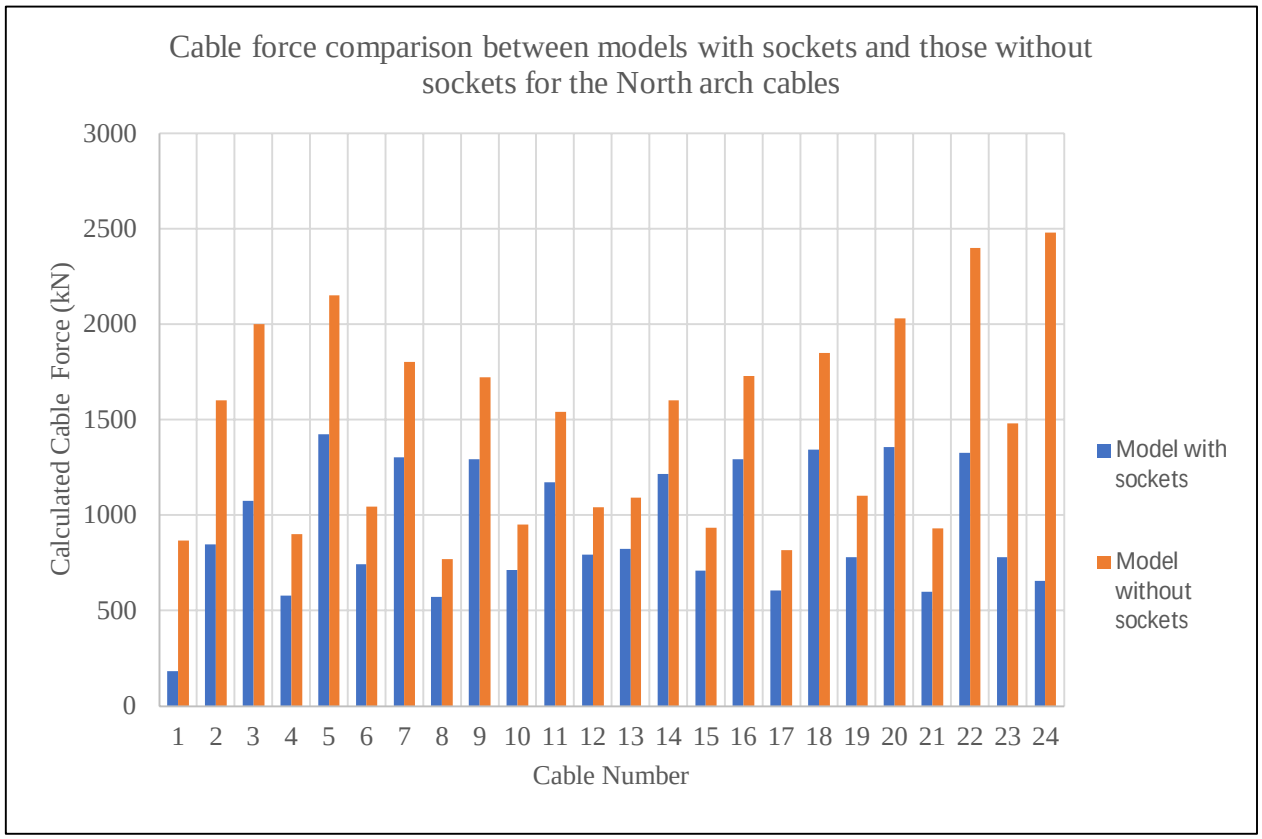

Figure 4-8: Force comparison between models with sockets and models without sockets for the north arch cables

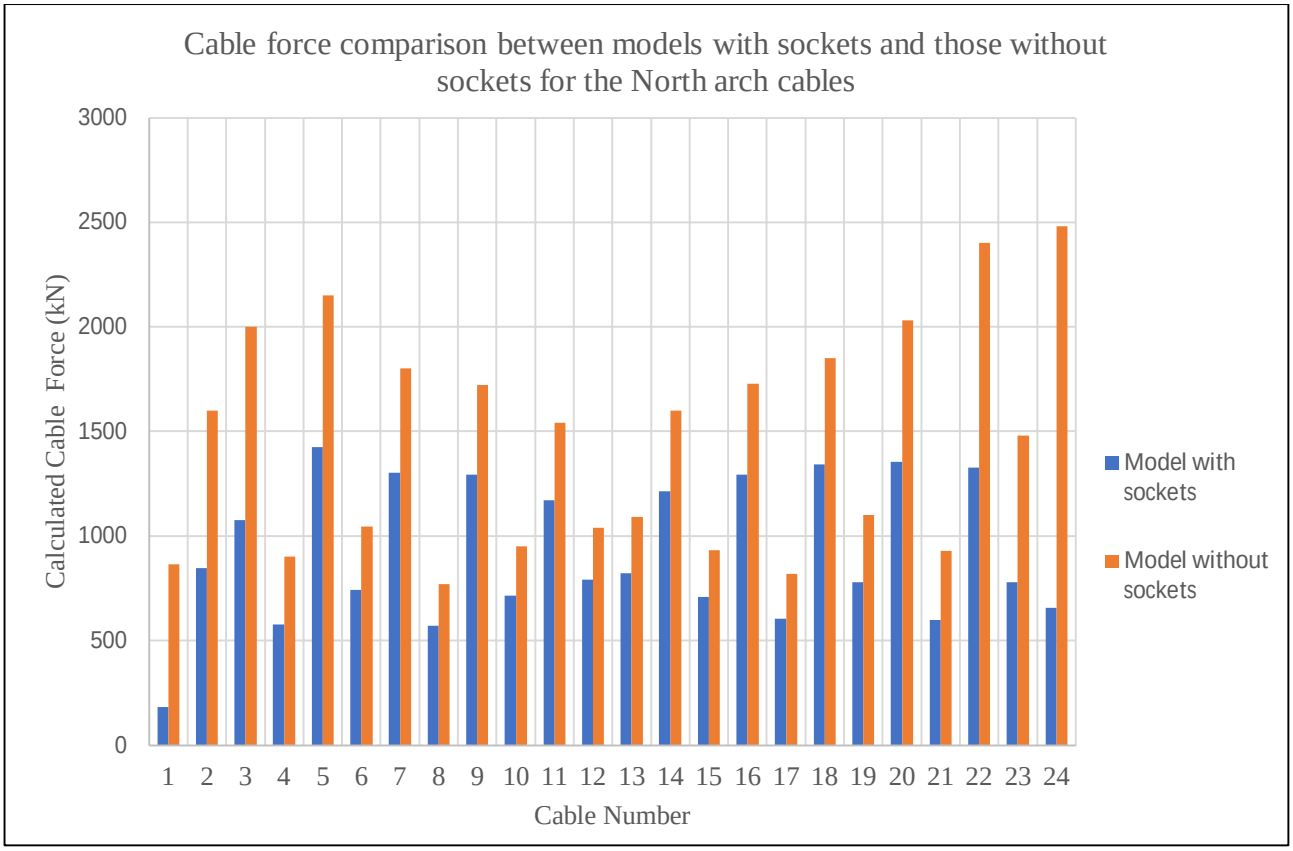

Figure 4-9: Force comparison between models with sockets and models without sockets for the south arch cables

The estimated forces in the models without the sockets are higher than those estimated in models containing sockets because when the sockets are removed the length of the cable increases. From the fundamental vibration theory, the force in a cable is directly proportional to the square of its length $\left(T \propto {L_c}^2\right)$. Hence it follows that the force in the cable will increase substantially with an increase in the cable length. A key observation in the differences between the models is that the percentage difference between the estimated forces increases significantly from the longest (12 and 13) to the shortest cables (1 and 24) as illustrated in Table 4-10.

Table 4-10: Estimated force comparison

Cable Number	North Arch Cables			South Arch Cables		
	Estimated Force from Model with sockets (kN)	Estimated Force from Model without sockets (kN)	% Difference	Estimated Force from Model with sockets (kN)	Estimated Force from Model without sockets (kN)	% Difference
1	182	865	375.33%	501	2100	318.89%
2	845	1600	89.27%	778	1458	87.37%
3	1076	2000	85.83%	961	1780	85.31%
4	578	900	55.69%	578	880	52.24%
5	1424	2150	50.98%	1356	2030	49.76%
6	741	1046	41.03%	682	960	40.88%
7	1304	1801	38.08%	1304	1801	38.08%
8	570	770	35.15%	642	880	37.11%
9	1293	1721	33.11%	1293	1721	33.11%
10	714	950	33.19%	630	855	35.76%
11	1172	1541	31.50%	1172	1541	31.50%
12	793	1041	31.25%	788	1041	32.07%
13	823	1091	32.45%	823	1091	32.50%
14	1215	1601	31.78%	1215	1601	31.78%
15	709	933	31.69%	709	933	31.69%
16	1293	1729	33.73%	1195	1631	36.50%
17	605	817	35.17%	637	880	38.18%
18	1343	1851	37.84%	1343	1851	37.84%

Table 4-10: Estimated force comparison (cont.)

Cable Number	North Arch Cables			South Arch Cables		
	Estimated Force from Model with sockets (kN)	Estimated Force from Model without sockets (kN)	% Difference	Estimated Force from Model with sockets (kN)	Estimated Force from Model without sockets (kN)	% Difference
19	779	1101	41.34%	718	995	38.63%
20	1356	2030	49.76%	1356	2030	49.76%
21	599	930	55.35%	653	990	51.57%
22	1326	2400	81.00%	1230	2250	82.93%
23	778	1480	90.19%	778	1480	90.19%
24	656	2400	277.92%	656	2400	571.02%

The increase in the percentage differences is influenced by proportions of the components of the cable. As seen in Table 4-11, the sockets make up more than 50% of the short cable system (1 and 24). Hence the removal of the sockets in these cable systems will have a greater impact on the estimated force than in the longest cables (12 and 13) in which the sockets make up about 13 % of the cable system.

Table 4-11: Components of the cable system

Cable No.	Pin-Pin length (mm)	% Fork Socket Part	% Adjustable Fork Socket Part	% Cable Part
1 & 24	4654	15.26%	39.11%	45.64%
2 & 23	9124	7.78%	19.95%	72.27%
3 & 22	9195	7.72%	19.79%	72.49%
4 & 21	13051	5.44%	13.95%	80.61%
5 & 20	13147	5.40%	13.84%	80.76%
6 & 19	16033	4.43%	11.35%	84.22%
7 & 18	16118	4.41%	11.29%	84.30%
8 & 17	18111	3.92%	10.05%	86.03%
9 & 16	18172	3.91%	10.02%	86.08%
10 & 15	19344	3.67%	9.41%	86.92%
11 & 14	19374	3.66%	9.39%	86.94%
12 & 13	19760	3.59%	9.21%	87.20%

In a second study, the stiffness values of the sockets were factored up and down to investigate the changes in the frequency of the cables as shown in Figure 4-10 and Figure 4-11. Increasing the stiffness of the sockets makes less than 6% difference to the frequencies because the sockets are inherently very stiff members at their initial stiffness value. However, a decrease in the stiffness values has a more significant effect on the frequency in the cables. The sockets act as rigid supports at the ends of the cables. Hence, a decrease in the stiffness, makes the ends less rigid which translates to a decrease in the frequency of the cable. The changes in the frequency are more pronounced in the shorter cables because the socket proportion of the entire cable system is greater in the shorter cables as shown in Table 4-11.

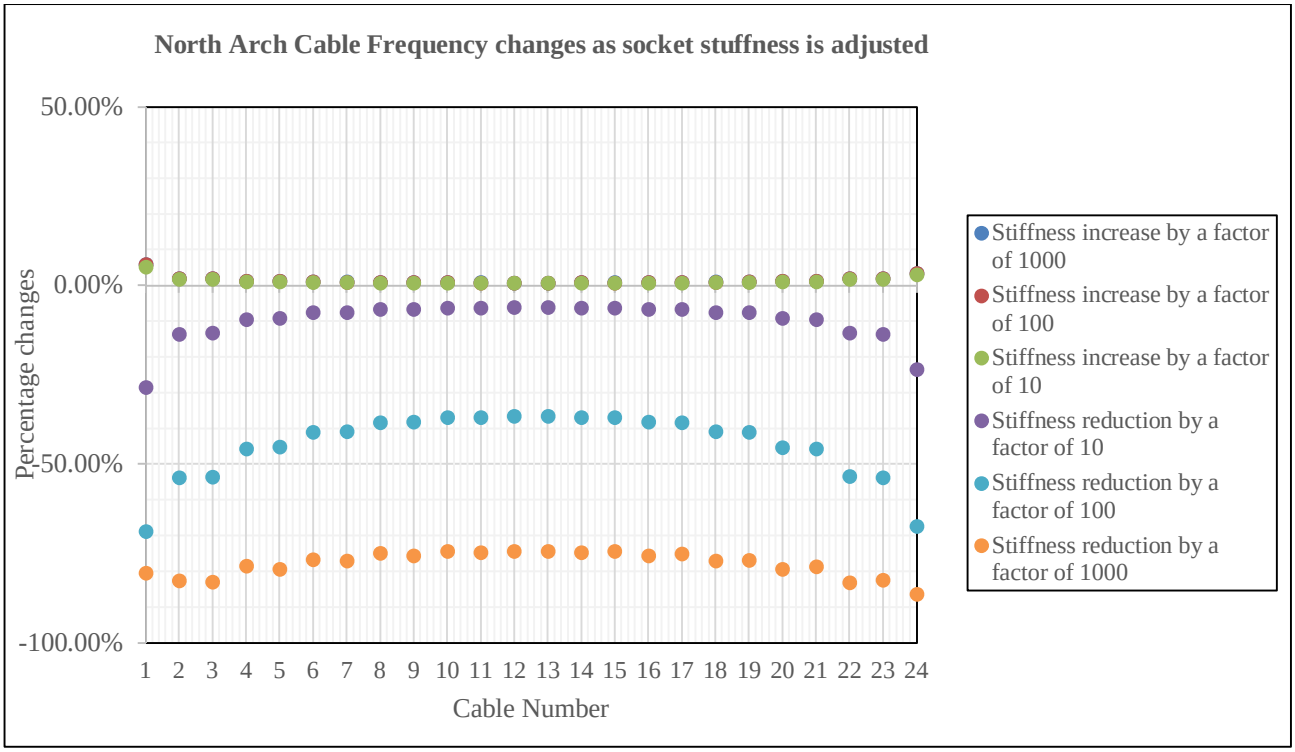

Figure 4-10: Frequency changes in the north arch cables as socket stiffness is adjusted

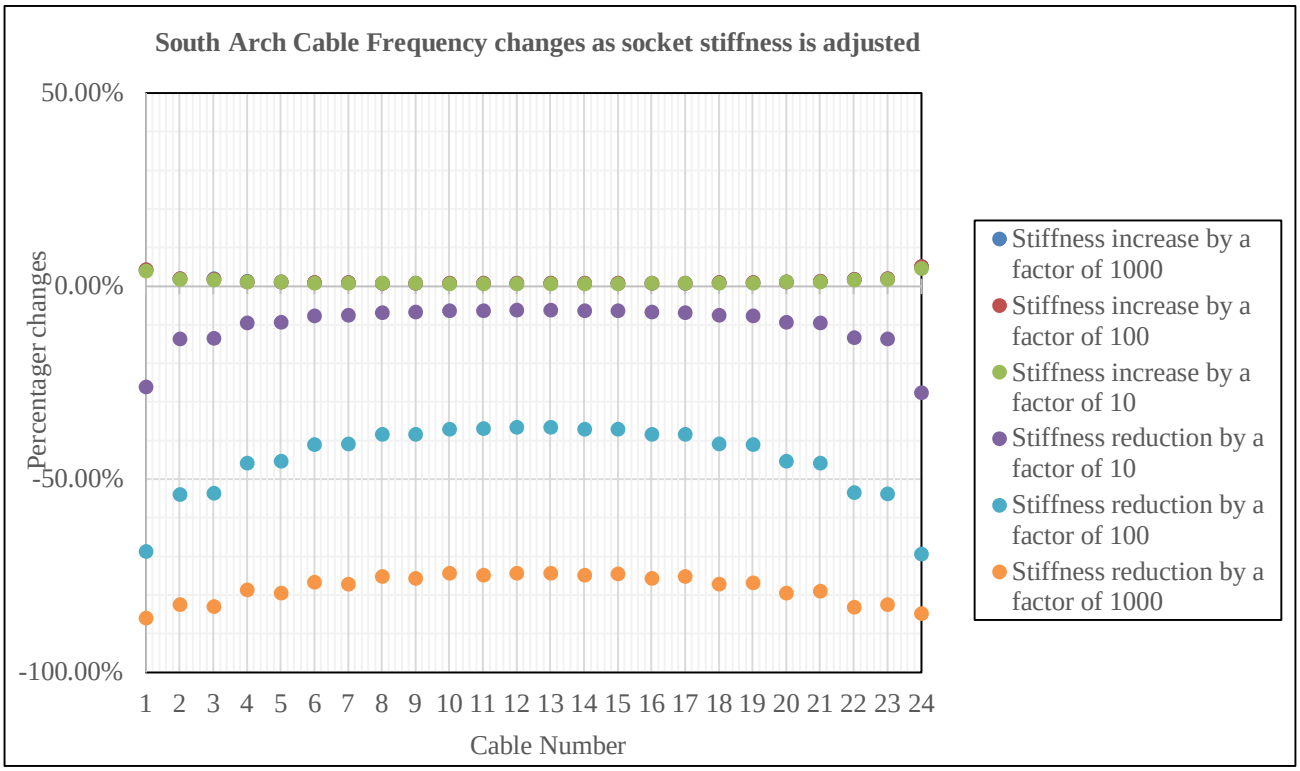

Figure 4-11: Frequency changes in the south arch cables as socket stiffness is adjusted

4.5 Summary of the Results and Discussions

The measured frequencies from the full-scale vibration tests corelated well with the ones predicted from the FEM at the end of construction. The main reason for the close corelation was that the arch, tie beam and deck concrete elements were modelled with self-weight and stiffness parameters that considered the actual reinforcement quantities and material tests results. Additionally, the post tensioning forces in the beams were also modelled as part of the superstructure. The spring stiffness values in the model were increased to get the measured frequencies and the model ones to within 10% of each other and thus create a benchmark calibrated model that can be used to isolate cable frequencies for the present and future tests. The frequencies and mode shapes of the cables were then presented after the calibration of the model.

The cable forces mostly matched the predicted ones with the total variation being -3.18% between the two. However, an individual cable variation check showed that as the cable length decreased, the variation between the predicted force and the force estimated from measured data increased. The forces in the bridge's shortest cables exhibited varying deviations from the predicted forces due to those cables' high sensitivity to temperature changes. A second measurement on the short cables adjacent to the spring points will be needed prior to the principal bridge inspections to ascertain the large variations in the forces observed in those cables. However, the primary method for engineer's approval relied on lift-off tests that ensured that the design force was achieved in all cables. The cables adjacent to the spring points must be inspected for fatigue during the principal bridge inspections.

The deviation of estimated forces from the predicted forces increases as the cable lengths decrease. This suggests that the cables start exhibiting beam behaviour because the proportions of sockets become larger in the cable system.

The fork sockets play an appreciable role in the forces and frequencies of the cables. Their removal from the analytical models coupled with the extension of the cable length to the pin connections results in the forces in the cables being overestimated. Factoring up the stiffness of the sockets results in a negligible increase in the frequency of the cable because the sockets are inherently very stiff components. However, factoring down the stiffness results in a large decrease in the frequencies of the cables because the cables become less restrained at the ends. The stiffness changes are also more pronounced in the shorter cables because the sockets form a larger part of those cable systems.

5 Conclusion and Recommendations

AVT provides a non-destructive method of checking the cable forces during and after construction. The objective of this study was to evaluate the cable forces at the Ashton Bridge as well as to investigate the effect of the fork sockets on the dynamic properties of the cables. The following sections provide the conclusions and recommendations pertaining to the study.

5.1 Conclusions

Analytical models of each cable were created and validated. Additionally, the bridge's FEM was calibrated using the results from the full scale AVT. The following conclusions were drawn based on the results from this dissertation:

i. The total variation between the forces estimated from the measured data and the forces predicted by the bridge's FEM is -3.18%. A second measurement on the short cables adjacent to the spring points will be needed prior to the principal bridge inspections to ascertain the large variations in the forces observed in those cables. The primary method for engineer's approval relied on lift-off tests that ensured that the design force was achieved in the cables,

ii. There is a large variation in forces in the short cables particularly in the ones adjacent to the spring points because they are more sensitive to temperature effects. The cables must be inspected for fatigue during the principal bridge inspections,

iii. The sockets are stiff elements that control the frequency in the cables depending on their proportion in the cable system. Hence, they should be modelled accurately to simulate the geometric and material properties,

iv. The effective length of the cable is essentially the length between the sockets. Any alteration of this value such as using the pin-to-pin length and disregarding the sockets results in the cable force being overestimated,

v. AVT can be conducted under operating conditions with minimal disruption to traffic,

vi. A full-scale dynamic test can be used to evaluate the stiffness of the bearings in the main model as part of the calibration exercise.

5.2 Recommendations

The following recommendations are given for future work pertaining to checking forces at the Ashton bridge as well as any other bridge with similar cable systems:

i. All asphalt paving and handrail works should be concluded prior to the final stage of tensioning. This would cut out the need to factor the additional load into the FEM to determine the forces to be evaluated through AVT after the final stage of tensioning,

ii. The short cables near the spring points must be inspected thoroughly for fatigue because of the large variation in their forces.

iii. A further study on the characterisation of the cable behaviour is needed. As the length of a cable decreases, the socket proportions become larger and more influential in the cable system behaviour. As a result, the cable may start to behave more as a beam than a cable. However, the point at which the cable transitions to beam behaviour or the combination of the cable and beam behaviour is not known and therefore requires further research,

iv. Future investigations on the effect of the bending stiffness especially in short cables should be carried out,

v. After the final tensioning sequence of the cables, lift-off tests should be conducted on all cables. This would provide an additional tool to compare and verify the forces predicted by the model as well as the ones determined through AVT.

6 References

Abramson, L.W. & Green, G.E. 1985. *Reliability of Strain Gauges and Load Cells for Geotechnical Engineering Applications.* Libary of Congress Cataloging in Publication Data. DOI: 10.1016/0148-9062(86)91794-8.

AccuWeather. 2021. *Ashton Western Cape South Africa Monthly Weather*. Available: https://www.accuweather.com/en/za/ashton/301231/december-weather/301231?year=2021 [2022, September 29].

BDI. 2020. *ST350 Strain Transducer*. Available: https://bditest.com/product/st350-strain-transducer/ [2022, July 24].

Bletzinger, K.U. & Ramm, E. 1999. A general finite element approach to the form finding of tensile structures by the updated reference strategy. *International Journal of Space Structures*. 14(2):131–144. DOI: 10.1260/0266351991494759.

Brownjohn, J.M.W., Dumanoglu, A.A. & Severn, R.T. 1992. Ambient vibration survey of the fatih sultan mehmet (second Bosporus) suspension bridge. *Earthquake Engineering & Structural Dynamics*. 21(10):907–924. DOI: 10.1002/eqe.4290211005.

Brüel & Kjær. n.d. *Type 8210*. Available: https://www.bksv.com/en/transducers/vibration/impact-hammers/8210 [2022, July 24].

British Standards Institution. 1991 *BS 3100 Steel castings for general engineering purposes*. Board of BSI

Caetano, E. 2007. *Cable Vibrations in Cable-Stayed Bridges*. SED 9th ed. Zürich, Switzerland: International Association for Bridge and Structural Engineering. DOI: 10.2749/sed009.

Caetano, E., Bartek, R., Magalhães, F., Keenan, C. & Trippick, G. 2013. Assessment of cable forces at the London 2012 Olympic Stadium roof. *Structural Engineering International: Journal of the International Association for Bridge and Structural Engineering (IABSE)*. 23(4):489–500. DOI: 10.2749/101686613X13627351081713.

Chang, C.C., Chang, T.Y.P. & Zhang, Q.W. 2001. Ambient vibration of Long-Span Cable-Stayed Bridge. *Journal of Bridge Engineering*. 6(1):46–53.

Chen, C.C., Wu, W.H., Chen, S.Y. & Lai, G. 2018. A novel tension estimation approach for elastic cables by elimination of complex boundary condition effects employing mode shape functions. *Engineering Structures*. 166:152–166. DOI: 10.1016/j.engstruct.2018.03.070.

Cho, S., Yim, J., Shin, S.W., Jung, H.-J., Yun, C.-B. & Wang, M.L. 2013. Comparative Field Study of Cable Tension Measurement for a Cable-Stayed Bridge. *Journal of Bridge Engineering*. 18(8):748–757. DOI: 10.1061/(asce)be.1943-5592.0000421.

Committee of Land Transport Officials. 1998. Standard Specifications for Road and Bridge Works for State Road Authorities. Halfway House: South African Institute of Civil Engineers

Geier, R., De Roeck, G. & Petz, J. 2005. Cable Force Determination for the Danube Channel Bridge in Vienna. *Structrual Engineering International*. (3):182–185.

Irvine, H.M. 1981. Dynamics of a suspended cable. In *Cable Structures*. The MIT Press. 87–133.

Irvine, H.M. & Caughey, T.K. 1974. The linear theory of free vibrations of a suspended cable. In *Proceedings of the Royal Society of London. A. Mathematical and Physical Sciences*. V. 341.

299–315. DOI: 10.1098/rspa.1974.0189.

Joaquim, A.R., Cismasiu, C. & Caetano, E.D.S. 2017. Estimation of the tensile force in the stay-cables of Salgueiro Maia bridge using ambient vibration tests. In *International Symposium on the Dynamics and Aerodynamics of Cables - ISDAC 2017*. 237–246.

Kangas, S. 2009. Experimental Modeling and Stay Force Estimation of Cable-Stayed Bridges. PhD Thesis. University of Cincinnati.

Kangas, S., Helmicki, A., Hunt, V., Sexton, R. & Swanson, J. 2010. Identification of Cable Forces on Cable-Stayed Bridges: A Novel Application of the MUSIC Algorithm. *Experimental Mechanics*. 50(7):957–968. DOI: 10.1007/s11340-009-9263-4.

Kim, B.H. & Park, T. 2007. Estimation of cable tension force using the frequency-based system identification method. *Journal of Sound and Vibration*. 304(3–5):660–676. DOI: 10.1016/j.jsv.2007.03.012.

LCM Systems. 2017. *Annular Load Cells Measure Tension in Wire Ropes*. Available: https://www.lcmsystems.com/annular-load-cells-measure-tension-in-wire-ropes [2022, July 20].

Lewis, W.J. 2003. *Tension Structures Form and Behaviour*. London, United Kingdom: Thomas Telford. DOI: 10.4324/9780203641651-8.

Mansour, A., Mekki, O. Ben, Montassar, S. & Rega, G. 2018. Catenary-induced geometric nonlinearity effects on cable linear vibrations. *Journal of Sound and Vibration*. 413:332–353. DOI: 10.1016/j.jsv.2017.10.012.

Mehrabi, A.B. & Tabatabai, H. 1998. Unified Finite Difference Formulation for Free Vibration of Cables. *Journal of Structural Engineering*. 124(11):1313–1322. DOI: 10.1061/(asce)0733-9445(1998)124:11(1313).

Morgenthal, G., Rau, S., Taraben, J., Abbas, T. & Hallermann, N. 2018. Determination of stay cable forces using highly mobile vibration measurement devices. *Journal of Bridge Engineering*. 23(2):04017136-1-04017136–13. DOI: 10.1201/9781315189390-346.

Radaelli. 2017. *Amsteele Ashton Tied Arch Bridge Certification book*. Milan.

Ren, W.X. & Peng, X.L. 2005. Baseline finite element modeling of a large span cable-stayed bridge through field ambient vibration tests. *Computers and Structures*. 83(8–9):536–550. DOI: 10.1016/j.compstruc.2004.11.013.

Ren, W.X., Liu, H.L. & Chen, G. 2008. Determination of cable tensions based on frequency differences. *Engineering Computations (Swansea, Wales)*. 25(2):172–189. DOI: 10.1108/02644400810855977.

Ronné, P., Newmark, A., Du Toit, N. & Van Wijk, H. 2018. New Ashton Arch-functional assessment of direct and indirect construction costs and evaluation of service life with respect to flooding risk. In *International Conference on Concrete Repair, Rehabilitation and Retrofitting (ICCRRR 2018)*. V. 199. Cape Town. 4–9. DOI: 10.1051/matecconf/201819906003.

Schwarz, B.J. & Richardson, M.H. 1999. Experimental Modal Analysis. In *CSI Reliability Week*. Orlando Florida. 1–12. Available: https://dokumen.tips/documents/experimental-modal-analysis-reliability-week-orlando-fl-october-1999-page-1.html?page=1.

Sipple, J.D. & Sanayei, M. 2014. Full-Scale Bridge Finite-Element Model Calibration Using Measured Frequency-Response Functions. *Journal of Bridge Engineering*. 20(9). DOI: 10.1061/(asce)be.1943-5592.0000705.

Sofistik AG. 2022a. *ASE General Static Analysis of Finite Element Structures*. Nuremberg, Germany.

Sofistik AG. 2022b. *SOFiLOAD Loads and Load Functions*. Nuremberg, Germany.

Starossek, U. 1991. Dynamic Stiffness Matrix of Sagging Cable. *Journal of Engineering Mechanics*. 117(12):2815–2828. DOI: 10.1061/(asce)0733-9399(1991)117:12(2815).

Suangga, M., Candra, H., Hidayat, I. & Yuliastuti. 2019. Temperature Effect on Tension Force of Stay cable of Cable-Stayed Bridge. *International Journal of Engineering and Advanced Technology*. 9(1):2251–2257. DOI: 10.35940/ijeat.A9724.109119.

Teufelberger Radaelli. 2022a. *Full Locked Coil*. Available: https://www.redaelli.com/products/ropes/locked-coil-ropes/full-locked-coil [2022, August 02].

Teufelberger Radaelli. 2022b. *Adjustable fork socket*. Available: https://www.redaelli.com/products/sockets/tbf [2022, August 02].

Teufelberger Radaelli. 2022c. *Fork socket*. Available: https://www.redaelli.com/products/sockets/ttf [2022, August 02].

Triantafyllou, M.S. 1984. The dynamics of taut inclined cables. *The Quarterly Journal of Mechanics and Applied Mathematics*. 37(3):421–440.

Veenendaal, D. & Block, P. 2012. An overview and comparison of structural form finding methods for general networks. *International Journal of Solids and Structures*. 49(26):3741–3753. DOI: 10.1016/j.ijsolstr.2012.08.008.

van Wijk, H. 2019. Validation of the deck behaviour due to post-tension loading of Ashton Arch Bridge. MEng Thesis. University of Cape Tow. Available: https://hdl.handle.net/11427/31783.

Xia, Y., Hao, H., Zanardo, G. & Deeks, A. 2006. Long term vibration monitoring of an RC slab: Temperature and humidity effect. *Engineering Structures*. 28(3):441–452. DOI: 10.1016/j.engstruct.2005.09.001.

Zhang, L., Qiu, G. & Chen, Z. 2021. Structural health monitoring methods of cables in cable-stayed bridge: A review. *Measurement: Journal of the International Measurement Confederation*. 168(August 2020):108343. DOI: 10.1016/j.measurement.2020.108343.

Zhou, Y., Sun, L. & Sun, S. 2013. Temperature field and its effects on a long-span steel cable-stayed bridge based on monitoring data. In *Proceedings of the 13th East Asia-Pacific Conference on Structural Engineering and Construction, EASEC 2013*. 11 - 13 September 2013. Saporo, Japan.

Zui, H., Shinke, T. & Namita, Y. 1996. Practical Formulas for Estimation of Cable Tension by Vibration Method. *Journal of Structural Engineering*. 122(6):651–656. DOI: 10.1061/(asce)0733-9445(1996)122:6(651).

Appendix A : Sequence 1 Residual Force Records

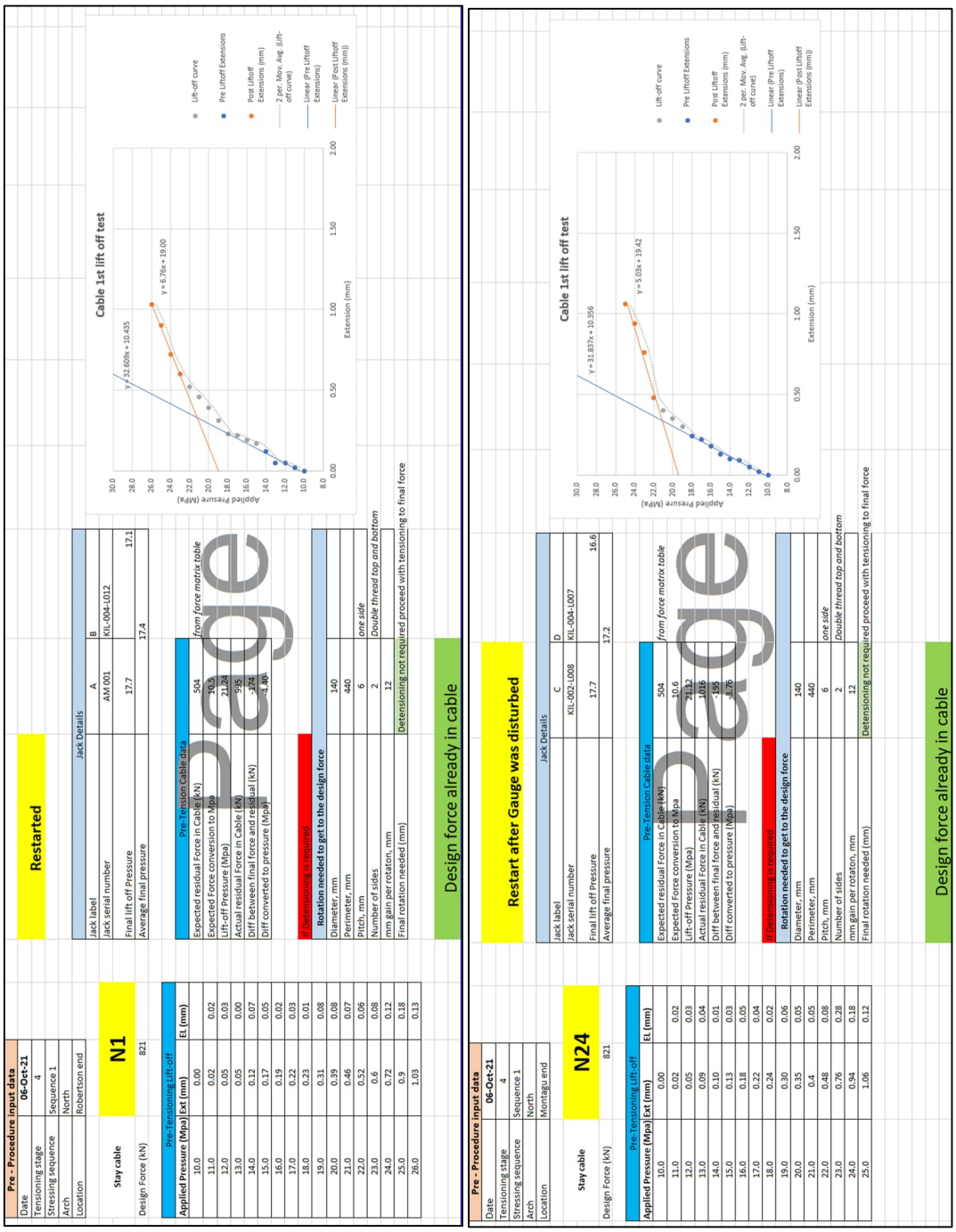

Pre - Procedure input data	
Date	06-Oct-21
Tensioning stage	4
Stressing sequence	Sequence 1
Arch	South
Location	Robertson end

Restart Gauge disturbed

Stay cable	S1
Design Force (kN)	821

Jack Details		
Jack label	A	B
Jack serial number	AM 001	KIL-004-L012
Final lift off Pressure	17.7	17.1
Average final pressure	17.4	

Pre-Tensioning Lift-off		
Applied Pressure (Mpa)	Ext (mm)	EL (mm)
10.0	0.00	
11.0	0.03	0.03
12.0	0.07	0.04
13.0	0.10	0.03
14.0	0.13	0.03
15.0	0.15	0.02
16.0	0.19	0.04
17.0	0.24	0.05
18.0	0.30	0.06
19.0	0.40	0.10
20.0	0.52	0.12
21.0	0.64	0.12
22.0	0.78	0.14

Pre-Tension Cable data		
Expected residual Force in Cable (kN)	504	*from force matrix table*
Expected Force conversion to Mpa	10.5	
Lift-off Pressure (Mpa)	17.97	
Actual residual Force in Cable (kN)	846	
Diff between final force and residual (kN)	25	
Diff converted to pressure (Mpa)	-2.13	

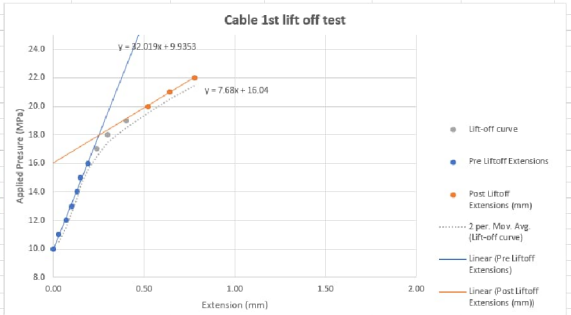

If Detensioning is required

Rotation needed to get to the design force		
Diameter, mm	140	
Perimeter, mm	440	
Pitch, mm	6	*one side*
Number of sides	2	*Double thread top and bottom*
mm gain per rotaton, mm	12	
Final rotation needed (mm)	Detensioning not required proceed with tensioning to final force	

Design force already in cable

Pre - Procedure input data	
Date	06-Oct-21
Tensioning stage	4
Stressing sequence	Sequence 1
Arch	South
Location	Montagu end

Restart

Stay cable	S24
Design Force (kN)	821

Jack Details		
Jack label	C	D
Jack serial number	KIL-002-L008	KIL-004-L007
Final lift off Pressure	17.7	16.6
Average final pressure	17.2	

Pre-Tension Cable data		
Expected residual Force in Cable (kN)	504	*from force matrix table*
Expected Force conversion to Mpa	10.6	
Lift-off Pressure (Mpa)	17.83	
Actual residual Force in Cable (kN)	856	
Diff between final force and residual (kN)	-35	
Diff converted to pressure (Mpa)	-0.46	

Pre-Tensioning Lift-off		
Applied Pressure (Mpa)	Ext (mm)	EL (mm)
5.0	0.00	
6.0	0.03	0.03
7.0	0.06	0.03
8.0	0.08	0.02
9.0	0.12	0.04
10.0	0.14	0.02
11.0	0.15	0.01
12.0	0.19	0.04
13.0	0.23	0.04
14.0	0.26	0.03
15.0	0.29	0.03
16.0	0.34	0.05
17.0	0.39	0.05
18	0.47	0.08
19	0.57	0.10
20	0.72	0.15
21	0.91	0.19

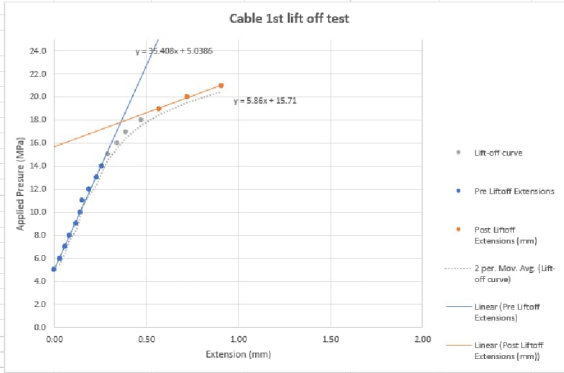

If Detensioning is required

Rotation needed to get to the design force		
Diameter, mm	140	
Perimeter, mm	440	
Pitch, mm	6	*one side*
Number of sides	2	*Double thread top and bottom*
mm gain per rotaton, mm	12	
Final rotation needed (mm)	Detensioning not required proceed with tensioning to final force	

Design force already in cable

Appendix B : Socket Length and Gap Calculation

Cable N6 Example

Fork Socket

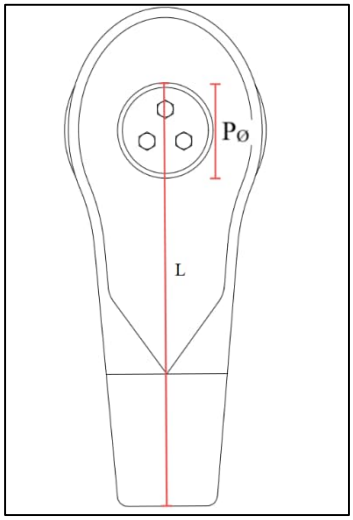

Length from the beginning of the socket to the end of the pin plate (L) = 798 mm

Diameter of pin plate ($P_Ø$) = 180mm

Length from the centre of the pin hole $= 798 - \frac{180}{2} = 708 \approx 710mm$ for all cables

Adjustable Fork Socket

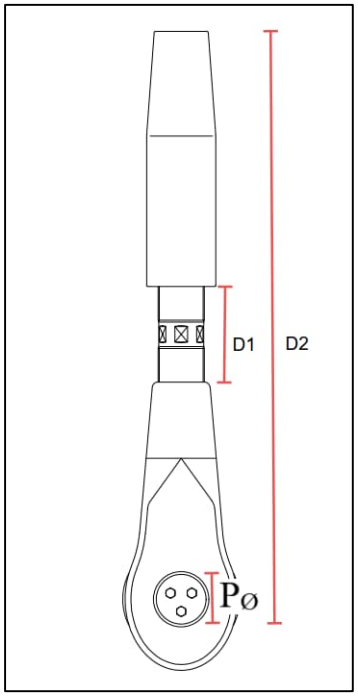

Diameter of pin plate ($P_Ø$) = 180 mm

D2 (before tensioning) = 1911mm

D1 (before tensioning) = 293mm

D1 (after tensioning) = 278mm

Length from the centre of the pin hole $= 1911 - (293 - 278) - \frac{180}{2} = 1806mm$

North Arch Cable Measurements						
Cable Number	**D1 initial (mm)**	**D2 initial (mm)**	**D1 after tensioning (mm)**	**Diameter of pin plate (mm)**	**Length from the centre of the pin (mm)**	**Note**
1	297	1927	276	180	1816	Design Force already in cable. Stage 3 tensioning measurements used
2	277	1903	269	180	1805	
3	323	1936	319	180	1842	
4	289	1939	281	180	1841	
5	299	1924	288	180	1823	
6	293	1911	278	180	1806	
7	299	1917	283	180	1811	
8	290	1917	279	180	1816	
9	310	1932	287	180	1819	
10	292	1918	278	180	1814	
11	309	1934	281	180	1816	
12	309	1918	281	180	1800	
13	309	1918	276	180	1795	
14	300	1918	278	180	1806	
15	279	1907	270	180	1808	
16	302	1930	282	180	1820	
17	281	1900	270	180	1799	
18	314	1936	301	180	1833	
19	278	1893	271	180	1796	
20	308	1936	303	180	1841	
21	304	1920	298	180	1824	
22	336.5	1853	288	180	1714.5	
23	319	1942	314	180	1847	
24	307	1942	280	180	1825	Design Force already in cable. Stage 3 tensioning measurements used
		Average	285	Average	1815	

South Arch Cable Measurements						
Cable Number	D1 initial (mm)	D2 initial (mm)	D1 after tensioning (mm)	Diameter of pin plate (mm)	Length from the centre of the pin (mm)	Note
1	299	1920	270.89	180	1802	Design Force already in cable. Stage 3 tensioning measurements used
2	280	1902	271	180	1803	
3	323	1936	320	180	1843	
4	315	1951	309	180	1855	
5	323	1939	311	180	1837	
6	286	1911	273	180	1808	
7	310	1912	291	180	1803	
8	289	1901	274	180	1796	
9	313	1919	289	180	1805	
10	305	1915	293	180	1813	
11	315	1927	289	180	1811	
12	299	1915	273	180	1799	
13	296	1908	271	180	1793	
14	323	1947	303	180	1837	
15	289	1913	277	180	1811	
16	309	1936	291	180	1828	
17	292	1902	280	180	1800	
18	304	1920	293	180	1819	
19	295	1931	282	180	1828	
20	299	1931.5	289	180	1831.5	
21	304	1920	298	180	1824	N21 cable measurements used because of error in the readings for S21
22	349	1960	346	180	1867	
23	312	1928	305	180	1831	
24	336	1960	308	180	1842	Design Force already in cable. Stage 3 tensioning measurements used
		Average	292	Average	1825	

Average of socket gap from the North Arch = 285mm

Average of socket gap from the South Arch = 292mm

Socket gap to be used in cable models = $\frac{285+292}{2}$ = 288mm ≈ 290 mm

Average length from centre of the pin from the North Arch = 1815mm

Average length from centre of the pin from the South Arch = 1825mm

Standardised socket length from the centre of the pin = $\frac{1815+1825}{2}$ = 1820mm

Appendix C : Socket Geometry and Self Weight

Fork Socket

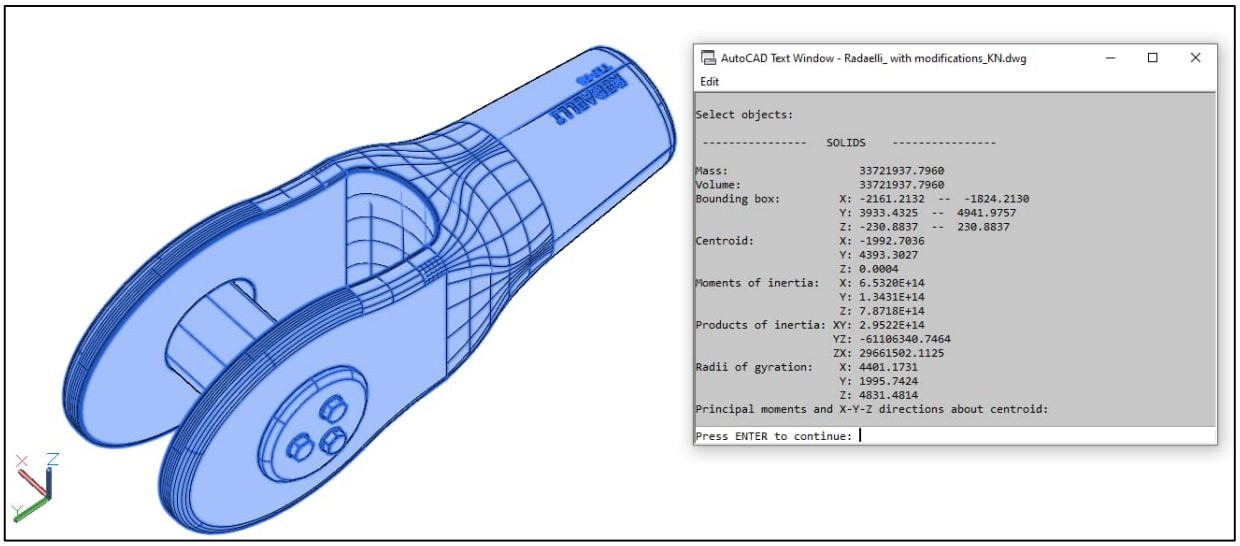

Total volume (V) = 33 721 937.7960 mm^3 (from AutoCAD)

Length from the centre of the pin FEM (L) = 710mm (from Appendix B)

Equivalent Diameter (D)

$$V = \frac{\pi D^2}{4} \times L \rightarrow D = \sqrt{\frac{4V}{\pi L}} = \sqrt{\frac{4 \times 33\,721\,937.7960}{\pi \times 710}} = 246\text{mm}$$

Mass of fork socket = 216 kg (from manufacturer specification booklet)

1 kN = 101.97 kg

$\therefore 216\ kg = 2.11827\ kN$

$$\therefore \text{Weight per unit volume} = \frac{2.11827\ \text{kN}}{33\,721\,937.7960 \times 10^{-3}\text{m}^3} = 62.82\ \text{kN/m}^3$$

Adjustable Fork Socket

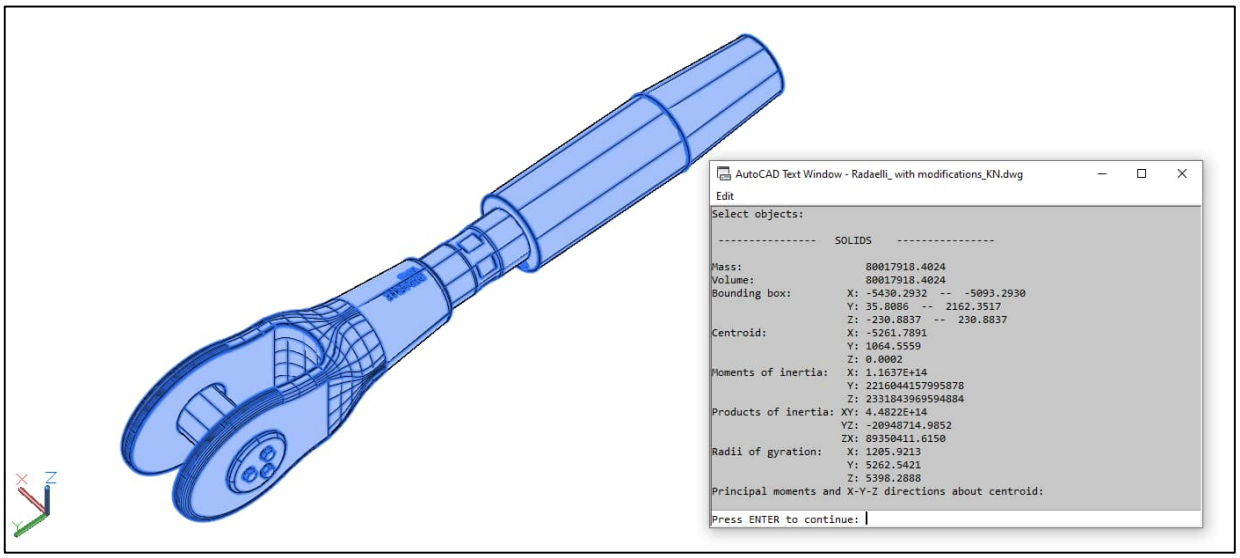

Total volume (V) = 80 017 918.4024mm^3 (from AutoCAD)

Length from the centre of the pin FEM (L) = 1820mm (from Appendix B)

Equivalent Diameter (D)

$$V = \frac{\pi D^2}{4} \times L \rightarrow D = \sqrt{\frac{4V}{\pi L}} = \sqrt{\frac{4 \times 80\,017\,918.4024}{\pi \times 1820}} = 237\text{mm}$$

Mass of adjustable fork socket = 442 kg (from manufacturer specification booklet)

1 kN = 101.97 kg

$\therefore 442\ kg = 4.33561\ kN$

$$\therefore \text{Weight per unit volume} = \frac{4.33561\ \text{kN}}{80\,017\,918.4024 \times 10^{-3}\text{m}^3} = 54.17\ \text{kN/m}^3$$

Appendix D : Analytical Model Validation

The validation calculation is based on cable S6.

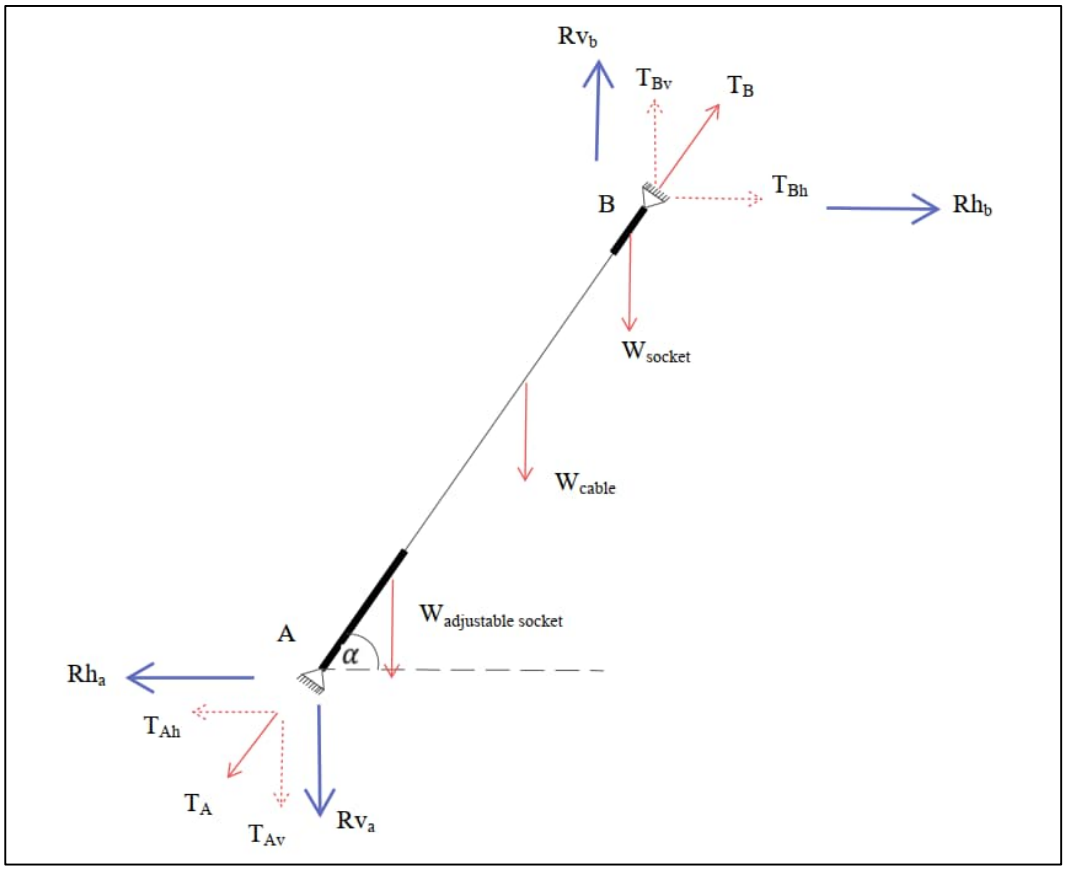

The cable details are as follows

Prestress Force : 695 kN
Unit Weight : 81.45 kN/m^3
Diameter : 70.8mm
Length of Cable : 13.503m
Inclination Angle : 77°

Validation conditions

$$Rv_a + Rv_b \cong W_{socket} + W_{cable} + W_{adjustable\ socket} + T_{Av} + T_{Bv}$$

$$Rh_a + Rh_b \cong T_{Ah} + T_{Bh}$$

$$T_B > T_A$$

Weight of components

W_{socket} = 2.12 kN (from Appendix C)
$W_{adjustable\ socket}$ = 4.34 kN (from Appendix C)

$$W_{cable} = Unit\ Weight \times volume = 81.45 \times 13.503 \times \pi \times \frac{0.0708^2}{4} = 4.33\ kN$$

Prestress Force Components

For a prestress force of 695 kN the resulting force in the cable after form finding is illustrated in the following figure from Sofistik Graphic.

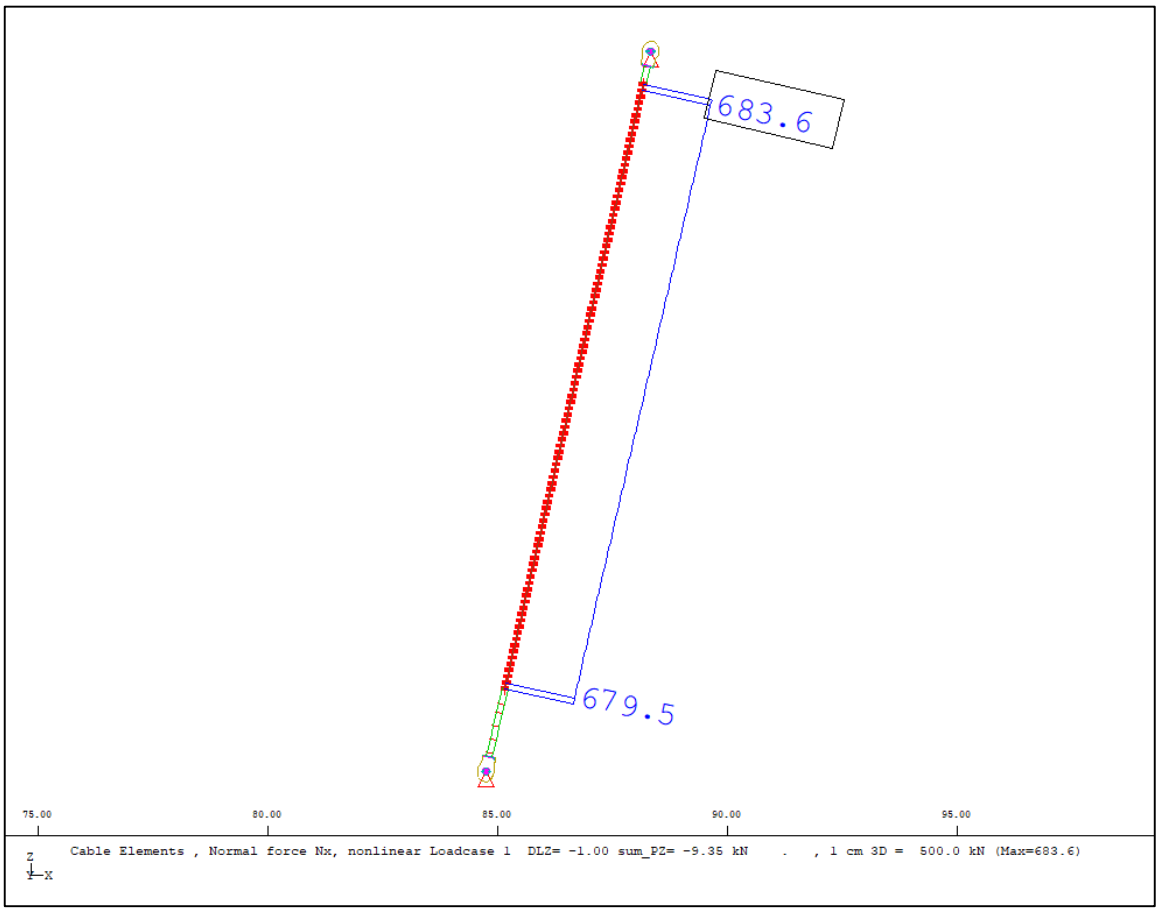

However, for the model verification process, the axial force in the sockets is taken because these are the elements directly connected to the pin connection. The forces in the sockets are then extracted from Sofistik graphic as follows

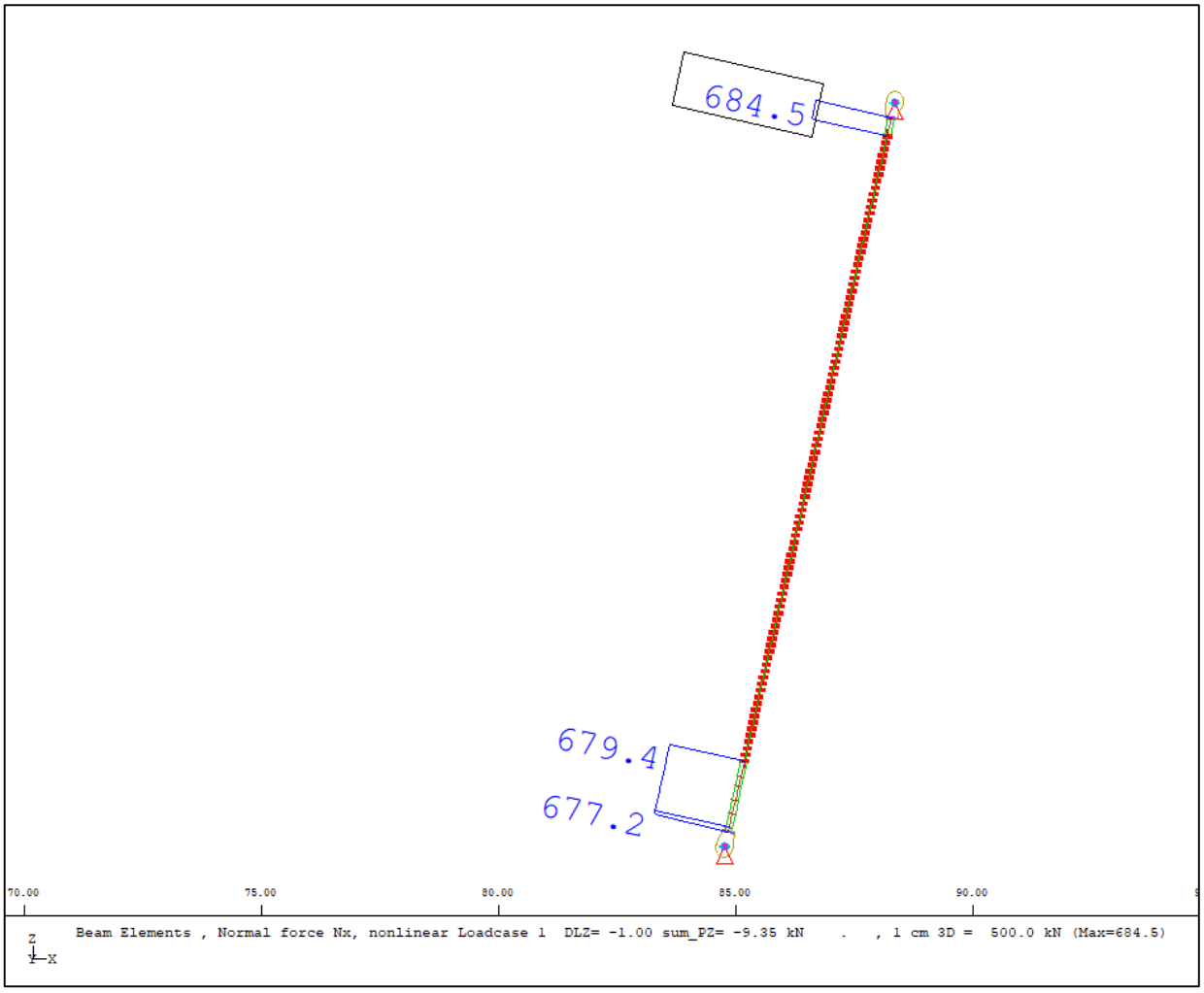

In this instance one of the conditions for validation, $T_B > T_A$ is satisfied because 684.5 kN > 677.2 kN

In the hand calculations for reactions, T_A and T_B were assumed to be equal. Therefore the total force is taken as $\frac{677.2+684.5}{2} = 681\ kN$

Horizontal force component

$T_{Ah} = T_{Bh} = Tcos\alpha = 681 \cos 77 = 153\ kN$

Vertical force component

$T_{Av} = T_{Bv} = Tsin\alpha = 681 \sin 77 = 664 kN$

Reaction check

Vertical forces

$Total\ downward\ vertical\ force = W_{socket} + W_{cable} + W_{adjustable\ socket} + T_{Av}$

$Total\ vertical\ force\ at\ A = 2.12 + 4.33 + 4.34 + 664 = 675\ kN$

$Total\ upward\ vertical\ force = T_{Bv} = 664\ kN$

Comparison with Sofistik results

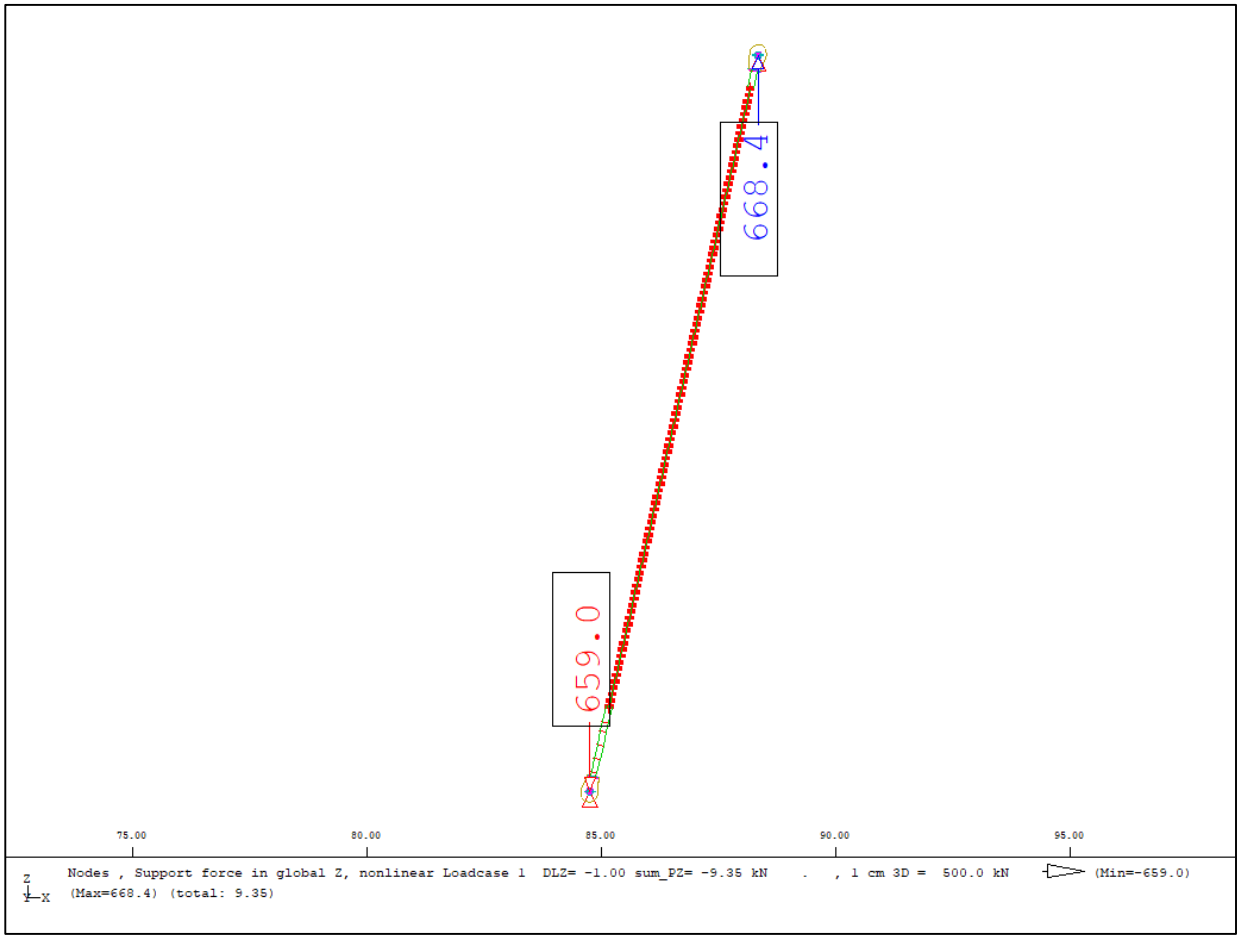

Parameter	Hand Calculation answer (kN)	Sofistik Answer (kN)	% Difference	Comment
Total downward Vertical Force	675	659	2	Valid
Total Upward Vertical Force	664	668.4	-0.7	Valid

Horizontal forces

Hand Calculation answer = 153 KN. Sofistik Answer = 151.8 kN.

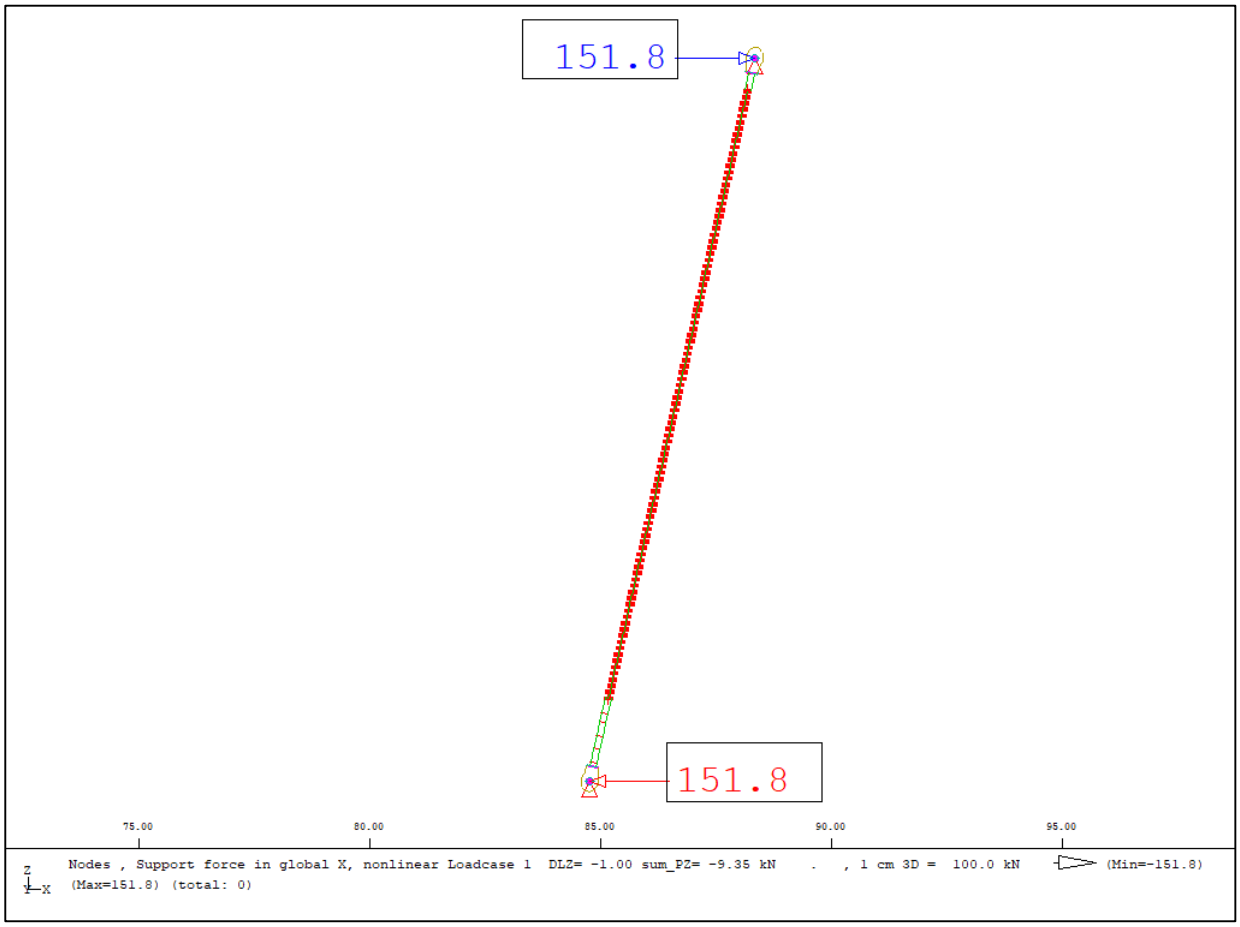

Parameter	Hand Calculation answer (kN)	Sofistik Answer (kN)	% Difference	Comment
Horizontal force magnitude	153	151.8	0.8	Valid.

Furthermore, the horizontal force components cancel out. Therefore, the model is validated.

Appendix E : Temperature Effects Calculation

The temperature effects calculation will be based on cable N19

The cable details are as follows

Cable length = 13 503 mm
E = 158 312 N/mm^2

Diameter = 70.8mm

$$\therefore Cross\ Sectional\ Area = \pi \times \frac{70.8^2}{4} = 3937\ mm^2$$

Coefficient of thermal expansion (φ) = $12.5 \times 10^{-6}\ ^0C^{-1}$

Change in temperature (ΔT) = 9℃

$$\Delta F_{cable} = EA\varphi\Delta T = 158312 \times 3937 \times 12.5 \times 10^{-6} \times 9 = 70\ kN$$

$\Delta F_{due\ to\ structural\ deformation}$

Bridge Deformation when temperature increase by 9℃

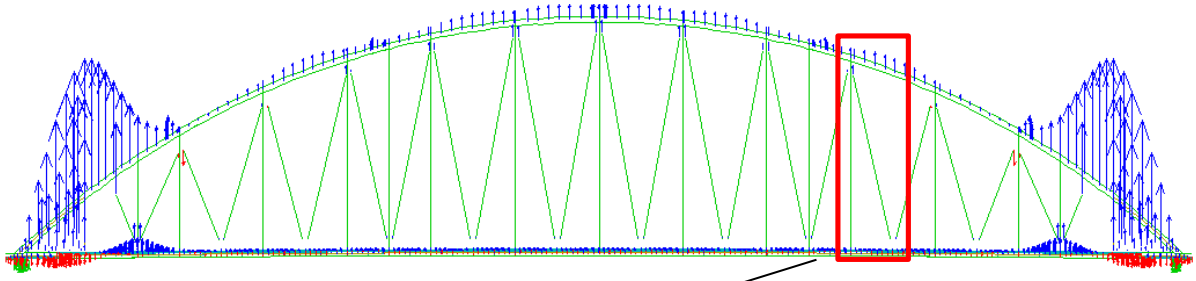

Close up view at Cable N19

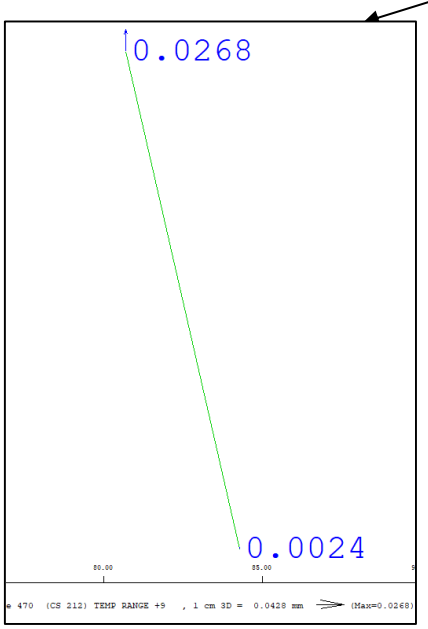

$Total\ change\ in\ length = 0.0268 - 0.0024 = 0.0244\ mm$
$Cable\ inclination\ angle = 77°$

Total length change along the axis of the cable

$$\Delta L_{cable\ axis} = \frac{0.0244}{\cos 77} = 0.108\ mm$$

$$\Delta F_{due\ to\ structural\ deformation} = EA\ \frac{\Delta L}{L_i} = 158312 \times 3937 \times \frac{0.108}{13503} = 5\ kN$$

Total change in force due to temperature effects

$\Delta F_{total} = \Delta F_{cable} + \Delta F_{due\ to\ structural\ deformation}$
$\Delta F_{total} = \Delta F_{cable} + \Delta F_{due\ to\ structural\ deformation} = 70 + 5 = 75\ kN$

When the temperature decreases by 9 ℃, the force changes by – 74 kN

The predicted force for N19 is 737kN

$\therefore The\ upper\ bound\ force\ value\ is\ 737 + 74 = 812\ kN$
$The\ Lower\ bound\ force\ value\ is\ 737 - 74 = 662\ kN$

The force evaluated in the N19 local model should be in the 737 ± 74 kN range